INSTITUTO TECNOLÓGICO Y DE ESTUDIOS SUPERIORES
DE MONTERREY

MONTERREY CAMPUS

GRADUATE PROGRAM IN ENGINEERING AND
INFORMATION TECHNOLOGIES

REAL-TIME SENSING SYSTEM TO CHARACTERIZE THE STATE OF RAT STEM CELL CULTURE THROUGH ECIS INTERROGATION

THESIS

PRESENTED AS PARTIAL FULFILLMENT OF THE REQUIREMENTS
FOR THE DEGREE OF:

MASTER OF SCIENCE WITH SPECIALTY IN ELECTRONICS ENGINEERING
(ELECTRONIC SYSTEMS)

BY:

GERMÁN MOLINA LUCIO

MONTERREY, N.L. Deccember 2013

INSTITUTO TECNOLÓGICO DE ESTUDIOS SUPERIORES DE MONTERREY

SCHOOL OF ENGINEERING AND INFORMATION TECHNOLOGIES

GRADUATE PROGRAM

The members of the thesis committee hereby approve the thesis of Ing. Germán Molina Lucio as a partial fulfillment of the requirements for the degree of Master of Science with specialty in Electronics Engineering (Electronic Systems).

Thesis Committee:

_____

Dr. Graciano Dieck Assad
Thesis Advisor

_____

Dra. María Teresa González Garza
Sinodal

_____

Dr. Sergio Omar Martínez Chapa
Sinodal

_____

Dr. Gabriel Campuzano Treviño
Director of the Graduate Program of Electronics Engineering
December 2013

REAL-TIME SENSING SYSTEM TO CHARACTERIZE THE STATE OF RAT STEM CELL CULTURE THROUGH ECIS INTERROGATION

BY:

GERMÁN MOLINA LUCIO

THESIS

Presented to the Graduate Program in Engineering
And Information Technologies

This Thesis is a partial requirement for the degree of
Master of Science with Specialty in Electronics Engineering (Electronics Systems)

INSTITUTO TECNOLÓGICO Y DE ESTUDIOS
SUPERIORES DE MONTERREY

December 2013

ABSTRACT

There is a huge variety of biochemical assays to characterize stem cells at molecular level. However, even when these assays have helped us to improve our understanding of basic cell biology down to gene and protein expression, most of these techniques are not able to characterize cells without affecting their therapeutic potential. The introduction of real-time, non-invasive sensing methods enables a major reliability, repeatability and sensibility than traditional methods; as well as the possibility to successfully translate the stem cell technology to real therapeutic applications. This is achieved through the use of specific biosensors that monitor various physical, chemical or biological parameters in the surrounding environment and provide representative signals that can be measured or stored.

Since the late 90's the enthusiasm around stem cell research took a new strength and the actual possibilities for this science branch range nowadays from immunotherapy to tissue culture, which are promising development areas in biology, bioengineering, chemistry, and medicine. Currently, most such culture processes are conducted at laboratory bench scale by a manual operator. Therefore, handling a wide repertory of cell cultures rapidly becomes unfeasible because of the bench scale properties. Here, high amount of time consumption stands as the major drawback. In the future, cell-based therapies will require cell culture expansion in vitro to provide sufficient functional biological material. Automatic culture methodologies open up the possibility to industrial production of novel applications in fields like tissue and regenerative medicine.

The goal of this work is to propose and validate a real-time, non-invasive sensing system through bioimpedance sensing capable of characterize the state (confluence, media state and specific cellular physical changes) of the rat stem cells (rSCs) culture with minimum human intervention using inter-digitized electrodes. The underlying low cost sensing system suitable for continuous monitoring, and the characterization of the bioimpedance curve during rat stem cell differentiation into motor and dopaminergic cells, are the main novelties of this thesis. The biosensor consists of an impedance measurement device, microfabricated inter-digitized electrodes from Applied Biophysics. The real-time impedance measurement device is based on Analog Devices AD5933 integrated circuit. Thesis focuses on the development of integrated, accurate, rapid and continuous monitoring of rSCs cultures. Obtained results are compared to data obtained by traditional protocol analysis performed by lab technicians as microscopy analysis and dying techniques.

ACKNOWLEDGEMENTS

This work would not have been possible without the support from the research Chair of "Sistemas Biointeractivos y BioMEMS" of the Engineering School (EITI) and the research Chair of "Terapia Celular" of the Medical School and TEC-Salud, both at Tecnológico de Monterrey, Monterrey campus in México.

There are so many people who have been involved in the creation of this work. Some have been intricately involved in the technical details while others have enriched my life in other ways. If I neglected to mention your name, you know who you are and how you have helped me through this process, and I thank you.

I would like to thank my advisor, Dr. Graciano Dieck Assad for his friendship, spirit and enthusiasm. Under his tutelage and guidance, I have developed myself into a more creative and critical professional. This work would have not been possible without his both invaluable and inspiring support and guidance during the past years, and I am truly thankful. He has taught me to push myself and has encouraged me to continuously seek new insights from existing knowledge. With his mentorship and patience, I have grown as a scientist; moreover, I have learned about my true nature as a person and, for this, I am deeply indebted to this dear friend. I look forward to continued interactions and collaborations with him in the future.

My sincere appreciation goes to Dr. María Teresa González for advice, correction and encouragement. You always warmly encouraged, and helped me to see my flaws during laboratory experiments. Her experience and insights were invaluable as I struggled to grasp the biological aspects of this work. I wish to thank her for her significant technical contribution and for always being interested in my work.

I also want to thank Dr. Sergio Omar Martínez, Dr. Raúl Hernández, Dr. Sergio Camacho and Dr. José Gómez for your advice, shared knowledge and assistance through this entire process. I truly appreciate the opportunity to interact and work with such gifted persons. Their friendship and professional help have been greatly appreciated.

I want to thank Dr. Alberto Yúfera who helped in the selection of techniques and models for the development of this thesis. His valuable expertise with electrical interrogation systems was invaluable. His help was critical for the development of this thesis.

I would like to thank Amada Abrego and Christian Mendoza with whom I have worked during these two years; you have been amazing – thank you! You have, in your own way, made the task of developing this thesis bearable. I appreciate the camaraderie, the useful technical discussions, and your friendship. I will truly miss our daily interactions.

I would also like to thank my fellow companions in this master program Rubén R. López and Javier A. Hernández who, while not being involved with any of this research, have helped to keep me sane during the process. Thanks to Luis Licón, Diana Arocha, Bernardino Ramirez, Chimina Molina and José Molina for supporting me, making me laugh and raising my spirit when things were not working out; your friendship and support have been greatly appreciated.

I want thank all my friends, the faculty and staff of El Tecnológico de Monterrey Campus Ciudad Juárez, Campus Monterrey, and Campus Guaymas. I specially want to thank the mother Juana Cadena Montaño, who turned me into the right direction at the right moment in my academic life. From my hearth thanks you for everything.

Finally, I want to thank my mother and father, Antonia Lucio and German Molina, for making the sacrifices which allowed me to attend college and for their endless love and support. They have taught me the value of hard work, honesty and integrity. Without all you have done for me, I would have not been finishing this master today. Thank you for everything.

CONTENTS

LIST OF FIGURES

LIST OF TABLES

CHAPTER 1 – INTRODUCTION

The study of cellular function and response has increased tremendously for decades to better understand the working of the body. As technology has advanced, the capabilities and sensitivity of cellular studies have greatly improved. Current techniques allow for examination of single cell electrical characteristics either *in vivo* (within the body) or *in vitro* (outside the body). Also, recent developments allow simultaneous examination of cell population.

Electrical bioimpedance measurements have been proved to be appropriate method for assessment of body composition. They can therefore provide with direct indicators of cell morphology evolution. Such ability of electrical bioimpedance technology allows the detection of cell membrane changes, motility, migration, cytotoxity, etc. These biologically relevant signals can be directly measured using microelectrodes which provide a stable, non-invasive interface for monitoring population of cells. Due to its capability to monitor morphology, the potential use for such cell based biosensors include environmental monitoring, pharmaceutical screening, drug discovery or delivery and basic neuroscience.

1.1 Justification

The increase of adult stem cells (ASCs), as promising candidates to be used in cell therapies for degenerative illness procedures, has pushed the need of automated cell culture systems. Such systems will have an important role in overcoming issues associated with the translation of emerging regenerative medicine technologies from laboratory to the clinic. Nowadays these systems have been already reviewed and compared with traditional ASCs culture with positive results [1-3]. Applications of ASCs are of particular interest because they can be isolated from bone marrow, fat tissues, placenta and umbilical cord blood and multiplied relatively easily *in vitro*. Moreover, having the potential to differentiate into cells of different lineages, such as cartilage, neural, bone, or muscle, they hold large potential in therapeutic markets. Furthermore, they are potentially valuable in promoting angiogenesis, and they have immunomodulatory properties indicating possible application for allogeneic as well as autologous therapies.

As suggested before, it is clear that cell-based therapies will require automated cell culture systems capable of in vitro expansion to provide sufficient functional biological material. Currently, most culture processes of this type are conducted at laboratory bench scale by manual operators. Therefore, meeting the high quantity and quality standards in a short window of time this new therapies need, rapidly becomes unfeasible because of the bench scale properties. Here, high amount of time consumption analyzing the cultures state stands as the major drawback. The possibility of fatigue, prompted by the long hours of repetitive work, may manifest as failure developing important manual tasks or activities of interpretation, compromising the final manufactured product. For this reason, it is suggested the implementation of an automatic real-time non-invasive sensing cell based biosensors to eliminate the time wasted in cyclic analysis present in bench scale. It has already been proved successfully by some research groups the possibility of monitoring platforms for stem cell culture and cell populations [4-5]. The improvements achieved by the use of those systems would be reflected in two major areas, reliability of cell culture analysis (cost-effectiveness, controllability, low volume, high resolution, and sensitivity) and the health of the cell cultures (increasing cell viability and reducing cell stress) [6].

Automatic real-time non-invasive sensing system require the following important parameters and variables in cell cultures: pH, glucose, lactate, dissolved oxygen, temperature, cytokine, CO^2, confluence, nutrient concentration, cell mechanical stress, and the medium exchange rates [7]. The interpretation of those parameters and the impact of the variables will allow to determine cell growth, cell health, cell differentiation and culture confluence without the use of traditional microscopy and dying techniques and avoiding the destructive impact of some other techniques. As implied, with measurements of one or some of these parameters is possible to characterize the state of the cell culture through time, and take adequate decisions and actions in dependence of that state.

1.2 State of the Art

Electrical impedance sensing, often referred as electric impedance spectroscopy (EIS) [8] or electric cell-substrate impedance sensing (ECIS) [9], is a well-known method for characterizing the electric and dielectric properties of a culture under test. This sensing method has been used to measure biological material, such as tissue samples and cell suspensions for over a hundred years [10-11]. The first reported system using EIS to measure cell cultures was first mentioned by Hause, et al. while measuring bacterial growth [12]; and the first time microelectrodes and ECIS were used was to study the characteristics of anchorage dependent cell lines by Giaever and Keese in 1984 [13]. Both methods apply an alternating voltage or current via electrodes to the culture under test and monitor the system response which is due the momentary change of electrical impedance as a particle replaces electrolyte in the sensing zone over the electrodes. Thirty years later from its first implementation, electrical impedance sensing has become a reliable low cost, real-time, label-free, and non-invasive method to study the activities of cells response to various stimuli in tissue culture.

The ECIS is a device developed by Giaever and Keese [13] that monitors the impedance of small gold electrodes used as substrata for cells in culture. The system has been extensively studied and can be used to detect subtle changes in the cell-substrata interactions including cell motion. Since the publications between the years 1991-1994 made by Giaever and Keese research team [14-19], on the use of ECIS for measuring cell adhesion, motility, toxicology, electroporation and change in cell shape in real-time, this strategy has become more important each year. In the thirty years since its invention, characterization of different processes through the frequency response of the cell-electrode heterojunction impedance has become a commonly referred topic in biosensor publications [20-24]. It has been demonstrated that it can detect cell migration [25], cell attachment & spreading [26], cell invasion & extravasation [27], barrier function [14], real-time electroporation [28], cell proliferation [29], toxicology impact [30-31], signal transduction [32] and even characteristics of cells under flow [33].

As explained by Shwan [34], the wide range of measurements this method has is due the electric and dielectric properties of the tissue under test, properties that are determined by its physiological and morphological properties. Following this chain, since electric and dielectric properties of a sample can be determined by recording the electrical impedance over a frequency range, the physiological events and morphological properties of biological tissue should be determinable by electric impedance measurements. In the past decade and due the advances in micromachining many publications have appeared.

At the beginning of the past decade, Hautmann and Müller presented a micro machined full bridge sensor system to characterize the impedance of bio suspensions of different kind of cells at frequencies

above the 500 kHz [35]. In 2002 Xiao, et al., following Giaever publications, conducted an in-depth analysis of ECIS to study attachment and spreading of cells in culture realizing that the resistance measured would be proportional to the area covered by the cells, and therefore proportional to the cell number, giving the insight that ECIS profile can be related to a traditional model of cell expansion [36]. A few years later Thielecke, et al. [37] while studying the possibility to characterize small biological samples (cell quantity) using impedance spectroscopy his research team showed experimentally that using frequencies above 100 kHz the EIS system can determine intracellular resistances in addition to the extracellular composition, while extracellular resistance is dominant under the 100kHz. Other efforts include the design and fabrication of the first interdigitated bioimpedance sensing systems to characterize bacterial concentration [38] which demonstrated the possibility of using different microelectrode structures for impedance measurement.

In 2004 the first major breakthrough in determination of cell shape was made by Arndt, et al. who showed the impact cell membrane had on the extracellular impedance measurement [39]. In 2008 Zheng, et al. [40] showed that it was possible to determine the cell composition while characterizing human blood cells at different frequencies and in the same year Cho used high and low (ECIS) frequency EIS to characterize both cellular growth and membrane composition in time [26]. These changes in the membrane were also used to characterize the toxicity in field water by Curtis, et al [33]. However it wasn't until 2010 when the first study involving cell differentiation was published by Hyo Eun Park, et al. [41], were the process of neural differentiation of human mesenchymal stem cells was monitored in real-time with great results. Finally, there are even cases where both cell growth and differentiation has been addressed in the same publication; in 2012 the work of Bagnaninchi [42] where human adipose derived ASCs were induced toward osteogenesis and adipogenesis showed that cell differentiation processes generate different impedance profiles.

In a different topic of impedance measurement publications, recently (2006) the manufacturer of integrated circuits, Analog Devices, introduced in the market the first integrated system dedicated to measure electric bioimpedance: the AD5933. The availability of this electric bioimpedance spectrometer device opens up new horizons for the integration of the measurement systems of electric bioimpedance into low cost and portable systems. In 2008 Ibañez [43] implemented an electrical bioimpedance monitoring system using an AD5933 and developed a MATLAB based software capable of obtaining vector analysis, however it remarked the frequency limitations of the integrated circuit for the development of composition analysis at frequencies higher than 100 kHz (AD5933 highest frequency). In 2009 Ansede [44] studied the suitability of a spectrometer based on an AD5933 for bioimpedance measurements, concluding that a significant repercussion in economic terms can be achieved due the high integration of the integrated card, and that new horizons for the creation of bioimpedance portable and wearable systems are open with this kind of platform. In the same year, Aliakbar [45] presented a design of a handheld impedance based biosensor for glucose monitoring using an AD5933 as low cost and energy consumption option, marking the first time the hardware was reported to be used to sense concentration of analytes in a solution. But it wasn't until 2012 when Rösner, et al. presented at the 2012 Micromechanics and Microsystems European Conference (Ilmenau, Deutschland) [46] an AD5933 based bio instrument for impedance sensing to determine viability of cells, showing that the capabilities of the system could be also applied into a real-time non-invasive bio impedance sensing platform.

The literature review on technologies of cell culture analysis provides a solid platform to perform a strategy to use impedance measurements. The application of this strategy allows us to visualize an automated culture sensor system that could provide the cell culture confluence state and a characterization of the differentiation process.

1.3 Problem Description

This work intends to implement a bioimpedance measurement system based on electric cell-substrate impedance sensing (ECIS) in order to examine the electrical characteristics of the cell membrane. Commercial electrodes arrays will be used as the substrate for the culture of anchorage dependent cell types. The ECIS system will be used to observe if the changes in impedance due to cell grow and differentiation can be monitored in real-time using extracellular electrodes, and determine if there is a possible application to design a cell culture automatized system. The ultimate goal of this study is both to develop a technique which would allow the action of different differentiation agents to be deduced and characterized, and to determine the confluence state of the culture by the measured cellular response.

1.4 Objectives

The research methodology focus on the characterization of small animals (rats) stem cells (rSCs) under different paths of differentiation through ECIS technique. Particular objectives are:

- To perform a cell culture of rSCs using specialized electrodes.
- To use a specialized data acquisition system to obtain real-time impedance measurements from 16 wells simultaneously.
- To demonstrate the application of a platform based ECIS in rSCs cultures as a real-time non-invasive viable technique for growth and differentiation.
- To detect cell growth through time.
- To detect rSCs culture differentiation in two cell groups:
    - Dopaminergic
    - Motor Nerve
- To compare impedance measurements with microscopy images to validate the cell math model of growth.
- To compare impedance measurements with microscopy images to validate the differentiation impedance characterization.

1.5 Overview of this Thesis

This thesis is organized as follows:

A. Chapter 1 describes the historical and state of the art background of ECIS impedance measurements on cultured stem cell systems. These from the basis of goals and objectives upon which this research was built.
B. Chapter 2 gives some fundamental background on stem cell research and the theory of cellular function with emphasis placed on cellular construction, cellular adhesion, motility, differentiation and bases of the impedance membrane properties. The anticipated cellular

response to external stimuli will also be explored as it will impact in cellular impedance modulation.

C. Chapter 3 focus on the general impedance measurement and microelectrode theory. The basic theory and models of microelectrodes for tissue culture impedance monitoring will be discussed.
D. Chapter 4 reviews the characteristics of ECIS technique. Its specific application, models, data analysis and presentation as well as the involved devices to perform the technique are presented.
E. Chapter 5 proposes the measurement methodology and instrumentation used in the biological tests. Also explanations of the instrumentation and specification of the experiments are provided.
F. Chapter 6 discusses the impedance response of biological samples using microelectrodes. Models of the cell/electrode interface, microscopy and dying imagery, and comparison with selected studies are presented to validate the obtained results and to determine the impact of the developed system.
G. Chapter 7 concludes with a discussion of the utility and limitations of the whole cell based biosensor system developed. Possible directions for future research will also be described.

References

[1] M. Kempner, and R. Felder, **"Review of cell culture automation,"** *Journal Laboratory Automation*, vol. 7, no. 2, pp. 56 – 62, 2002.

[2] Thomas RJ, Chandra A, Liu Y, Hourd PC, Conway PP, Williams DJ. **"Manufacture of a human mesenchymal stem cell population using an automated cell culture platform,"** *Cytotechnology*, 55, pp. 31-39, 2007.

[3] Schmidt BT, Feduska JM, Witt AM, Deasy BM. **"Robotic Cell Culture System for Stem Cell Assays,"** *Industrial Robot: An International Journal*, vol. 35, no. 2, pp. 116 – 124, 2008.

[4] Yue X, Drakakis EM, Lim M, Ye H, Mantalaris A, Radomska A, Cass A, Panoskaltsis N. **"A Real-Time Multi-Channel Monitoring System for Stem Cell Culture Process,"** *IEEE Transactions on Biomedical Circuits and Systems*, vol. 2, no. 2, pp. 66-77, 2008.

[5] Gottschamel J, Richter L, Mak A, Jungreuthmayer C, Birnbaumer G, Milnera M, *Br*ückl H, Ertl P. **"Development of a Disposable Microfluidic Biochip for Multiparameter Cell Population Measurements,"** *Anal. Chem.*, 81, pp. 8503-8512, 2009.

[6] M. Ni. et al. **"Cell culture on MEMS platform: A review,"** *International Journal of Molecular Science*, vol. 10, no. 12, pp. 5411 – 5441, 2009.

[7] M. Kallos, and L. Behie. **"Inoculation and growth conditions for high-cell-density expansion of mammalian neural stem cells in suspension bioreactors,"** *Biotechnology and Bioengineering Wiley Periodicals*, vol. 63, no. 4, pp. 473 – 483, 1999.

[8] Asami K. **"Characterize of heterogeneous systems by dielectric spectroscopy,"** *Prog. Polym. Sci.*, 27, pp. 1617-1659, 2002.

[9] Giaever I. and Keese, CR. **"Micromotion of Mammalian Cells Measured Electrically,"** *PNAS USA*, 88, pp. 7896 – 7900, 1991.

[10] Schanne OF. and Ruiz E. Impedance Measurements in Biological Cells. John Wiley & Sons, 1978.

[11] Schwan HP. **"Linear and nonlinear electrode polarization and biological materials,"** *Ann. Biomed. Eng.*, 20, pp. 269-288, 1992.

[12] Hause LL, Komorowski RA, Gayon F. **"Electrode and Electrolyte Impedance in the Detection of Bacterial Growth,"** *IEEE Transactions on Biomedical Engineering*, vol. 28, no.5, pp. 403-410, 1981.

[13] Giaever I, Keese CR. **"Monitoring Fibroblast Behavior with an Applied Electric Field,"** *PNAS*, 81, pp. 3761-3764, 1984.

[14] Tiruppathi C, Malik AB, Del Vecchio PJ, Keese CR, Giaever I. **"Electrical method for detection of endothelial cell shape change in real-time: Assessment of endothelial barrier function,"** *Proc. Natl. Acad. Sci.*, 89, pp. 7919-7923, 1992.

[15] Keese CR, Giaever I. **"A biosensor that monitors cell morphology with electrical fields,"** *Engineering in Medicine and Biology Magazine*, vol. 13, no. 3, pp. 402-408, 1994.

[16] Giaever, I. and Keese, C.R., **"Use of Electric Fields to Monitor the Dynamical Aspect of Cell Behavior in Tissue Culture,"** *IEEE Trans. Biomed.Eng.*, 33, pp. 242-247, 1986.

[17] Lo CM, Keese CR, Giaever I. **"Monitoring motion of confluent cells in tissue culture."** *Exp Cell Res,.* vol. 204, no. 1, pp. 102-109, 1993.

[18] Giaever I. and Keese CR. "**Toxic? Cells Can Tell,**" *Chemtech*, pp. 116-125, Feb. 1992.

[19] Mitra P, Keese C, Giaever I. **"Electric Measurement Can Be Used to Monitor the Attachment and Spreading of Cells in Tissue Culture"** *BioTechniques,* 4, pp. 504-510, 1991.

[20] Qiu Y (2010) Impedance sensing for cellular response studies. ProQuest Dissertations and Theses. Doctoral Dissertation

[21] Seriburi P (2008) Using Electric Cell-Substrate Sensing (ECIS) to Measure Properties of an Individual Adherent Cell. ProQuest Dissertations and Theses. Doctoral Dissertation

[22] Montgomery S (2008) Impedance Measurement System for Embryonic Stem Cell and Embryoid Body Cultures. Master Dissertation.

[23] McEwan GD (2012) Raman Microspectroscopy, Atomic Force Microscopy, and Electric Cell-Substrate Impedance Sensing for Characterization of Biointerfaces: Molecular, Bacteria, and Mammalian Cells. All Graduate Theses and Dissertations. Paper 1251.

[24] Borkholder DA (1998) *Cell Based Biosensors Using Microelectrodes*. Doctoral Dissertation.

[25] Stolwijk JA, Hartmann C, Balani P, Albermann S, Keese CR, Giaever I, Wegener J. **"Impedance analysis of adherent cells after in situ electroporation: Non-invasive monitoring during intracellular manipulations,"** *Biosensors and Bioelectronics*, 26, pp. 4720-4727, 2011.

[26] Cho S, Thielecke H. **"Electrical characterization of human mesenchymal stem cell growth on microelectrode,"** *Microelectronic Engineering*, 85, pp. 1272-1274, 2008.

[27] Keese CR, Bhawe K, Wegener J, Giaever I. **"Real-Time Impedance Assay to Follow the Invasive Activities of Metastatic Cells in Culture,"** *BioTechniques*, 33, pp. 842-850, Oct. 2002.

[28] Wegener J, Keese CR, Giaever I. "**Electroporation of adherent cells on a conductive substrate and electrical in situ monitoring of the cell response.**" *Biotechniques*, 33, pp. 348-357, 2000.

[29] Zudaire E, Cuesta N, Murty V, Woodson K, Gonzalez N, Martinez A, Narayan G, Kirsch I, Hirsch F, Birrer M, Cuttitta F. "**The aryl hydrocarbon receptor repressor is a putative tumor gene in multiple human cancers.**" *J. of Clinical Investigation*, vol. 118, no.2, pp. 640-650, 2008.

[30] Xiao C, Lachance B, Sunahara G, Luong JHT. **"Assessment of Cytotoxicity Using Electric Cell-Substrate Impedance Sensing: Concentration and Time Response Function Approach,"** *Anal. Chem.*, 74, pp. 5748-5753, 2002.

[31] Curtis TM, Tabb J, Romero L, Schwager SJ, Widder MW, van der Schalie WH. **"Improved cell sensitivity and longevity in a rapid impedance-based toxicity sensor,"** *Journal of Applied Toxicology*, 2009.

[32] Chongxiu Sun, Mack H. Wu, Mingzhang Guo, Mark L. Day, Eugene S. Lee, and Sarah Y. Yuan. **"ADAM15 regulates endothelial permeability and neutrophil migration via Src/ERK1/2 signaling,"** *Cardiovasc Res.*, published 10 April 2010, 10.1093/cvr/cvq060.

[33] DePaola N, Phelps JE, Florez L, Keese CR, Giaever I, Minnear FL, and Vincent P. "**Electrical Impedance of Cultured Endothelium Under Fluid Flow,**" *Annals of Biomedical Engineering*, 29, pp. 1-9, 2001.

[34] Schwan HP. **"Mechanisms Responsible for Electrical Properties of Tissue and Cell Suspension,"** *Med. Prog. Technol.*, 19, pp. 163-165, 1993.

[35] Hauttmann S., Müller J. **"In-situ biomass characterization by impedance spectroscopy using a full-bridge circuit,"** *Bioprocess and Biosystems Engineering*, 24, pp. 137-141, 2001.

[36] Xiao C, Lachance B, Sunahara G, Luong JHT. **"An In-Depth Analysis of Electric Cell-Substrate Impedance Sensing to Study the Attachment and Spreading of Mammalian Cells,"** *Anal. Chem.*, 74, pp. 1333-1339, 2002.

[37] Thielecke H, Fleckenstein J, Bartholoma P, Rübe C. **"Evaluation of Impedance Spectroscopy for the Characterization of Small Biological Samples in Tissue-based Test Systems,"** *Proceedings of the 26th Annual International Conference of the IEEE EMBS*, 2004.

[38] Radke SM, Alocilja EC. **"Design and Fabrication of a Microimpedance Biosensor for Bacterial Detection,"** *IEEE Sensors Journal*, vol. 4, no. 4, pp. 434-440, 2004.

[39] Arndt S, Seebach J, Psathaki K, Galla HJ, Wegener J. **"Bioelectrical impedance assay to monitor changes in cell shape during apoptosis,"** *Biosensors and Bioelectronics*, 19, pp. 583-594, 2004.

[40] Zheng S, Nandra MS, Shih CY, Li W, Tai YC. **"Resonance impedance sensing of human blood cells,"** *Sensors and Actuators A*, 145-146, pp. 29-36, 2008.

[41] Park HE, Kin D, Koh HS, Cho S, Sung JS, Kim JY. **"Real-Time Monitoring of Neural Differentiation of Human Mesenchymal Stem Cells by Electric Cell-Substrate Impedance Sensing,"** *Journal of Biomedicine and Biotechnology 2011*, pp. 1-8, 2011.

[42] Bagnaninchi P, Drummond N. **"Real-time label-free monitoring of adipose-derived stem cell differentiation with electric cell-substrate impedance sensing,"** *PNAS*, vol. 108, no. 16, pp. 6462-6467, 2011.

[43] Ibañez D (2008) Implementation of an Electrical Bioimpedance Monitoring System and a Tool for Bioimpedance Vector Analysis. Master Dissertation.

[44] Ansede A (2009) A Feasibility Study of the Suitability of an AD5933-based Spectrometer for EBI Applications. Master Dissertation.

[45] Aliakbar AM (2009) Handheld Impedance Based Biosensor System for Glucose Monitoring. Master Dissertation.

[46] Rösner A, Frank T, Tobehn I (2012) Bio instrument for determining the viability of cells on the basis of the impedance measurement. European Micromechanics and Microsystems Conference 2012

Chapter 2 – CELLULAR THEORY

2.1 Introduction

A good understanding of biochemistry, metabolism molecular biology and genetics is necessary to completely understand cell biology. However, the study of these fields is beyond the scope of this work and the knowledge of this Thesis. Thus, this chapter focuses on the fundamentals of cellular function as its electrical activity. This includes: cellular membrane impedance characteristics, cell adhesion and motion for both, animal cells and animal adult stem cells (ASCs). Cellular adhesion, motility, growth and differentiation greatly impact impedance measurements using extracellular electrodes. Thus, an understanding of the mechanisms responsible for these phenomena is critical for interpretation of the measured impedance and development of appropriate control experiments.

This chapter will begin with a short introduction to tissue culture and the mechanisms responsible for cellular adhesion to solid substrates, cellular motility, differentiation and growth. Cell membrane impedance basic characteristics are also addressed as they are the main focus of this work. Finally, a detailed analysis of stem cells, types and major characteristics, as well as an analysis of the research in the area is presented.

2.2 Tissue Culture

The first successful cell culture was achieved by Harrison in 1907 [13], but it was not until the 1950's when cell culture became available as a tool for scientists. Nowadays, tissue culture or cell culture is one of the major tools used in life sciences. While cultured cells systems are not identical to those found *in vivo*, they do allow study of animal cells without the complications of systemic variation due to the normal physiology of the animal or stresses induced by invasive experimental procedures. It consists in the growth of tissues in an artificial environment that can be easily manipulated and analyzed (cells *in vitro*). Such environment consists of a suitable culture vessel (glass or plastic) containing a liquid or semi-solid medium that supplies the nutrients essential for survival and growth. Regardless of the cell type and substrate, maintenance of the living culture requires precise control of temperature, pH, ion concentrations, total solution osmolality, O_2 and CO_2 which constitute the *physiochemical* environment [7]. However, the poorly defined (but well controlled) *physiological* environment (growth factors, hormones, etc.) is also critical and often requires supplementation of the media with serum or other compounds derived from living organisms which cannot be synthetically produced. Variations of any or all of these parameters can greatly influence cellular health as well as the development and proliferation of individual cells. Thus, culture of living tissue is as much an art as a science, and even when the advances in the past hundred years have been consistent there is still much to be done.

2.2.1 Cellular Adhesion

One the most important characteristics while working with adherent cell tissue cultures is adhesion. The surroundings of the extracellular membrane consists of a collection of fibrous collagen proteins, hyaluronic acid, proteoglycans and glycoproteins. Their understanding is necessary to comprehend cellular adhesion. This is collectively known as the extracellular matrix (ECM). Its composition varies depending on the cell type, tissue type, and culture conditions, but

the majority of the required components are contained within standard cell culture medium containing serum. It is this matrix that forms the connections between cells *in vivo* and allows cells to attach to surfaces *in vitro*. Since it is responsible for the attachment of cells to a substrate in culture, the extracellular matrix exerts some control over cellular shape (cells are spherical in suspension and flatten out as they attach to a surface). By changing the surface properties of the cell culture substrate (addition of proteins), binding of the ECM to the surface, and therefore cell attachment, can be controlled. Attachment factors, such as collagen, gelatin, fibronectin and laminin, can also be used as coatings to improve the adhesion of normal cells. Thus, adhesion controls the shape of adherent cells, and can directly influence cell life and death [8].

There is a great effort in biology research aimed to improve the understanding of ECM components and their effects on cellular shape and function. At this point, we need to know that the ECM creates a bridge between the cellular membrane and the substrate upon which the cells are cultured. However, an understanding of the adhesion mechanism is important for interpretation of impedance data obtained with extracellular electrodes.

As a cell comes into contact with a solid surface, there are specific sites where adhesion occurs known as focal contacts or adhesion plaques. Borkholder [12] sets an example from which the mechanism of cell adhesion can be extracted. He states that the formation of adhesion sites typically depends on two proteins found in serum containing culture media and forming part of the ECM: fibronectin and vitronectin. Those proteins bind to the culture surface and express specific sequences which are recognized by cell-surface receptors called integrins. As shown in Figure 2.1, integrins are transmembrane proteins that bind to the fibronectin, vitronectin, or some other component of the ECM. A chain of other proteins such as talin, vinculin, or α-actin connects the integrin to an actin filament, thereby effectively coupling the cytoskeleton to the cell culture substrate. These focal contact areas are generally oval patches roughly 1 μm long and separated from the substrate by 1 to 50 nm [12].

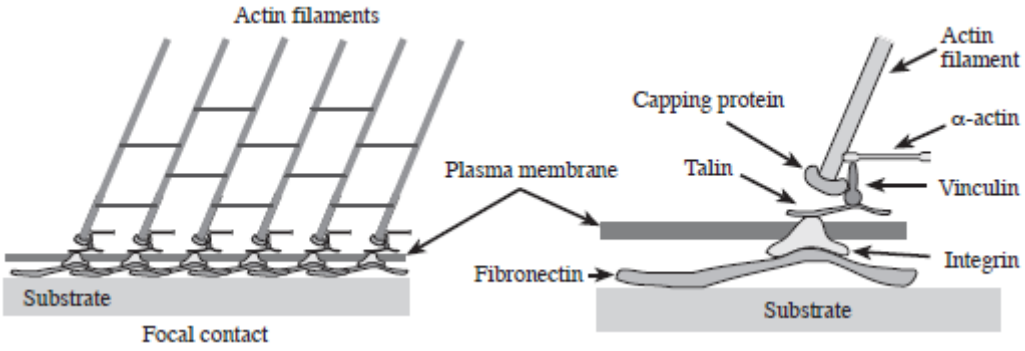

Figure 2.1. Focal contact or adhesion plaque. The actin cytoskeleton is attached to the ECM (represented by fibronectin) via a chain of proteins connected to the integral protein integrin [12].

2.2.2 Cellular Motility

Another important characteristic pertaining to this research is the ability to regulate movements, which is a fundamental property of most eukaryotic cells. According to the book Rho GTPases [4], cell motility can be described in four components which are illustrated in Figure 2.2:

1) Polarization of the cytoskeleton.
2) Extension of the leading edge of the cell.
3) Attachment of this new extension to the substrate and releasing of preexisting contacts.
4) Contraction of the rear portion of the cell using the newly formed focal contact as an anchorage.

This cycle is repeated as necessary for the cell to move in response to chemical, physical, or other environmental stimuli [9]. With a migrating cell, new focal contacts are made at the leading edge of the cell while focal contacts further back detach. Thus, the cellular membrane rolls over the top of the cell while the base remains fixed in space. Eventually, the plaques released become the trailing edge that can track the movement of the cell. While the details of cellular movement are certainly cell specific, this simplistic model is useful for the purpose of this research. With this understanding of the underlying mechanisms of cellular motility, it is possible to design experiments that take this motion into account and perhaps eliminate the motion effects completely.

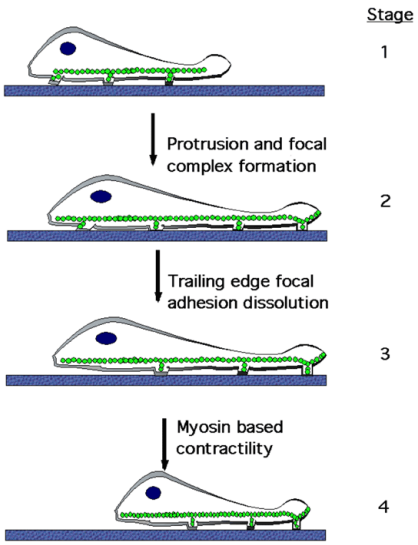

Figure 2.2. Generalized model for cellular motility [4]

2.2.3 Cellular Growth and Differentiation

Growth and differentiation are additional key characteristics which are relevant to electric interrogation techniques such as bio-impedance methodologies. All eukaryote cells (organisms containing nuclei and organelles) at some point in their lives can reproduce and differentiate, but those capabilities become a liability when cells are trying to coexist in a community. This is particularly true for a community as complex as an animal's body. The human brain, for example, contains billions of neurons constructed during embryonic development. Once established, this network would be destroyed if the cells continued dividing, in other words, they become post-mitotic (lose the ability to divide) soon after an individual is born. Many other organs, such as spinal cord, heart, kidneys, and muscles, adhere to the same development pattern. The loss of cell division in an animal´s body is a trade-off that allows the cell community to produce organs of a predictable size and shape. The problem arises when a person suffers a disease or trauma such as

a heart attack. In this case the post-mitotic cells, myocytes, are unable to repair the damage. Nevertheless, some of our tissues and organs, such as skin, liver, and bone marrow, retain the power of division throughout the life span of the individual. In the case of blood cells, which are replaced on daily basis, stem cells located in the bone marrow, divide and differentiate into both red and white blood cells, thus replacing them as they wear out. As mentioned before, in cell culture, cells will grow if the environment in which they exist meets the necessities of the cells; In this case, those cultures have loose the post-mitotic characteristic and they can keep growing while the environment is positive for their development. Referring to differentiation, it can be met *in vitro* but the correct differentiation media must be used as the cells in culture are not in direct contact with the tissues it may differentiate to. As expected, the rates of replication and differentiation pathways the tissue culture follows depend upon the richness of the media, the growth and differentiation factors and the space where the cells are being cultured. However, cell tissue culture characteristics and development also depend of the space where they are being cultured as well as depending on the substrate as it has been mentioned before.

2.2.3.1 Growth Factors

Growth factors are proteins that bind to cell-surface receptors, each of which activates a signaling pathway, leading to the phosphorylation (on and off) of many cytoplasmic proteins. Protein growth factors bind to their receptors as dimers. Each growth factor binds its own specific receptor, which activates a unique set of signaling molecules. This is the reason that some growth factors stimulate cell division, but not necessarily differentiation, while others stimulate differentiation as well as proliferation. Current hot research topics in biology include: identification of signaling molecules, signal pathways for cancer, and aging cell mechanisms. As an example, nowadays some cells simply will not grow well unless fetal bovine serum (FBS) is added to the culture media; and even then the exact composition of the FBS is still a mystery for science. There are many growth factors yet to be discovered, and the stimulation of stem cells to grow and differentiate will become a much more precise science when growth factor signaling pathways are understood in greater detail.

2.3 Cellular Membrane

Every cell consists of a lipid bilayer membrane surrounding an intracellular fluid containing numerous organelles (mitochondrion, nucleus, endoplasmic reticulum, lysosomes, etc.) The Figure 2.3 illustrates with some detail the cell membrane and its associated components. The membrane stands as the most important part of the cells for bioimpedance measurements due to its polarization properties when electric fields are applied. Overton discovered the cellular membrane in 1899 and Höber in 1910 gave electrical evidence of the presence of a thin, poorly conducting layer containing an electrolytic cytoplasm. Nowadays, the cellular membrane stands as the base in every impedance measurement, its interactions with the ECM can be detected and its composition can be described in detail.

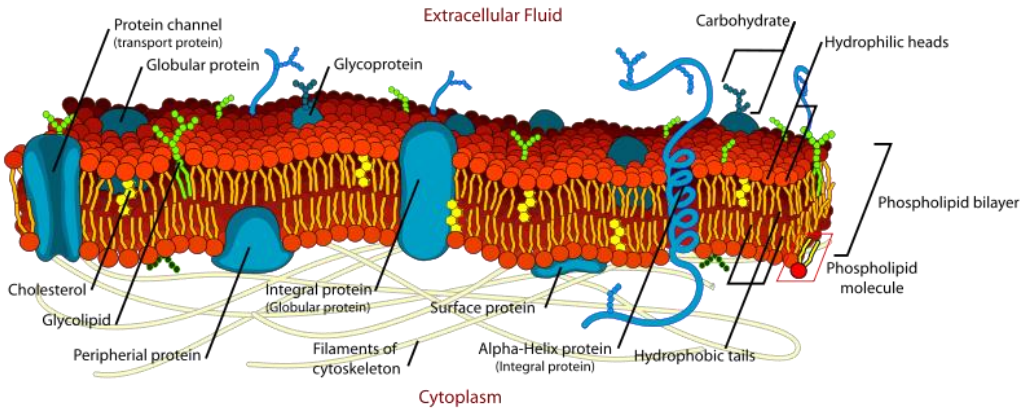

Figure 2.3. Schematic of cell membrane (lipid bilayer) [14]

2.3.1 Membrane Impedance

Impedance techniques have become a reliable tool used through the years to study organs in the body, explanted neural tissues, whole blood and erythrocytes, cultures cell suspension, bacterial growth, and anchorage dependent cell cultures. There is a great deal of relevant information regarding the characteristics of biological material, and impedance measurements have provided information about proliferation, motility, and cellular adhesion for both electrically active and nonelectrically active cell types. In many cases, the capacitance of the cell membrane, cell/substrate separation, and cell/cell can all be monitored and determined. While all of these measurements provide biologically relevant information, there is still a need to examine the membrane properties of cultured cells. In particular, the effects of different compounds on the ionic channels of populations of cell cultured in vitro should be considered.

Biological material presents frequency dependent dielectric properties that provide important insights about the expected behavior. Figure 2.4 shows the adhesion process that cells follows once they reach the substrate. The cells reach the substrate with an almost spherical morphology; then the area of closest contact between basal membrane and surface rather initially small, increases continuously while the cell spreads [9]. Since the cell membrane is essentially insulating and restricts current flow, current leaving the electrode in the adhesion area has to flow in the narrow clefts underneath the cells before it can escape in the bulk electrolyte at the cell perimeter. Current flow within the adhesion area is furthermore dependent on the applied frequency.

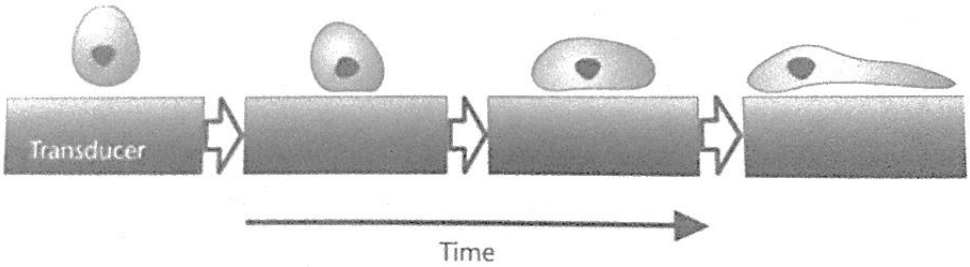

Figure 2.4. Time course of cell spreading on a culture substrate and the concomitant increase in the adhesion area's projection on the substrate [22]

The impedance characteristics of the cell lipid bilayer can be described as a component of a mostly capacitive and a slightly resistive component due to the channels that control the transmembrane transport of specific ions. The most interesting property of this membrane is that the membrane composition (equivalent resistance and capacitance) may change during differentiation, motility, apoptosis and adhesion. This change can be sensed to determine cell morphological characteristics and state through electrical interrogation [16-18].

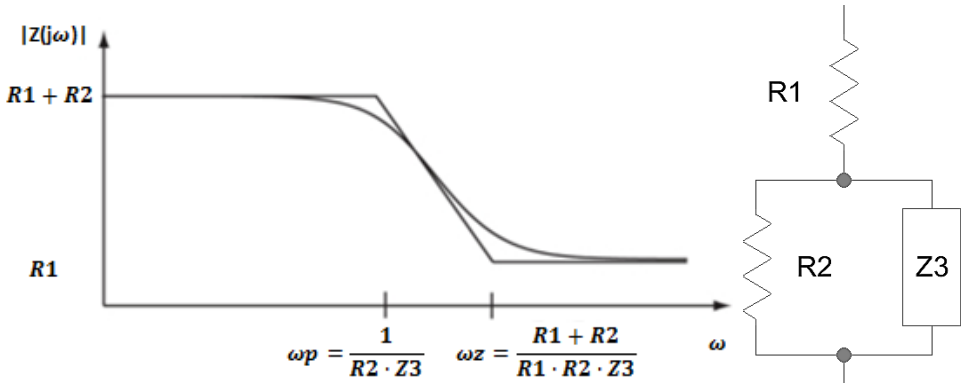

Figure 2.5. (a) Specific impedance of guinea pig liver as a function of the alternating current measuring frequency (ω). (b) Equivalent circuit proposed for several tissues. Cm=Z3 and Rm=R2 are attributed to the cell membrane capacity and resistance and Ri=R1 to the cytoplasm resistance [15]

Historically, this technique has been used since 1922, when Philippson performed and modeled the first measurement of impedance (|Z|=V'/I') in a culture over a range of frequencies [15]. The impedance curve is similar to the one presented in Figure 2.5.a. The data was interpreted by Philippson in terms of the circuit of Figure 2.5.b, in which R_i represented the resistance of the cell cytoplasm and R_m, C_m represent the resistance and capacity, respectively, of the membrane, neglecting any current flow around and between the cells. The concept of impedance as a vector on the R, X plane and techniques for analysis were well established and used by Philippson. However, the complex impedance Z=R+ jX with the imaginary operator $j = (-1)^{1/2}$ was soon found more convenient and came into common usage. The application of this particular use of impedance for electrical interrogation will be discussed later.

2.4 Stem Cells

Back in the 1960s Drs. Ernest McCulloch and James Till, then professors at the University of Toronto and the Ontario Cancer Institute, reported for the first time the discovery of stem cells. Nowadays stem cells are in the hype, being labeled as the "new medicine" by some or a "fools dream" by others; either in a positive or negative way stem cells research is a topic of modern world. However, the present interest and controversy around stem cell research did not truly begin until the 1990s with two major breakthroughs:

1. The successful cloning of "Dolly" by Ian Wilmut, Keith Campbell and coworkers in 1997 [1]
2. The establishment of human embryonic stem cell (ECS) lines by the laboratory of James Thomson in 1998 [2]

Since those first steps, and without any doubt, this new technology has found its way in the human mind. It has given a new perspective to tissue engineering and organ transplants. At no

other time in the history in biomedical research discoveries have had such repercussion on a global scale. Stem cells have demonstrated their potential to develop into all kinds of specialized cells and tissues in the body. For this reason the possibility to rejuvenate or replace defective organs and the tissues in human body now sounds like a plausible idea and not just a dream. However, this new technologies are not just about finding cures for diseases, they are also helping scientists to understand a wide range of biological processes under new perspective.

2.4.1 Definition

Stem cells are a special kind of cells that have the ability to divide for an indefinite period and can give rise to a wide variety of specialized cell types. This ability is known as plasticity and is a common trait of fertilized eggs and early embryonic cells. Fertilized egg, being able to give rise to all of the body's cells, has the highest degree of plasticity and, thus, is said to be totipotent. As time passes, a five-day-old human embryo (blastomeres) can only give rise to a limited range of cells types and, accordingly, are said to be pluripotent. As development progresses, individual cells become multipotent (able to give rise to only a few cell types) before assuming their final form as a specialized cell that can only give rise to other cells of its kind (unipotency). Plasticity also varies depending on whether the stem cells originate from an embryo or from an adult organism. In summary, stem cells from embryos are pluripotent, whereas stem cells from adults are multipotent.

All stem cells, regardless of their source, have three general properties [5]:

1. They are capable of dividing and renewing themselves for long periods of time.
2. They are unspecialized.
3. They can give rise to specialized cell types.

The stem cell types that exist are displayed in Table 2.1.

Table 2.1. Stem cells and abbreviations [6]

CELL	ABBREVIATION
adult stem cell	ASC
bone marrow stem cell	BMS cell
cardiac stem cell	CSC
embryonic stem cell	ESC
Embryonic germ cell	EGC
Endothelial progenitor cell	EPC
Induced pluripotent stem cell	iPSC
Umbilical cord stem cell	UCS cell

Hematopoietic stem cell	HSC
Human embryonic stem cell	hESC
Mesenchymal stem cell	MSC

When placed in culture, stem cells grow and divide indefinitely and scientists are still learning how to coax then into producing cells types that may be used to cure many diseases. Stem cells may be isolated from embryos, umbilical cords, and adult tissues. When isolated from embryos or umbilical cords, they are equivalent to pluripotent blastomeres; while the isolated from adult tissues are usually multipotent, but pluripotent forms have been identified. Most recently, stem cells have been produced by reprogramming skin cells, an advance that is expected to revolutionize the field of disease treatment [3]. Stem cells therapies may be able to treat cardiovascular diseases, spinal cord disorders, Parkinson´s disease, Alzheimer´s disease, and some cancers. Leukemia, a cancer affecting white blood cells (WBCs), is already being treated by replacing the cancerous cells with stem cells programmed to differentiate into healthy WBCs. Diseases that affect the brain, spinal cord, or heart are ideal candidates for stem cell therapy because these organs have lost the talent that stem cells retain; in particular the ability to proliferate (grow and reproduce) and differentiate.

At the present time, stem cell research is focused on embryonic stem cells (ESCs), adult stem cells (ASCs), therapeutic cloning, and induced pluripotent stem (iPS) cells. This thesis will just focus in the widely used ASCs.

2.4.1.1 Embryonic Stem Cells

Considered the ultimate stem cell, the fertilized egg is a totipotent cell that can give rise to an entire organism consisting of hundreds of different kinds of cells. Human, mouse, and amphibian blastomeres retain the totipotency and are good examples of embryonic stem cells in their first stages (two- or four-cell embryos). In the case of mammalian stem cells, these are obtained exclusively from the inner cell mass (ICM) of a blastocyst, and when placed in cell culture they can differentiate into many kinds of cells. However, once the association between the ICM and the trophoblast is disrupted (when placed in culture), the ESCs lose the capacity to develop into an embryo. For this reason, they are said to be pluripotent rather than totipotent.

An important fact of the ESCs is that the ones that are now being isolated and cultured are good only for basic research and not for the treatment of human diseases. This is because the ES cells, being allogeneic, will be destroyed by GVHD (Graft-Versus-Host-Disease), the same way the immune system rejects foreign hearts, livers, or kidneys. Even when further investigation must be done in this area, the future application of these cells in the treatment of human diseases looks grim as the lack of consistent results plus the ethical impact of their use put its development in a deadlock.

2.4.1.2 Adult Stem Cells

Adult stem cells (ASCs) are collected from adult tissues or organs. The term also applies to stem cells collected from children, infants, and even umbilical cord blood. ASCs are still a novel topic, not long ago, scientists believed all repairs in the adult body were carried out by the affected tissue (if the skin is cut, other skin cells divide and migrate to seal the wound) and not by ASCs present in the tissues. In fact, other organs such as the brain and heart that were thought to be incapable of self-repair since the myocytes and neurons were known to be post-mitotic are repaired by the action of these stem cells. The picture, as expected, has become more complex and, from a clinical point of view, much more interesting now that ASCs have been identified.

The first ASCs to be characterized were found in the bone marrow and are called hematopoietic stem cells (HSCs). They are majorly known to be responsible for replenishing blood cells. Now, science knows that the bone marrow contains other types of stem cells, such as endothelial progenitor cells (EPCs) and Mesenchymal stem cells (MSCs). The former ones have the potential to differentiate into endothelial cells (cells that line blood vessels and the digestive tract) and the later ones can form many types of cells, including bone, fat, and cardiomyocytes. Since this discovery, many scientists believe that most repairs in adult tissues are carried out by stem cells and that organs such as the brain and heart, with the help of specialized stem cells, may have some ability to heal themselves [19-21].

An important example is the blood isolated from human umbilical cords to extract adult stem cells. In fact, umbilical cord stem cells (UCS) appear to have a developmental plasticity equal to that of ESCs (pluripotency). The collected blood from umbilical cords (UCs) from millions of infants could become an extremely valuable tissue bank that could be used to treat many diseases without causing immune rejection and without raising the ethical problems associated with ESCs. Currently, there are more than 250,000 units of umbilical cord blood banked for public use, and more than 8,000 UCS cells transplants have been performed.

Table 2.2. Adult tissues and organs known to have stem cells [6]

SOURCE	DESCRIPTION
Bone marrow	These occur as hematopoietic stem cells, which give rise to red and white blood cells. The bone marrow also contains Mesenchymal stem cells, which differentiate into cartilage and bone, and endothelial progenitor cells, which differentiate into blood vessels and cardiomyocytes.
Brain	Stem cells of the brain can differentiate into the three kinds of nervous tissue-astrocytes, oligodendrocytes, and neurons-and, in some cases, blood-cell precursors.
Digestive system	Located in intestinal crypts, or invaginations. These stem cells are responsible for renewing the epithelial lining of the gut.
Heart	Stem cells have been isolated from the heart, where they reside in small

	clusters. The extent to which these cells repair the heart is unknown.
Pancreas	Many types are believed to exist, but examples have yet to be isolated. Some neural stem cells are known to generate pancreatic β cells.
Skeletal muscle	These stem cells may be isolated from muscle or bone marrow. They mediate muscle growth and may proliferate in response to injury or exercise.
Skin	Stem cells of the skin are associated with the epithelial cells, epidermal cells, hair follicle cells, and the basal layer of the epidermis. These stem cells are involved in repair and replacement of all types of skin cells.

Nevertheless, identifying ASCs is not always easy. ASCs account for only 1/100000 of the total cell population (bone marrow), so odds of finding one, at the best of times, are small indeed. Adding to the problematic, stem cells have a simple morphology, and even when that might seem that it could set them apart from other cells in the body, there are many differentiated cells that have similar size and shape. Indeed, no one knows the ultimate source of these cells. Some scientists have suggested that they are embryonic cells, set aside during development of each tissue, while others believe they may have been part of a migrating population of embryonic cell that took up residence in various parts of the body during the processes or neurulation and organogenesis. A third possibility is that stem cells were produced after embryonic development was completed by the dedifferentiation of a select group of cells within the various tissues of the body. Until now it is not clear why these cells are able to repair some tissue but not others. Consequently, it is almost impossible to separate stem cells from differentiated cells by simple visual inspection, and even through a series of specialized laboratory proceedings results a complex enterprise [6].

However, the existence of ASCs is extremely important for future treatment of human diseases, since they resolve the ethical problems and the problem of tissue rejection that are associated with the use of ESCs. The limited plasticity of ASCs is a major hurdle to overcome before they will be a practical alternative to the ESCs plasticity. However and even when lacking plasticity, ASCs have shown to have the important characteristic that after being injected into mice, they appear to *"know"* where home (tissue from where they were isolated) is and consequently where they migrate. Due to this special characteristic and that many researchers believe that the limits of plasticity can be overcome, the future of ASCs shines brightly.

2.4.1.3 Stem Cell Differentiation

Once the stem cells are collected, they can be grown in culture and stimulated in various ways to determine the types of cells they may produce. This process is called directed differentiation. All stem cells have the ability to proliferate in culture and can differentiate into many different kind of cells. However, there is a problem with adult bone marrow stem cells, as they tend to differentiate spontaneously when placed in culture. In the process of proliferation, the stem cells are difficult to

maintain over a continuous culture due to the fact that there is no way to stop its differentiation. So far, only mouse embryonic stem cells are able to proliferate *in vitro* for an indefinite period of time while retaining an embryonic phenotype.

So far, adult and embryonic stem cells have been stimulated to produce several cell types, either through exposure to various growth factors or by being incubate in mice to produce teratomas. Selecting growth factor for these experiments is an example of educated guesswork. If the intention of the experiments is to produce neurons or epithelial cells, the investigators will select growth factors such as epidermal growth factor (EGF) and nerve growth factor (NGF), both of which are known to influence the proliferation of these cells in vivo. Other growth factors, such as transforming growth factor (TGF) or the hormone insulin, are known to influence tissue such as muscle and cartilage. In some cases, the growth factors producing a certain kind of cell are unknown; this occurs when stem cells differentiate in vivo or when they are cultured in the presence of FBS, which contains many yet-to-be identified growth factors.

Table 2.3. Directed differentiation of human adult stem cells [6]

SOURCE	CONDITIONS	RESULTING CELL TYPES
bone marrow	teratoma	hepatocyte, myocyte, adipocyte, chondrocyte, red blood cell, white blood cell, cardiomyocyte
bone marrow	EGF, NGF, FRN	Neuron
Brain	teratoma, FCS	myocyte, astrocyte, neuron, oligodendrocyte
Liver	teratoma	red blood cell, white blood cell

**Note: EGF (epithelial growth factor), NGF (neurotrophic growth factor), FRN (fetal rat neuron), FCS (fetal calf serum)*

A simple example of cell differentiation can be addressed making reference to the plasticity mentioned before. ASCs have less plasticity than ESCs, so when stem cells from an adult mouse brain are placed in culture, they differentiate into neural tissue but not the variety of cell types that are produced by ESCs. Likewise, ASCs from the bone marrow differentiate *in vitro*, into blood cells, neurons, and fat cells but not glandular tissue. Moreover, and in part due the spontaneous differentiation of adult stem cells, scientists have less control over the differentiation process of ASCs than that of ESCs. In treatment, that is not a possible guess that can be taken, bone marrow ASCs are still not used to treat diseases as the responsiveness is extremely important when treat a patient. For example, to repair a damaged heart, cultured ESCs, kept in stock for years, would be stimulated to differentiate into myocytes, after which they would be injected into the circulatory system of the patient which would be impossible with the ASCs due their spontaneous differentiation. However it is important to mention that it is necessary to ensure the cells are only

partially differentiated (myocyte precursors); otherwise they would be unable to repair the heart as they will form teratomas as they do when injected in mice. If injected myocyte precursors, as suggested earlier in this chapter, the cells will home into the parent organ, the heart, to initiate repairs. For the present, even when is possible to differentiate stem cells in a huge variety of specialized cells, scientists simply do not know what a precursor cell will do when it reaches the home organ and, perhaps more important, in the case of heart treatment with myocytes no one knows how the heart will respond and research in that area has not shown encouraging results [6].

Even when directed differentiation of cultured human stem cells is an important research topic that has led to the production of many cell types, in most cases scientists do not fully understand the details of the process. Manipulating the culture conditions, by adding a growth factor or a molecule that influences gene expression, may cause the stem cells to differentiate into nervous tissue or bone, but the intermediate steps that lead to the transformation are still obscure. Consequently, directed differentiation requires a good deal of guesswork. Various compounds known to influence gene expression can be added to the culture media to see if they will stimulate differentiation and, if they do, which kind of cell is produced. In this way, scientists are in the process of constructing a catalogue of culture additives that will lead to the production of specific cell types from cultured ES and AS cells. The study of directed differentiation may also help scientists understand the molecular nature of plasticity and the factors that distinguish ES and AS cells. This new information could open the way to effective therapies bases solely on the use of ASCs.

Table 2.4. Cells produced by stem cell differentiation [6]

CELL	DESCRIPTION
Adipocyte	Cells that make and store fat compounds
Astrocyte	A type of glia (glue) cell that provides structural and metabolic support to the neurons
Cardiomyocyte	Cells that form the heart, also called myocytes
Chondrocyte	Cells that make cartilage
Dendritic cell	Antigen-presenting cell of the immune system
Endothelial cell	Cells that form the inner lining (endothelium) of all blood vessels
Hematopoietic cell	Cells that differentiate into red and white blood cells
Keratinocyte	Cells that form hair and nails
Mast cell	Associated with connective tissue and blood vessels
Neurons	Cells that form the brain, spinal cord, and peripheral nervous system

Oligodendrocyte	Myelin-forming glia cells of the central nervous system
Osteoblast	Give rise to osteocytes, or bone-forming cells
Pancreatic islet cells	Endocrine cells that synthesize insulin
Smooth muscle	Muscle that lines blood vessels and the digestive tract

2.4.2 Stem Cell Research

Through the 1990s, when scientists were studying stem cells from rodents, standard protocols were developed for culturing, testing and manipulating cells. Other stem cells, from different species or from adult tissues, are now studied by using those protocols so that one type of stem cell can be easily compared with another. Booth in vivo and in vitro behavior is covered by these protocols. One of the most important *in vivo* characteristic is the cell's ability to proliferate (grow and divide) for an indefinite period of time, while maintaining their phenotype. Phenotype, used in this case, refers to all observable characteristics of the cell (physical morphology); its behavior (interaction with other cells); and the composition of the glycocalyx (cell membrane). Proteins in the membrane are different from those of a fully differentiated adult cell, so glycocalyx varies depending on the differentiation state of the cell.

Studying embryonic stem cells is a difficult and demanding enterprise, not only because of the science, but because of the greater social issues associated with any experiment in which a human being, no matter at what stage of development, is the guinea pig. Ethical issues in research of this kind set the pace and the scope of the experiments that are allowable. While many people are willing to accept the isolation of stem cells from human blastocysts that are only a few days old most oppose to the use of highly developed human fetuses as a source for these cells, particularly if they can be obtained in some other way. Until recently, there was no way to remove cells from the ICM of a human blastocyst without killing the embryo. But in January 2008, researchers at Advanced Cell Technology (ACT) in Worcester, Massachusetts, reported some success with harvesting once or two blastomeres without killing the embryo [6]. The problem is that while the procedure itself does not kill the embryo, it will die nonetheless as is highly improbable that parents in in-vitro fertilization clinics will choose embryos that have been tampered. The use of human fetuses for stem cell research is carefully regulated by the American Public Health Service Act, and scientists must obtain special permission to conduct these experiments, including informed consent from the parents.

In recent years, the limited versatility of AS cells has been challenged by Dr. Catherine Verfaillie in a series of studies she conducted at the University of Minnesota and more recently at the Catholic University of Leuven in Belgium, where she serves as the director of the Stem Cell Institute. In 2002, Verfaillie provided convincing evidence, contrary to the common view, that mouse AS cells isolated from bone marrow can be stimulated in vitro to differentiate into a wide variety of cell types, representing mesoderm, neuroectoderm, and endoderm, the three fundamental germ layers. Consequently, Verfaillie calls her ASCs multipotent adult progenitor

cells, or MAPCs. In 2005, Verfaillie and her group confirmed and extended their original observations and presented detailed protocols for the growth, stimulation, and maintenance of ES and AS cells. In 2007, the team described a method for reconstituting healthy bone marrow in vivo from isolated MAPCs. And finally, in 2008, Verfaillie's team showed that MAPCs could restore vascular and skeletal muscle growth in mice suffering from limb ischemia due to peripheral vascular disease (i. e., muscle degeneration due to poor blood circulation). Most important, they found that the limbs could also be repaired with human MAPCs [6].

It has been also discovered that although allogeneic (i. e., not from the patient being treated), are less inclined to stimulate graft-versus-host disease (GVHD) when compared to allogeneic ESCs. This disease is caused by the immune system, which is programmed to reject foreign cells, tissue, and organs. The cost of this procedure is not likely to exceed a standard bone marrow transplant and would take but a few weeks to administer. For the treatment of blood disorders such as leukemia, this is an ideal procedure and is now a routine medical therapy. Brains disorders can also be treated in this way, since ASCs isolated from bone marrow can be directed to differentiate into neurons and glia cells. However, marking this procedure applicable to all forms of disease requires new methods that would enhance the developmental plasticity of the AS cells. As cells can be obtained from other organs, such as the pancreas or liver, which would allow production of a wider variety of cell types, but obtaining them would require costly surgeries [11].

Most of what is known about stem cells has come from studying mice and rats. All of the protocols investigators now use to evaluate stem cells come from on those animals, and many scientists continue using rodents to gain a deeper understanding of what it is that makes a stem cell tick. But stem cells from mice cannot be used to cure human disease, repairing a severed spinal cord or curing Parkinson's disease can only be attempted with human stem cells (as shown in the ASCs investigations). Consequently, many scientists are eager to study human stem cells and are hoping they will keep on showing the same properties of plasticity and proliferation demonstrated by rodent stem cells.

The speed at which stem cell research is progressing is such that is expected that within 10 years ASCs will be used routinely to repair or replace any tissue in the body. ESC research will decline and eventually disappear entirely. This will come about, in part, through a better understanding of growth factors in order to augment the plasticity of ASCs. Initially, BMS cells, UCS cells or even MAPCs will be the starting material for the therapies. But eventually it will be possible to take a simple tissue scrape from inside a patient's mouth to obtain skin cells that will be reprogrammed to become a stem cell and then directed to differentiate into a different kind of cell, depending on what the patient requires (induced pluripotent cells - iPS) [10].

References

[1] Wilmut I, Schnieke AE, McWhir J, Kind AJ, Campbell KH. **"Viable offspring derived from fetal and adult mammalian cells,"** *Nature*, no. 385, pp. 810, 1997.

[2] Thomson JA, Itskovitz-Eldor J, Shapiro SS, Waknitz MA, Swiergiel JJ, Marshall VS, Jones JM. **"Embryonic stem cell lines derived from human blastocysts,"** *Science*, no. 282, pp. 1145, 1998.

[3] Cell Journal. *2012 Nobel Laureates*. Retrieved from http://www.cell.com/cellpress/nobelprize2012

[4] Symons M (Editor) *Rho GTPases. Rho GTPases and Cell Motility*. ISBN: 0-306-47992-3. Consulted on the Landes Bioscience Madame Curie Database website at

http://www.landesbioscience.com/curie/chapter/4250/

[5] Ho AD, Hoffman R, Zanjani ED (Editors) *Stem Cell Transplantation.* Wiley-VCH. First Edition, Germany, 2006.

[6] Panno J. *Stem Cell Research – Medical Applications & Ethical Controversies*. Revised Edition, USA, 2010.

[7] *General Guide for Identifying and Correcting Common Cell Culture Growth and Attachment Problems*, Corning Life Sciences Technical Bulletin. Consulted on the Corning Life Sciences web site at www.corning.com/lifesciences

[8] Chen CS, Mrksich M, Huang S, Whitesides GM, Ingber DE. **"Geometric control of cell life and death,"** *Science*, no. 276, pp. 1425-1428, 1997.

[9] Fuhr G. **"Examples of three-dimensional micro-structures for handling and investigation of adherently growing cells and submicron particles,"** *Analytical Methods & Instrumentations, Special Issue µTAS ´96*, 1996.

[10] Takahashi K, Yamanaka S. **"Induction of Pluripotent Stem Cells from Mouse Embryonic and Adult Fibroblast Cultures by Defined Factors,"** *Cell*, no. 126, pp. 663-676, 2006.

[11] Barker JN, Rocha V, Scaradavou A. **"Optimizing unrelated donor cord blood transplantation,"** *Journal of the American Society for Blood and Marrow Transplantation.*, vol. 15, no. 1 Suppl., pp. 154-161, 2009.

[12] Borkholder DA. *Cell Based Biosensor Using Microelectrodes*, Ph.D. dissertation, Stanford University, Palo Alto, CA, 1998.

[13] Harrison RG. **"Observations on the living developing nerve fiber,"** *Proc. Soc. Exp. Biol. Med.*, 4, pp. 140-143, 1907.

[14] Block W (2008) *A Multinutrient Approach to Alzheimer's Disease. Life Enhancement magazine*. Consulted on the Life Enhancement magazine website at http://www.life-enhancement.com/magazine/article/1967-a-multinutrient-approach-to-alzheimers-disease

[15] Cole KS (1968) *Membranes, Ions and Impulses; A Chapter of Classical Biophysics*. University of California Press, USA.

[16] Giaever I and Keese CR, **"Micromotion of Mammalian Cells Measured Electrically,"** *PNAS USA*, 88, pp. 7896-7900, 1991.

[17] Tiruppathi C, Malik AB, Del Vecchio PJ, Keese CR, Giaever I. **"Electrical method for detection of endothelial cell shape change in real time: Assessment of endotelial barrier function,"** *Proc. Natl. Acad. Sci.*, 89, pp. 7919-7923, 1992.

[18] Bagnaninchi P, Drummond N. **"Real-time label-free monitoring of adipose-derived stem cell differentiation with electric cell-substrate impedance sensing,"** *PNAS*, vol. 108, no. 16, pp. 6462-6467, 2011.

[19] Bolli R, et. al. **"Cardiac stem cells in patients with ischaemic cardiomyopathy (SCIPIO): initial results of a randomized phase 1 trial,"** *Cardiology & Vascular Medicine. The Lancet*, vol. 378, no. 9806, pp. 1847-1857, 2011.

[20] Cattaneo E (Coordinator) (2013) *Neural Stem Cells in Development and for Brain Repair Course. Neuroscience School of Advanced Studies (NSAS)*; University of Milan, Italy. Consulted on the NSAS website at http://www.nsas.it/neural-stem-cells-for-development-and-repair

[21] ReNeuron Limited (2013) *Pilot Investigation of Stem Cells in Stroke (PISCES)*. United Kingdom: Medicine and Healthcare Products Regulatory Agency. ClinicalTrial.gov Identifier: NCT01151124.

[22] Wang P, Liu Q (editors), *Cell-Based Biosensors; Principles and Applications*. Norwood, MA: Artech House. 2010.

Chapter 3 – BIOIMPEDANCE CELL CULTURE MEASUREMENTS

3.1 Introduction

Bioimpedance has been discussed for a long time, covering the electric currents and biopotentials associated with the life processes. This technique is non-invasive, simple and inexpensive considering the associated electronics involved. Bioimpedance measurements probe the electrochemical processes in the cell and tissue, providing a capability of monitoring physiological changes (cell growth, cell activity, changes in cell composition, shapes or cell locations) and deciphering the information hidden inside a cell, which may not be possible to detect using classical analytical techniques. Frequency dependent analyses, impedance measurement ranging from kilohertz to hundreds of megahertz, is mainly affected by the shape of the cells, the structure of the cell membrane, and the amount of intra and extra cellular solution. Many investigators have used this data to exploit the technology potential in areas such as electrical impedance tomography, body composition, identification of cell types, cell micromotion, organ viability, skin hydration, skin pathology, etc. [1].

The historical perspective and methodological development of impedance spectroscopic studies of tissue and cell suspensions have been reviewed elsewhere [2-3]. Impedance spectroscopic studies of cells in suspension have provided insight into the function and properties of cells [4]. However, this technique gained its practical application to cell-based screening only in the last decades, greatly promoted by the emergence of microfabrication technology. The research on cell impedance sensing can be divided into two main categories: a) adherent cells grown on planar electrodes and, b) cells transported and/or immobilized in microfluidic channels. The former category is vastly reported and researched for its comparative simplicity, while the latter one is expected to be a new trend for its precise control and measurement of single cell.

Microelectrodes have been used to study behavior of analytes, such as adherent cells, for more than three decades [5-6]. Most of the experiments were performed with electrogenic cells (cells that generate an electrical signal) such as neurons and cardiac myocytes or other adherent cells such as fibroblasts, endothelial cells, and epithelial cells. There are many publications reporting the progress using microelectrodes through the years to study both electrogenic and non electrogenic cells using amperometric detection, potentiometric detection or conductometric detection. However, this research will only focus on the use of microelectrodes as impedance based sensors using the conductometric detection.

This chapter discusses the impedimetric biosensing technique applied to biological samples. First, the principle of impedance change sensing using microelectrodes for monitoring is discussed. Second, the impedance characteristics (electrode-electrolyte and electrode-cell) are reviewed in order to understand its interactions while covered by an electrolyte and tissue culture. Finally, the chapter presents a discussion of cell-tissue culture's impedance models, as well as a short analysis of possible noise sources.

3.2 Impedance Measurement Principle

In impedimetric or conductometric biosensor, the binding between recognition and biomaterial occurs above the surface of electrodes; this change is scanned by electrode electric field which results in an impedance change. The used electrodes could be either circular with a counter electrode or interdigitated; in fact in 1997 Ehret et al. demonstrated that interdigitated electrode structures are capable of sensing impedance measurements, sometimes with less noise than circular electrodes [7]. The change of pathway of these electrical fields will cause a signal that can be interpreted as the presence of an analyte over the electrode. The electrode array and the corresponding electric fields are shown in Figure 3.1 (simple and interdigitated).

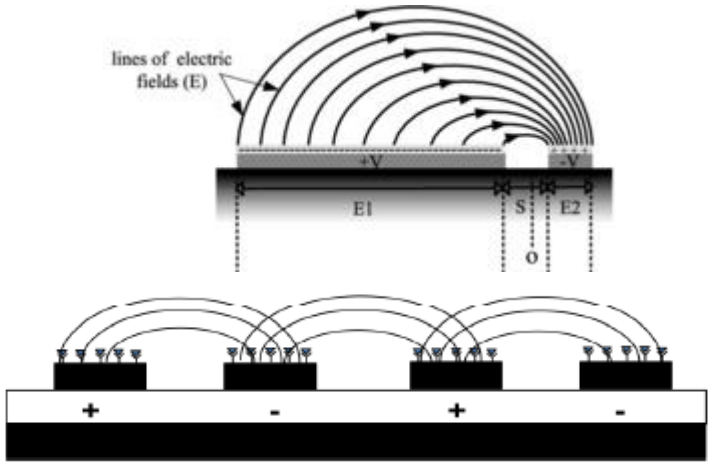

Figure 3.1. (a) Circular electrode (b) Interdigitated electrode and their respective electrical fields [8]

As can be seen in Figure 3.2, the electric field on the top of the electrode has an inverse relation to the distance from the electrode. Applying the Laplace equation $\nabla^2\varphi = 0$, the value and maximum distance of electric field penetration can be calculated. After calculation, electric field at point x and y above the electrode (Figure 3.2) could be derived from the following equation [9].

$$\Phi(x,y) = \frac{V}{2K\left(\sin\frac{\pi W_{sp}}{2L}\right)} Re\left(F\left(Asin\left(\frac{\sin\left(\pi\left(\frac{x+iy}{L}\right)\right)}{\sin\left(\frac{\pi W_{sp}}{2L}\right)}\right), \frac{\pi W_{sp}}{2L}\right)\right) \quad (3.1)$$

Where, V is the voltage between electrodes, K (k) is complete elliptical integral of with modulus k, F (α,β) is an incomplete elliptical integral which α is amplitude and β is modular angle [10]. Assuming the spacing between the electrode (W_{sp}) and their width (W_{el}) is equal and the voltage is applied differentially as (-V/2 , V/2), the equation (3.1) provides solutions that are illustrated in Figure 3.2.

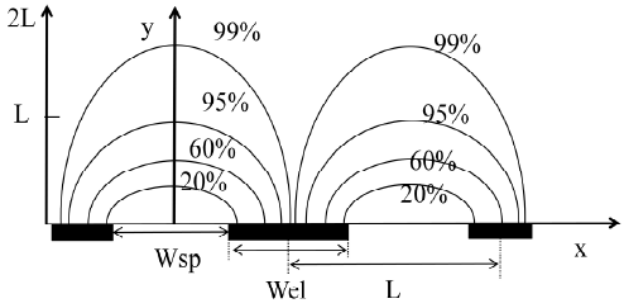

Figure 3.2. Percentage of change in current that happens at certain distances from electrodes [8]

The impedance is calculated using a ratio of voltage over current. Changes of dielectric medium above the electrode will cause the current to change between the interdigitated electrodes. Figure 3.2 illustrates that up to 99% of change in current happens within a distance of 1.6L. This means that any change in dielectric above 1.6L will have minimum effect on the current measured in such electrodes. If the space between 0.5L and 1L contribute around a 65% to current change, we can assume that electrode field penetration and sensitivity is at 0.5L above the electrodes [11].

This thesis uses interdigitated electrodes with 250µm diameter and having a distance L of 1250µm, which mean that adhered stem cells must be at least at a distance of 625µm to interact into the most sensible range.

3.3 Impedance Spectroscopy Technique

Impedance spectroscopy (conductometric detection) is a powerful method for characterizing electrical properties of material and their interfaces with electrically conducting electrodes. Generally, the impedance *Z* of a system is determined by applying an electrical voltage perturbation (stimulus signal) of small amplitude and detecting the current response passing through the measured sample. From its definition, impedance is the quotient of the voltage-time function *v(t)* and the resulting current-time function *i(t)*:

$$Z = \frac{v(t)}{i(t)} = \frac{V_m \sin(\omega t)}{I_m \sin(\omega t + \theta)} \tag{3.2}$$

$$Z(\omega) = \frac{V(j\omega)}{I(j\omega)} = Z' + jZ'' = |Z|\cos(\theta) + j|Z|\sin(\theta) \tag{3.3}$$

The impedance is a complex value, since the current does not only vary in the amplitude (as is the case for a pure ohmic resistance), but also shows a phase shift θ compared to the voltage-time function. Equation (3.2) can be transformed to complex domain as (3.3). Thus, the value can be described either by the modulus $|Z|$ and the phase shift ϕ or alternatively by the real part and the imaginary part of the impedance. Impedance can be illustrated using Bode plot using $|Z|$ and ϕ as a function of log *f*.

Many processes account for the response of impedance measurement, which is mainly the transport of electrons or charged ions through the interfaces of bulk sample and electrodes besides the diffusion processes. For this reason the impedance spectrum is often analyzed by means of an equivalent circuit. In electrochemical impedance spectroscopy, usually four elements

are used for the description of the impedance behavior: ohmic resistance, capacitance, constant phase element and Warburg impedance. Electrical properties of the investigated system are modeled from experimental data.

3.3.1 The Solid-Electrolyte Interface

When a solid is placed into an electrolyte (a solution where charge is carried by the movement of ions), an electrified interface immediately develops. This occurs for any solid (metal, semiconductor, and insulator) immersed in an electrolyte [12]. At the instant when a metal, electrode, is placed in an ionically conducting solution, the metal and the solution become electroneutral. Chemical reactions occur immediately whereby electrons are transferred between the metal and the electrolyte ($A^+ + e^- \rightarrow A$). This results in the formation of an electric field between the electrode and the electrolyte that influences further chemical reactions (thus making them electrochemical). This induced electrical field inhibits the reduction reaction ($A^+ + e^- \rightarrow A$) while accelerating the oxidation reaction ($A \rightarrow A^+ + e^-$). These two competing reactions eventually reach an equilibrium condition whereby the currents due to electron transfer to and from the metal are equal. This equilibrium exchange where current density flows across the interface in both directions, results in a zero net current.

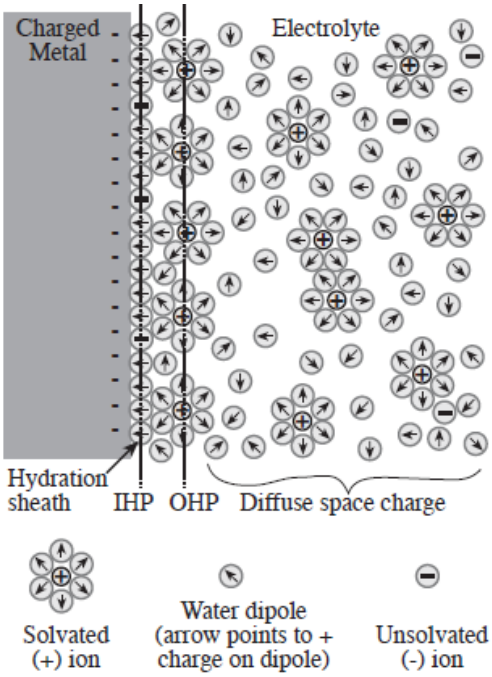

Figure 3.3. Adaptation of solid electrolyte interface of Borholder [13]

The electric field generated by these electron transfer reactions also has an impact in the electrolyte. Figure 3.3 shows how water dipoles orient themselves in the field over a layer at the metal surface forming what is known as the hydration sheath. Just beyond the water dipoles are solvated ions (the result of the electron transfer with the metal) that form a layer, the locus of which is known as the outer Helmholtz plane (OHP). There is also specific adsorption of ions (cations or anions) at the electrode surface interspersed with the orientated water dipoles. The contact adsorption of these ions tends to be very chemically dependent and partly oblivious to the

charge on the metal. Anions can be adsorbed to the surface of a negatively charged metal. The locus of centers of these ions is known as the inner Helmholtz plane (IHP) (although in some texts it is the locus of the orientated water dipoles that is termed the IHP) and can affect the overall charge density profile of the interface. The net result of these reaction, adsorptions, and orientations is the creation of the electrical double layer (or simply double layer). This is an electrified interface describing the interphase region at the boundary of an electrolyte. Figure 3.3 shows the arbitrary case of positive ions at the OHP where electrons at the metal surface have been assumed. The choice of an unsolvated negative ion for specific adsorption was also arbitrary and independent of the other charges in the system. The space charge region shown has a graded profile with the strongest field at the interface, diminishing to zero in the bulk electrolyte as will be discussed in more detail below.

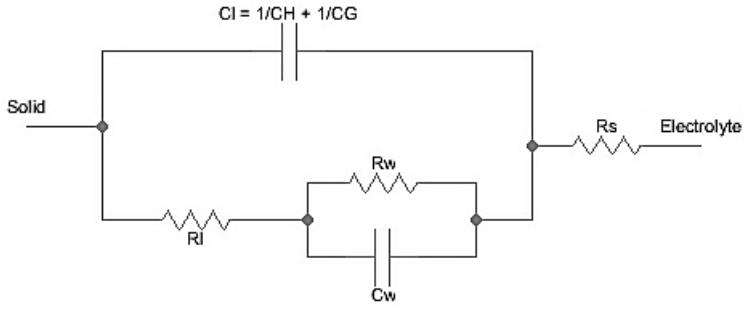

Figure 3.4. Equivalent circuit of interface between electrolyte and solid including the interfacial capacitor (Cl), charge transfer resistance (Rl), diffusion-related Warburg elements (Rw and Cw), and the solution (spreading) resistance (Rs)

Figure 3.4 illustrates a circuit impedance model described so far. This works well for simple electrode systems in pure electrolytes (those without proteins). Where proteins are present, empirical methods for determination are required to determine electrode parameter models. The parameters related to the electrode area must also be adjusted if the geometrical area of the electrode does not match the physical area.

3.3.2 Interfacial Capacitance: Helmholtz, Gouy-Chapman, and Stern

As mentioned above, when a metal and electrolyte are in contact, a space charge region is formed in the electrolyte at the interface. However, the exact structure of this region is difficult to determine. The Stern, a ramification of the Helmholtz and Gouy-Chapman models, is used to determine this structure.

In 1879, Helmholtz [14] assumed that charge of solvated ions was confined to a rigid sheet at the OHP, and was equal and opposite to that in the metal. With the water dipole layer acting as a dielectric, the model predicted that the interface would behave like a simple capacitor:

$$C_H = \frac{\varepsilon_0 \varepsilon_r}{d_{OHP}} \tag{3.4}$$

Where C_H is the capacitance per unit area (F/m^2), ε_0 is the permittivity of free space (8.85419 x 10^{-12} F/m), ε_r is the relative permittivity of the electrolyte, and d_{OHP} is the distance of the OHP from the metal electrode.

However, the simple model of Helmholtz neglected the dependence of capacity on potential that had been observed experimentally. Since the OHP was determined by how close the solvated ions could get to the electrode, there was no accommodation for movement of those ions. From 1910 to 1913, Gouy and Chapman modified the simple Helmholtz model (a rigid sheet of solvated ions) by considering mobile solvated ions at the electrode surface [15-16].

$$C_G = \frac{\varepsilon_0 \varepsilon_r}{L_D} \cosh\left(\frac{zV_0}{2V_t}\right) \tag{3.5}$$

Where the first term ($\varepsilon_0\varepsilon_r/L_D$) is simply the capacitance per unit area of two plates separated by a distance L_D and effects of mobile charges are compensated for by the hyperbolic cosine. L_D is the Debye length. The Debye length characterizes the spatial decay of potential and can be viewed as the characteristic thickness of the diffuse layer. V_0 is the potential at the electrode (x=0), and V_t is the thermal voltage (kT/q).

While Gouy-Chapman model was an improvement over that of Helmholtz, it generally overestimates the interfacial capacitance. The capacity varies more strongly with applied potential than is observed experimentally and it is too dependent on ionic concentration. Stern rectified this inconsistency by combining both models. He combined a layer bound ions at the OHP with a diffuse ion cloud beyond it [17]. The total interfacial capacitance was the series combination of both capacitances:

$$\frac{1}{C_I} = \frac{1}{C_H} + \frac{1}{C_G} \tag{3.6}$$

Where C_I is the total interfacial capacitance, C_H is the Helmholtz capacitance, and C_G is the Gouy-Chapman capacitance due to the diffuse ion cloud.

3.3.3 The Charge Transfer Resistance

The capacitance that develops at the electrode/electrolyte interface and how it changes with the concentration of the electrolyte and the applied potential has been discussed above, but this does not describe the entire electrical behavior. If a DC potential is applied across the interface, a current may flow under certain conditions. Thus, a resistive path in parallel to the capacitive is considered in the electrical model of this interface.

Wang and Liu [18] established that the theoretical value for the charge transfer resistance that appears in parallel with the interfacial capacitance under low field conditions (nonrectifying system) is:

$$R_t = \frac{V_t}{J_0 z} \tag{3.7}$$

In $\Omega \cdot cm^2$. V_t is the thermal voltage (kT/q); J_0 is the exchange current density (A/cm^2); and z is the valence of the ion involved in the charge transfer reaction. Here, the resulting current *(J)* can be calculated directly from Ohm's law:

$$J = \frac{\eta_t}{R_t} = \frac{J_0 z \eta_t}{V_t} \tag{3.8}$$

Where η_t is the overpotential due to charge transfer through the double layer.

For instances where higher currents are required (as in stimulation of neural tissue), it is no longer possible to define a pure resistance term. However, by assuming that one exponential term of (3.8) tends toward zero while the other increases in magnitude, the total current may be estimated by, where no rectifying system is assumed:

$$J = J_0 \exp\left(\frac{z\eta_t}{2V_t}\right) \tag{3.9}$$

3.3.4 Diffusion and Warburg Impedance

When the current density, either *AC* or *DC*, is very large (a couple of mA/cm^2) reactants are not able to diffuse from the bulk to the interface fast enough. The charge carriers are now diffused from the bulk into the interface and this generates a diffusion overpotential (η_d). An additional impedance must be placed in series with the charge transfer resistance (R_t), since physical diffusion and charge transfer must occur as a direct process from the bulk to interface. In this case reactants diffuse to the interface where they contribute to oxidation or reduction reactions.

Warburg proposed a model for this frequency dependent diffusion related impedance:

$$|Z_w| = \frac{k}{\sqrt{f}} \tag{3.10}$$

Where *k* is a constant determined by the electrochemistry and mobility of the ions involved in the charge transfer reaction and f is the excitation frequency [19].

The Warburg impedance elements may be theoretically determined [20] by the following equations, provided that the diffusion is dominated by a single ion and the electrode is operated near equilibrium:

$$R_w = \frac{10^3 V_t}{z^2 q n^0 \sqrt{\pi f D}} \tag{3.11}$$

$$C_w = \frac{1}{2\pi R_w} \tag{3.12}$$

$$R_w = \left[\frac{1}{R_w} + j2\pi C_w\right]^{-1} \tag{3.13}$$

Where *f* is the frequency in hertz, *D* is the diffusion coefficient (*cm^2/sec*) of the ion in question, R_w is in *Ω·cm^2*, and C_w is in *C/cm^2*. Substitution of (3.12) into (3.13) reveals that the Warburg impedance has a constant magnitude of:

$$|Z_w| = \sqrt{2} R_w \tag{3.14}$$

With a constant phase of -45°.

3.3.5 Spreading Resistance

The final circuit element that must be included in the basic electrode/electrolyte model is the spreading resistance. As the name implies, this resistance models the effects of the spreading of current from the localized electrode to a distant counter electrode in the solution. It can be

calculated by integrating the series resistance of shells of solution moving outward from the electrode where the solution resistance (*R* in *Ω*) is determined from

$$R = \frac{\rho L}{A} \tag{3.15}$$

Where *ρ* is the resistivity of the electrolyte (*Ω·cm*), *L* is the length (*cm*), and *A* is the cross-sectional area (cm^2) of the solution through which the current passes. Microelectrodes of interest are the ones fabricated using planar integrated circuit techniques which produce square and circular with one side exposed to the electrolyte. For a circular electrode of radius *r* (*cm*), the spreading resistance is given by:

$$R_S = \frac{\rho}{4r} = \frac{\rho\sqrt{\pi}}{4\sqrt{A}} \tag{3.16}$$

Where *A* is the area of the circular electrode in cm^2 [21]. For a rectangular electrode of length *l* and width *w* (both in *cm*), Kovacs calculated the spreading resistance using the formula:

$$R_S = \frac{\rho ln\left(4\frac{l}{w}\right)}{\pi l} \tag{3.17}$$

From these equations it can be seen that the spreading resistance varies with the square root of the electrode area (for symmetrical shapes) rather than being directly proportional, as was the case for the circuit elements discussed so far [20].

3.3.6 Electrical Model

Figure 3.4 shows the circuit model developed so far, this works well for simple electrode systems in pure electrolytes (those without proteins, etc.). However, the capacitance and resistance due to analyte in two electrodes arrangement has to be modeled. The electrical modeling provided by Figure 3.4 corresponds to a non-faradic biosensor. The impedance between two non-faradic electrodes can be modeled with different structures [22]; and Figure 3.5 illustrates the one which is commonly used.

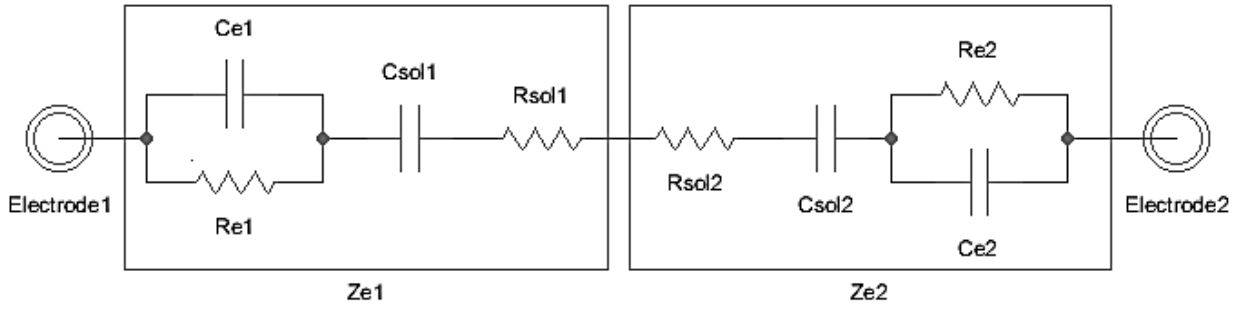

Figure3.5. Electrical model of electrodes covered by media

From Figure 3.5, C_{E1} and C_{E2} are overall capacitances of electrode 1 and electrode 2, respectively. These capacitances represent the analyte binding to both the immobilized layer and double layer capacitance on top of each electrode. Double layer capacitance produced by positioning of solution ions above the binding site. Although analyte molecules may be neutral,

they will have charge cloud distribution on their molecular structures. Once target analyte binds with immobilized layer, positive or negative ions from the solution will accumulate on top of target due to molecular charge clouds. R_{sol} and C_{sol} are solution resistance and capacitance, respectively and they are separated into two resistances and two capacitances to make calculation easier and symmetrical for both electrodes. R_{E1} and R_{E2} represent the charge transfer resistance of each electrode through the immobilized element. This is still a simplified model that can be used as the first insight in biological studies. However other detailed models [23] use additional structures to explain leaking ion currents, losses, noise and other non-ideal phenomena.

When an *AC* voltage is applied, impedance change in biosensor can be monitored before and after introducing the analyte on top of electrode. Measuring the impedance change over time is important because it provides an estimation of response time and other transient behavior issues which are very important for continuous-time monitoring applications. The principle and formulas for impedance measurements in order to provide a simple calculation of the impedance are reviewed as follows.

The electrical model of the impedance biosensor includes both capacitance and resistance. The capacitive impedance varies with frequency and can be calculated as follows:

$$Z(j\omega) = \frac{1}{j\omega C} \tag{3.18}$$

Where *C* is the capacitance value and ω is angular frequency, which is directly proportional to the frequency, *j* is the complex operator ($j = \sqrt{-1}$). The capacitance causes a lag in resulting current by $\pi/2$ when a sine wave circulates over it. The resistance magnitude does not change with the frequency; however it will change in the final value of impedance calculated as follows:

$$Z_1(j\omega) = \left(R_{sol1} + \frac{R_{E1}}{1-(\omega C_{E1}R_{E1})^2}\right) + j\left(\frac{1}{\omega C_{sol1}} - \frac{\omega C_{E1}R_{E1}^2}{1-(\omega C_{E1}R_{E1})^2}\right) \tag{3.19}$$

$$Z_2(j\omega) = \left(R_{sol2} + \frac{R_{E2}}{1-(\omega C_{E2}R_{E2})^2}\right) + j\left(\frac{1}{\omega C_{sol2}} - \frac{\omega C_{E2}R_{E2}^2}{1-(\omega C_{E2}R_{E2})^2}\right) \tag{3.20}$$

Total impedance is Z_1+Z_2. Replacing R_{sol1}+R_{sol2} with R_{sol} impedance calculated as:

$$Z(j\omega) = \left(R_{sol} + \frac{R_{E1}}{1-(\omega C_{E1}R_{E1})^2} + \frac{R_{E2}}{1-(\omega C_{E2}R_{E2})^2}\right) + j\left(\frac{\omega C_{sol}}{\omega^2 C_{sol1}C_{sol2}} - \frac{\omega C_{E1}R_{E1}^2}{1-(\omega C_{E1}R_{E1})^2} - \frac{\omega C_{E2}R_{E2}^2}{1-(\omega C_{E2}R_{E2})^2}\right) \tag{3.21}$$

The magnitude of complex number is calculated by the following formula:

$$Z(j\omega) = \sqrt{Real^2 + Imaginary^2} \tag{3.22}$$

Measured magnitude vs. frequency according to the above result is shown in Figure 3.6.

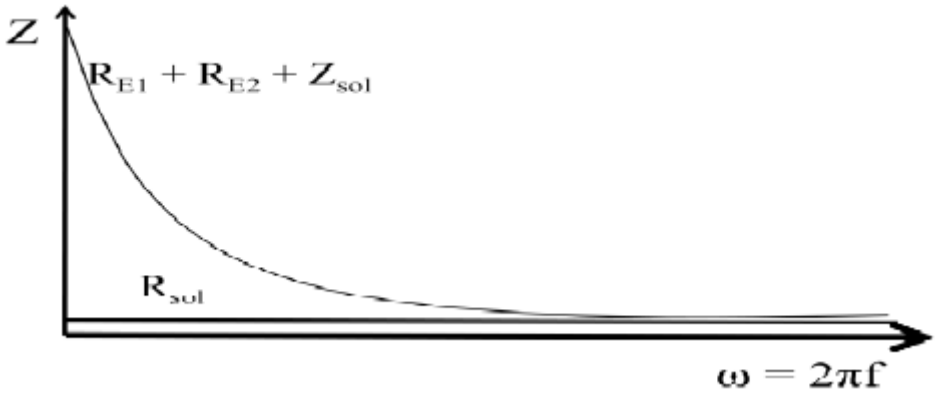

Figure 3.6. Response of impedance magnitude vs. frequency [33]

The impedance frequency response can be summarized as follows. At very high frequencies, the capacitance will act as a short circuit and the total impedance will be equal to $R_{sol}=R_{sol1}+ R_{sol2}$. However, at low frequencies, the contribution of capacitance to the impedance magnitude is noticeable and impedance is equal to $Z_{sol}+R_{E1}+R_{E2}$.

Siddiquei, et al. [8] used a simplification to this model while measuring the impedance of DF-1 cells using non planar electrodes. According to Siddiquei, when a ionic electrolyte is added to the electrode, a R_{med} and C_{med} are formed in series due the dielectric behavior of the media as mentioned before. Figure 3.7 shows the solid electrolyte interaction to represent a simplified equivalent circuit model.

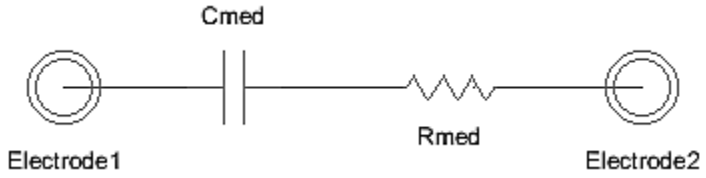

Figure 3.7. Siddiquei simplification to solid-electrolyte electrical model

However the model employed in this thesis is the reported by Yúfera [24], obtained using finite element method simulations by Huang [25] and Olmo [26]. The model in Figure 3.8 is a visual "simplification" of Figure 3.5 that considers that the sensing surface of e_1 is not filled by cells. For the two-electrode sensor the variables are: *A* as the sensing area of e_1 and *Z(w)* as the impedance by unit area of the empty electrode (without cells on top). In this model, the capacitance and media resistance are modeled as impedance per unit area dependent upon the frequency; and at high frequencies, R_S in series with R_{med} would turn dominant.

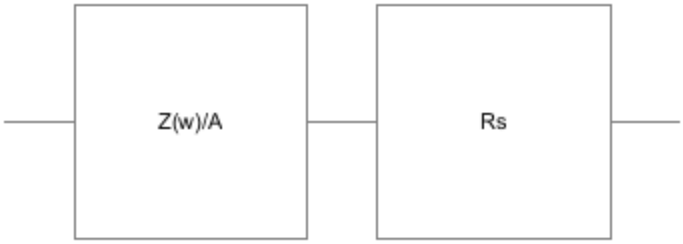

Figure 3.8. Simplification for Figure 3.4 electrical model by Yúfera [24]

3.4 Cell-Substrate Impedance

Measurement of Cell-Substrate Impedance is a relevant research topic that could reveal important characteristics of the cell behavior. Typically, optical methods including microscopy and fluorescence detection are used. Besides, mechanical, electrical, and sonic measurements have also gained popularity in the detection. Among them, electrochemical techniques provide the most convenient, inexpensive, and fast turnaround method. The use of bioimpedance technology has gained a lots of application in human body-related investigations, and *in vitro* tissue culture. Impedance sensing has become a very important and inspiring technology. As reviewed in Chapter 2, during cell culture, cells interact with substrate by changing their morphology according to the stiffness, energy, or some proteins on the substrate. Interconnection with adjacent cells through tight junctions is also subject to the stimulus factor surrounding their environment [27]. The common sense would suggest that the interaction between the cells and the substrate would be the same as the one between the electrolyte and the substrate. However, when a cell grows on a chip, we cannot expect that the lipid bilayer and metal from the substrate form a compact dielectric layer. As reviewed in Chapter 2, cell adhesion is mediated by protein molecules that protrude from the membrane and that are deposited on the substrate. These proteins keep the lipid core of the membrane at a certain distance from the substrate (gap). Nevertheless, this cell interaction with the substrate gives the possibility to use conductometric techniques and permits the modelation of the system as an electrical circuit.

Impedance measurement of biosensor could also be performed when an analyte or cells, are introduced over the electrode in addition to the previously mentioned electrolyte-substrate interaction. In this case, the previously stated electrical models result inaccurate and new models have to be taken into account to represent the presence of the analyte. The analyte change the media composition and interacts with the electrical fields shown in Figure 3.1. The new electrical models respond to the independent variables such as frequency and time, depending upon the technique of impedance measurement. As a matter of fact, both independent variables (time and frequency) could be controlled to obtain different measurements. A specific frequency could be applied to the electrodes and the impedance changes could also be monitored before and after (time) the analyte is immobilized. Moreover, the electrodes could be sweep through different frequencies to determine the composition of the analyte over the electrodes as suggested in Figure 3.6. The impedance change could be gradual or sudden depending how fast the binding reaction occurs. Figure 3.9 represents a classic curve of impedance change in measurements

before and after the analyte is immobilized. For the electrode and the interacting electric field, Z_0 is in fact the modeled impedance in the previous section.

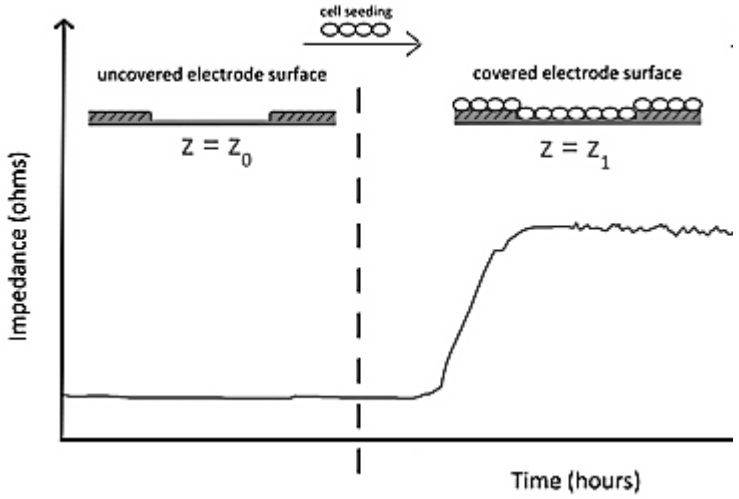

Figure 3.6. Classical impedance curve after and before analyte introduction (specific frequency during a span of time) [28]

3.4.1 Impedance Model of Single Cell

A schematic view of a cell positioned over a microelectrode was described in Chapter 2. The cell starts as an almost spherical body and then due to contact with the substrate the area of contact between the basal membrane and surface increases continuously as the cell spreads. Historically, the first impedance measurement of an individual cell on a microelectrode was reported by Lind et al. in 1991 [29]. This report provided the first evidence that the microelectrode could be used to sense the presence and movement of one individual cell. In 1995, Hagedorn et al. [30] presented evidence that motility of individual cells could be sensed and that cells will always maintain a gap between the cell and the substrate that would be filled by media. He also demonstrated that the transformation of the cell during cell adhesion seemed to correlate with the change in impedance measurement, which could also be extended to the changes during differentiation using stem cells. More recently a group from Carnegie Mellon University [25, 31], predicted the changes in impedance spectra due to differences in cell-substrate separation (R_{gap}) using FEMLAB simulation. They determined that the gap between the cell and the substrate could change the impedance measurement in an important way as shown in Figure 3.10. All these investigations have led to the design of electrical models for single adhered cells.

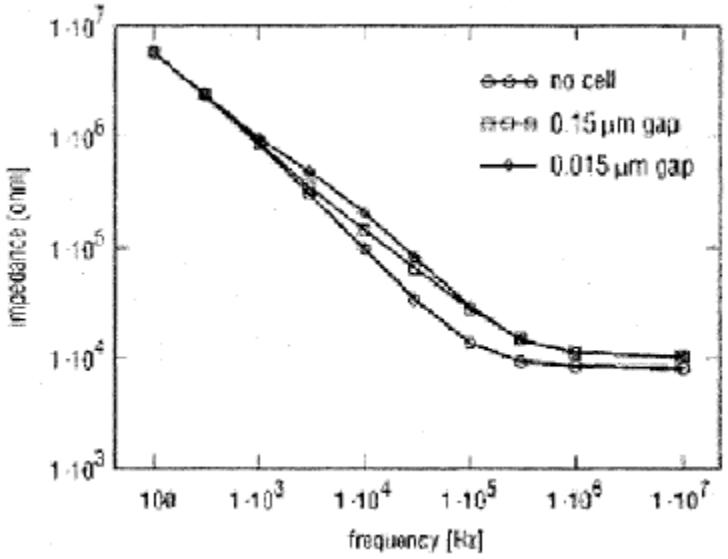

Figure 3.7. Impedance curve dependent upon the cell substrate separation (gap) [32]

Figure 3.11 illustrates the simplest model where the measured impedance consists of the electrode impedance (Z_e), the resistance between the electrode and the bulk electrolyte due to the layer of medium between the cell and the passivation layer (R_{seal}), the membrane capacitance and ion channel resistance over the electrode (C_{m1} and R_{ch1}), the membrane capacitance and ion channel resistance of the top and sides of the cell (C_{m2} and R_{ch2}), the solution resistance (R_{soln}) and the counter-electrode impedance (Z_{co}). The resistance R_{seal} is distributed with the capacitance and conductance of the membrane in the region over the passivation layer. For this measurement, the counter-electrode impedance, solution resistance, and electrode impedance should all be negligible (assuming platinized electrodes) so that the impedance measurement is dominated by the seal resistance and the cell membrane properties. R_{seal} must be equal or bigger than the membrane impedance if changes in membrane properties are to be observed [18].

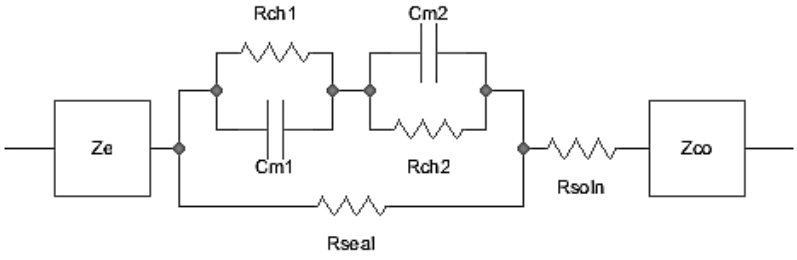

Figure 3.8. Simple electrical model for single cell over microelectrode

The model components ere estimated by assuming a circular cell of radius r_1 centered over a microelectrode of radius r_0. The total seal resistance was estimated by assuming a uniform cell to substrate separation (t) and using the standard formula given by equation (3.15). While changes in the effective resistivity of the solution are possible with small t, the effects are assumed to be negligible and the bulk resistivity of the medium was used. The seal resistance is calculated by

integration of (3.15) over the distance between the outer edge of the electrode and the outer edge of the cell, where the length *L* is equal to the incremental change in radius, and the area *A* is equal to the perimeter times the cell to substrate separation:

$$R_{seal} = \int_{r_0}^{r_1} \frac{\rho}{2\pi r t}\, dr = \left(\frac{\rho}{2\pi r t}\right) ln\left(\frac{r_1}{r_0}\right) \tag{3.23}$$

The capacitance and resistance values could be calculated from:

$$C_{m1} = \pi r_0^2 C_A \tag{324}$$

$$G_{m1} = \pi r_0^2 G_A \tag{3.25}$$

$$C_{m2} = \pi r_1^2 C_A \tag{3.26}$$

$$G_{m2} = \pi r_1^2 G_A \tag{3.27}$$

Where C_A and G_A are the capacitance and conductance for the cellular membrane per unit area.

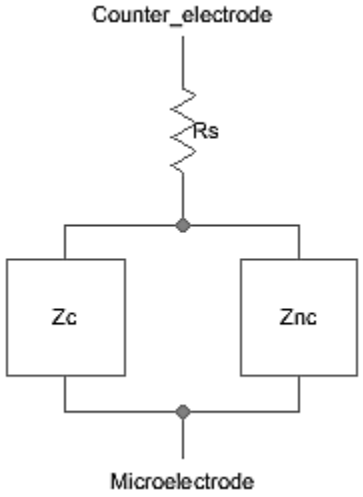

Figure 3.9. Modified electrical circuit for single cell over a microelectrode of [18] and [32]

Seriburi [32] describes that the model presented in Figure 3.11 can approximate $Z_{cell}(w)$ using Figure 3.12. The main difference is that Figure 3.12 takes into account the possibility that the cultured cell does not cover the entire electrode and the impedance of cell is modeled as single impedance. The model consists of three main elements representing the impedance across an electrode pair:

$$Z(w) = (Z_C || Z_{NC}) + R_S \tag{3.28}$$

Where Z_C is the impedance of a microelectrode covered by an individual cell and stands for the R_{seal} and the cellular resistance and membrane capacitance, Z_{NC} is the impedance of a microelectrode not covered by a cell, and R_S (spreading resistance) is the resistance of the cell medium between the microelectrode and the counter electrode. To calculate Z_C and Z_{NC} a modified form of the model proposed by Giaever and Keese [33] is used. The complete development of the proposed model can be found in [32].

3.4.2 Impedance Model of Population of Cells

The Giaever's model [33] is based on the fact that the cell monolayer geometrically blocks the current flow with respect to the current flow measured in the absence of cells, naked response. As well as in the single cell model, between the electrode surface and the bottom of the cells, there is a gap occupied by electrolyte. This gap is implicitly assumed to be larger than a few nanometers, and, therefore, even in the presence of cells, the electrical behavior of the current flowing through the electrode in contact with the electrolyte is analogous to the behavior of the naked electrode. Once it crosses the electrode medium interface, the current flows through different paths. The relative importance of the different paths depends on the specific impedances that are developed by the monolayer attached to the electrode. This model proposes that there can be two paths: either between the substrate-cell spaces or through the cell membrane.

In a simplified manner, the resistance produced by the cellular monolayer is due to the current passage underneath cells (distributed effect) and the current passage crossing intercellular spaces, through a junction resistance (lumped effect). The current that directly crosses the cell presents an essentially capacitive behavior.

As mentioned before, the analysis in a cellular unit provides the system response in the presence of cells. In this sense, cells are represented as circular disks of radius, r_C, and the analysis is carried out up to the one-cell limit where a proper boundary condition is imposed [18]. Figure 3.13 shows the outstanding variables in the current distribution, the drops in potential developed in the system, and the volume utilized for the integral analysis [33]. Electrical properties are considered by both the specific impedance of the naked electrodes, $Z_n(w)$, and the specific impedance due to the presence of cells (the impedance of two cellular membranes connected in series considering that each of both membranes only shows a capacitive behavior), $Z_m(w)$.

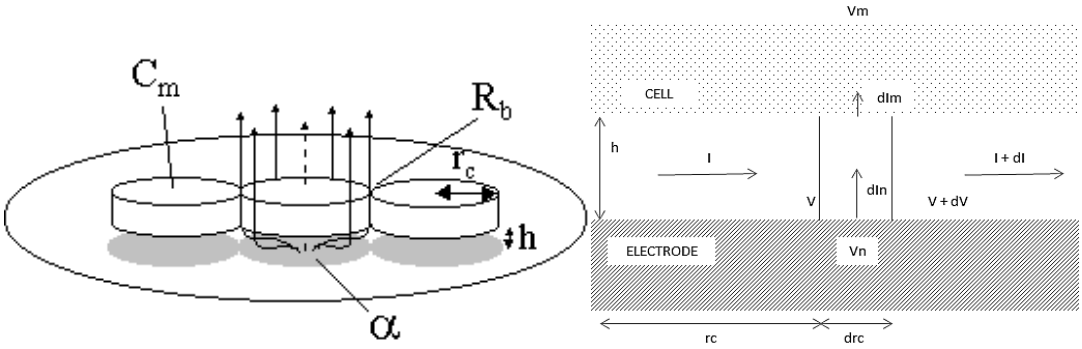

Figure 3.10. Giaever and Keese model emphasizing the spaces between the cell and the substratum. Cells are regarded as disk shaped when viewed from the top. The schematic side view diagram of cells is useful in constructing the differential equation (3.33) [33]

From Figure 3.13 and specific characteristics of the electrolyte and electrode is possible to obtain the follow equations:

$$-dV = \frac{\rho d_{r_c}}{2\pi h r_c} I \tag{3.29}$$

$$V_n - V = \frac{Z_n(v)}{2\pi r d_{r_c}} d_{I_n} \tag{3.30}$$

$$V - V_m = \frac{Z_m(v)}{2\pi r d_{r_c}} d_m \tag{3.31}$$

$$d_I = d_{I_n} - d_{I_m} \tag{3.32}$$

Where ρ is the resistivity of the solution, $Z_n(v)$ is the specific impedance of the electrode-electrolyte interface, $Z_m(v)$ is the specific membrane impedance of the cells. Using potential and current balances, a second order ordinary differential equation of for the potential in the cell-substrate space, *V*, can be obtained:

$$\frac{d^2V}{dr^2} + \frac{1}{r}\frac{dV}{dr} - \gamma^2 V + \beta = 0 \tag{3.33}$$

Where:

$$\gamma^2 = \frac{\rho}{h}\left(\frac{1}{Z_n} + \frac{1}{Z_m}\right) \tag{3.34}$$

$$\beta = \frac{\rho}{h}\left(\frac{V_n}{Z_n} + \frac{V_m}{Z_m}\right) \tag{3.35}$$

Because of the geometry assumed for the cell, the formulation is simplified when expressed in cylindrical coordinates. *P* is the known resistivity of the medium, *h* is the height of the cell-substrate space, V_n is the applied potential, and V_m is the potential beyond the monolayer.

The general solution of (3.34) is given by:

$$V = C_1 I_0(\gamma r) + C_2 K_0(\gamma r) + \frac{\beta}{\gamma^2} \tag{3.36}$$

Where I_0 and K_0 are the modified Bessel functions of first and second kind, respectively, of zero order.

Because K_0 diverges at the origin, the constant C_2 must be zero. The constant C_1 is determined with the boundary condition:

$$V_{r=r_c} - V_m = \frac{R_b}{\pi r_c^2} I_{r=r_c} \tag{3.37}$$

Where *I* is the current in the cell-substrate space and R_b is a resistance (per unit area) due to the formation of intercellular junctions. This condition implies that the potential drop at the end of the cell can be considered a lumped effect. The current under the cell that reaches its boundary cannot cross the limit of the system because the neighboring cell is identical to the cell under study; thus, by symmetry, in this region the current must axially cross the cells through a tight junction that acts electrically as a resistance. This type of analysis by unit cells is justified when all cells are equivalent. In such cases, the boundary condition (restricting the analysis to only one cell) results are simple, such as in the model descried in this section. However, the region studied, rigorously, is not a unit cell because it does not fill the space. In this analysis, there are spaces between consecutive regions that are not considered within any region. Nevertheless, this is a

minor concern, since the results obtained under this formulation agree with those obtained with a formulation based on regions of rectangular base that does fill the space.

Once the constants are determined, the variables of the system are defined, the inverse specific impedance of the cell-covered electrode can be given by:

$$\frac{1}{Z_{cov}} = \frac{1}{Z_n}\left(\frac{Z_n}{Z_n+Z_m} + \frac{\frac{Z_m}{Z_n+Z_m}}{\frac{\gamma r_c I_0(\gamma r_c)}{2I_1(\gamma r_c)}+R_b\left(\frac{1}{Z_n}+\frac{1}{Z_m}\right)}\right) \tag{3.38}$$

Where:

$$\alpha = r_c\sqrt{\frac{\rho}{h}} \tag{3.39}$$

This model has two parameters: α and R_b. A greater complexity can be achieved by considering the specific impedance through the cells, $Z_m(w)$, as a capacitive impedance with the particular value of the capacitance becoming and additional parameter [34].

Siddiquei, et al. [35] demonstrates that when cells are inoculated into the culture medium, they and their continuous growth causes changes of the electrode impedance as stated in this section. The impedance measurement from experimental data can be easily calculated where the impedance changes due to the cell growth as follows:

$$Z_{cell} = \frac{Z - Z_{initial}}{Z_{initial}} \tag{3.40}$$

Where $Z_{initial} = R_{med} + jX_{med}$ and $Z = R + jX$, is the value of impedance of the electrodes covered only by media before the cell inoculation. The total impedance is a combination of the cells´ capacitance denoted as C_{cell} and the resistance R_{cell}. Change in impedance values could be seen when there is an addition, movement or growth of cells. Figure 3.14 represents the equivalent circuit model proposed for the impedance of a cell culture inoculated in media. The total impedance is:

$$Z = R_{med} + \frac{(Xc_{cell}+R_{cell})Xc_{med}}{Xc_{cell}+Xc_{med}+R_{cell}} \tag{3.41}$$

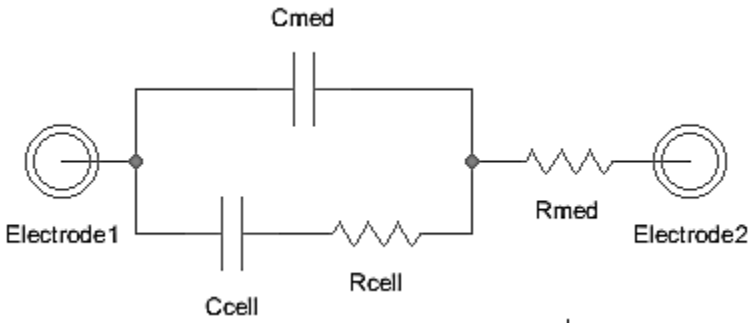

Figure 3.11. Siddiquei modification to electrical model for cell covered electrodes

The electrode electrode-cell/culture-electrolyte model used in this thesis is similar to the one proposed by Yúfera [36], where the given impedance comes per unit area. If e_1 is partially covered by cells in a surface A_c, $Z(w)/(A-A_c)$ the electrode impedance associated with the area not covered by cells, and $Z(w)/A_c$ is the impedance of the area covered. The resistance R_{gap} represents an opposition to the current flowing laterally in the electrode-cell interface, which depends on the electrode-cell distance at the interface (in the range of 15-150 nm) as showed in the previous section. R_s is the spreading resistance through the conductive solution. Parameter *ff*, called the fill factor, can be zero for $A_c=0$ (e_1 electrode empty), and 1 for $A_c=A$ (e_1 electrode full); and is used to study the difference between impedances while different percentages of the active area is covered. Figure 3.15 shows such model.

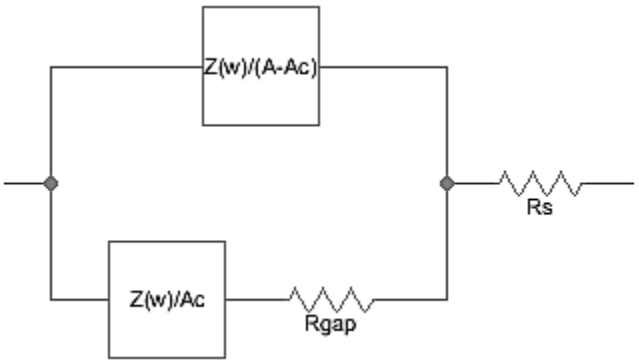

Figure 3.12. Electrical model for cell covered microelectrodes used in this research by Yufera [36]

3.4.3 Noise Sources in Impedance Measurements

Noise is very serious problem that can modify the results of any measurement. A good understanding of the noise sources is fundamental to provide feasible noise minimization solutions. According to [18], the main noise sources defined in electric cell culture measurements are the electrode noise, electromagnetic interference and biological noise.

3.4.3.1 Electrode Noise.

The intrinsic noise associated with the metal-electrolyte interface has been empirically shown to be thermal, following the standard Johnson noise equation for the rms voltage noise of a resistor:

$$V_{rms\ noise} = \sqrt{4kTR_N\Delta f} \tag{3.42}$$

Where k is the Boltzmann's constant ($1.38\text{x}10^{-23}$ J/K), T is the absolute temperature in Kelvin, R_N is the real part of the electrode impedance in ohms, and Δf is the bandwidth of interest.

The thermal noise voltage is plotted versus R_N in Figure 3.16. The resistance R_N will be attenuated with the electrode capacitance changes as the frequency increases.

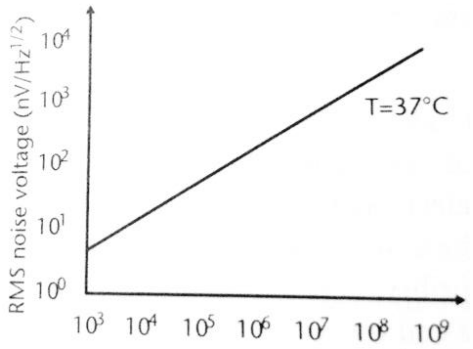

Figure 3.13. Theoretical noise voltage plotted versus the real part of the electrode impedance at 37°C. Noise if quoted as nV per root hertz, since it is the bandwidth not the actual frequency that is significant. [18]

In practical applications, the electrode impedance is measured in the bandwidth of interest, and the obtained resistance is used in (3.42) to estimate the thermal noise. The noise is compared to the anticipated signal levels to determine whether electrode impedance reduction is required. For impedance measurements where homodyning techniques are employed, the effective bandwidth of the measurements is significantly reduced, making this thermal noise less significant. However, this noise is so important because it may cause saturation in amplification systems prior to the homodyning stage [37].

3.4.3.2 Electromagnetic Interference

Electromagnetic interference (EMI; also called radio frequency interference or RFI) is an unwanted disturbance that affects an electrical circuit due to electromagnetic radiation emitted from an external source. The disturbance may interrupt, obstruct, degrade or limit the effective performance of the circuit. The source may be any object, artificial or natural, that carries rapidly changing electrical currents, such as an electrical circuit, the Sun, or the Northern Lights.

EMI can be induced intentionally for radio jamming, as in some forms of electronic warfare, or unintentionally, as a result of spurious emissions and responses, intermodulation products, and low frequency magnetic fields. EMI frequently affects the reception of AM radio in urban areas and it may also cause interference in cell phones, FM radio transmissions, and television reception.

3.4.3.3 Biological Noise

Ionic concentrations in the cellular media and membrane conductance exhibit some stochastic features. The activity of ionic membrane channels behaves as a transmitter that releases random noise in response to stimuli. Embedded in such a noisy environment, cells operate a spatial and temporal integration of the input stimuli, encoding them into firing or bursting patterns that carry information on the inputs in both spike rate and timing. These complex responses are generated through the activation of ionic channels, which behave as gates for transmembrane currents. The switching between opening and closing is almost stochastic, due to thermal excitation of channel macromolecules with multiple stable states. Recently, some studies have proposed a functional role in clustering ionic channel assemblies for preferred input processing, according to a phenomenon known as stochastic resonance.

References

[1] Grimmes S, Martin ØG. *Bioimpedance and Bioelectricity Basic*, San Francisco, CA: Academic Press, 200.

[2] Foster KR, Schwan HP. **"Dielectric Properties of Tissues and Biological Materials: A Critical Review,"** *Crit. Rev. Biomed. Eng.*, vol. 17, no. 1, pp. 25-104, 1989.

[3] Polk C, Postow E, *Handbook of Biological Effects of Electromagnetic Fields*, Boca Raton, FL: CRC Press, 1996.

[4] Gheorghiu E, Asami K. **"Monitoring Cell Cycle by Impedance Spectroscopy: Experimental and Theoretical Aspects,"** *Bioelectrochem. Bioenerg.*, vol. 45, no. 2, pp. 139-143, 1998.

[5] Giaever I, Keese CR. **"Proceedings of the National Academy of Sciences,"** 81, pp. 3761-3764, 1984.

[6] Thomas CA Jr., Springer PA, Loeb GE, Berwald-Netter Y, Okum LM. *Experimental Cell Research*, 74, pp. 61-66, 1974.

[7] Ehret R, et al., **"Monitoring of cellular behavior by impedance measurements on interdigitated electrode structures,"** *Biosensors & Biolectronics*, vol. 12, no. 1, pp. 29 – 41, 1997.

[8] Siddiquei H, et al., **"Electrical cell-substrate impedance sensing (ECIS) based biosensor for characterization of DF-1 Cells,"** *IEEE International Conference on Computer and Communication Engineering, 2010*, pp. 1 – 4, 2010.

[9] Van Gerwn, P, Laureyn W, et al. **"Nanoscaled interdigitated electrode arrays for biochemical sensors,"** *Sensors and Actuators B Chemical*, vol. 49, no. 2, pp. 73-80, 1998.

[10] Marrakchi M, Martelet C, et al. **"An enzyme biosensor based on gold interdigitated thin film electrodes for water quality control,"** *Analytical Letters*, vol. 40, no. 7, pp. 1307-1316, 2007.

[11] Aliakbar AM (2009) *Handheld Impedance Based Biosensor System for Glucose Monitoring*. Master Dissertation.

[12] Sui WM, Cobbold RSC. **"Basic properties of electrolyte-SiO_2-Si system: physical and theoretical aspects,"** *IEEE Transactions on Electron Devices*, vol. 26, no. 11, pp. 1805-1815, 1979.

[13] Borkholder DA. *Cell Based Biosensor Using Microelectrodes*, Ph.D. dissertation, Stanford University, Palo Alto, CA, 1998.

[14] Helmholtz HL, **"Studien über electrische grenzschichten,"** *Ann. Phys. Chem.*, 7, pp. 377-382, 1879.

[15] Gouy M. **"Sur la constitution de la charge électrique a la surface d'un electrolyte,"** *J. Phys.*, 9, pp. 457-468, 1910.

[16] Chapman DL, *Phil. Mag.*, vol. 25 no. 6, pp. 475, 1913.

[17] Stern O, **"Zur theorie der elecktrolytischen doppelschicht,"** *Z. Elektrochem.*, 30, pp. 508-516, 1924.

[18] Wang P Liu Q (editors), *Cell-Based Biosensors; Principles and Applications*. Norwood, MA: Artech House. 2010.

[19] Warburg E. **"Ueber das verhalten sogenannter unpolarisirberer electroden gegen wechselstrom,"** *Ann. Phys. Chem.*, 76, pp. 493-499, 1899.

[20] Kovacs GTA. *Microelectrode models for neural interfaces,* In Enabling technologies for cultured neural networks (Stenger DA and McKenna TM, eds.), pp. 121-165, Academic Press, New York, 1994.

[21] Newman J. **"Resistance for flow of current to a disk,"** *J. Electrochemical Society*, vol. 113, no. 5, pp. 501-502, 1966.

[22] Gamry Instruments (2013) *Basics of Electrochemical Impedance Spectroscopy*. Consulted on Gramry webpage at: www.gamry.com/application-notes/EIS/

[23] Marrakchi M, Martelet C, et al. **"An enzyme biosensor based on gold interdigitated thin film electrodes for water quality control,"** *Analytical Letters*, vol. 40, no. 7, pp. 1307-1316, 2007.

[24] Yúfera A, Cañete D, Daza P. **"A Microelectrode-Cell Sensor Model for Real Time Monitoring,"** *Second International Conference on Sensor and Device Technologies and Applications, SENSORDEVICES 2011*, pp. 143-146, 2011.

[25] Huang X, et al. **"Simulation of Microelectrode Impedance Changes Due to Cell Growth,"** *IEEE Sensors Journal*, vol 4, no. 5, pp. 576-583, 2004.

[26] Olmo A, Yúfera A. **"Computer Simulation of Microelectrode Based Bio-Impedance Measurements with COMSOL,"** *Third International Conference on Biomedical Electronics and Devices, BIODEVICES 2010.* pp: 178-182. Valencia, Spain. 2010.

[27] El-Ali J, Sorger PK, Jensen KF, **"Cells on Chip,"** *Nature*, vol. 442, no. 7101, pp. 403-411, 2006.

[28] Applied BioPhysics (2013) *ECIS Theory*. Consulted at the Applied BioPhysics webpage at: http://www.biophysics.com/ecis-theory.php

[29] Lind R, Connolly P, Wilkinson CDW, Breckenridge LJ, Dow JAT. *Biosensors and Bioelectronics*, 6, pp. 359-367, 1991.

[30] Hagedorn R, Fuhr G, Lichtwardt-Zinke K, Richter E, Hormung J, Voigt A. *Biochemica et Biophysica Acta*, 1269, pp. 221-232, 1995.

[31] Seriburi P (2008) *Using Electric Cell-Substrate Sensing (ECIS) to Measure Properties of an Individual Adherent Cell.* ProQuest Dissertations and Theses. Doctoral Dissertation.

[32] Giaever I, Keese CR. **"Micromotion of Mammalian Cells Measured Electrically,"** *Proc. Natl. Acad. Sci.*, 88, pp. 7896-7900, 1991.

[33] Urdapilleta E, Bellotti M, Bonetto FJ. **"Impedance Analysis of Cultured Cells: A Mean-Field Electrical Response Model for Electric Cell-Substrate Impedance Sensing Technique,"** *Phys. Rev. E.*, 74, 2006; 041908.

Chapter 4 – Electric Cell-Substrate Impedance Sensor (ECIS)

4.1 Introduction

During the past 20 years, there have been remarkable changes in technology and applications regarding cell impedance. Among Impedance Spectroscopy (IS) techniques for adherent cells, Electrical Cell-Substrate Impedance Spectroscopy (ECIS) [1] is the selected technique to measure bioimpedance of cell cultures in this research. Based on two-electrode setups, it allows the measurement of monolayer cell-culture impedances (Chapter 3) and makes it possible to determine the biological condition of a cell type and its relationship with the environment. The ECIS methodology is extensively used in the literature [2-11] to monitor cellular events such as adhesion and spreading on different substrates, barrier function of endothelial cells, micromotion, migration, morphology and shape change, and responses to cytotoxic compounds. Giaever and Keese [12] applied the ECIS technique to measure impedance in cell morphology monitoring using planar electrodes. This system is capable of real-time, noninvasive, label-free impedance measurements. To increase sensitivity, reproducibility, biocompatibility, cell number, and throughput, diverse electrode layouts and novel designs have been implemented. Furthermore, experiments and mathematical modeling have been developed to reveal the mechanism of impedance measurement of cellular behavior. During the last 20 years, impedance-based sensing technology has emerged as one of the most important and interesting label-free technologies for in vitro cell-based assays, real-time and dynamic technique to obtain information of cellular response.

4.2 ECIS Technique

ECIS is one of the most widely used electrochemical techniques that can be applied to monitor the adhesion and spread of mammalian cells quantitatively and in real time. In this technique, cell membrane is considered a high value capacitor with low conductivity (about 10^{-6} S/m), a cell membrane capacitance of approximately 1μF/cm^2, but complex pattern, which mainly consists of phospholipids that form a bilayer lipid membrane about 7 nm thick [13]. The cell maintains life activity by controlling the membrane permeability and if the integrity of membrane is destroyed, the cell dies. To measure the bioimpedance of cultured cell using this technique, gold film is deposited on proper substrate such as glass or silicon to fabricate specific electrode pattern. The method (described in Chapter 3) measures the changes in the effective electrode impedance (Figure 4.1). It is well known that when planar gold electrodes are immersed in culture medium, cells attach and spread on the electrode [14]. The impedance measurement technique has become one of the most used conductometric schemes due primarily to its simple methodology and readily available implementation.

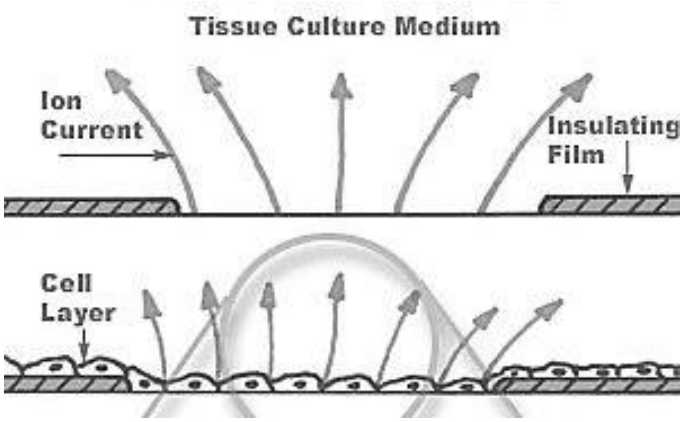

Figure 4.14. Principle of electrical impedance measurement on planar electrodes [15]

The impedance measurement in cell cultures using ECIS technique is frequency dependent. At *DC* and low frequencies, current passes beneath the cells and flows out beside cells. Figure 4.2 illustrates the way current is flowing from the electrodes. At high frequencies, above 1 MHz [16], current penetrates the cell membrane and the membrane effect disappears, ergo current flows according to local ionic conductivity as shown in Figure 4.3. Impedance changes can be interpreted to reveal relevant information about cell behavior, composition and coordination of many biochemical events [17]. This method has provided noninvasive techniques [8], as the small electrical current for measurements has no detectable effect on living cells, so that long-term experiments are reliable.

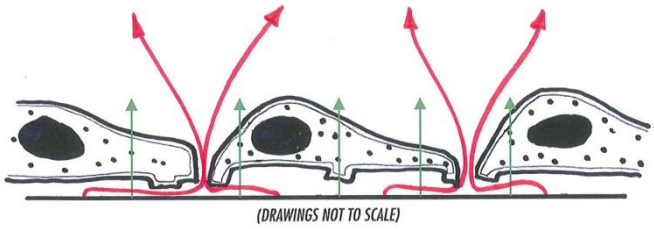

Figure 4.15. Behavior of ion currents at DC and low AC frequencies [18]

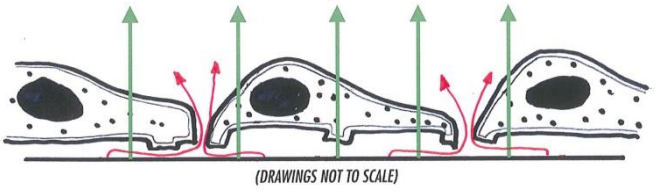

Figure 4.16. Behavior of ion currents at high AC frequencies [18]

Due to the nature of the attached cells, and the frequency dependence (normally between 1 kHz and 100 kHz) of experiments in ECIS technique, many research projects with different configurations have been reported. A change in impedance at 4 kHz over time has been used extensively [18] to study the behavior of adherent cells such as cell motility [12, 17, 19], proliferation [20-21], and cell morphological changes due to viral infection [22]. In other cases, a change in impedance at 400 Hz and 1 kHz over time was used to study cell-cell adhesion [23] and

cell morphological changes during apoptosis [11]. Moreover, a change in capacitance at 40 kHz over time was used to study the kinetics of cell spreading to various artificial surfaces [8]. Specific properties of the adherent cell monolayer such as the average cell-substrate separation and the average tight-junction gap resistance was obtained from the ECIS impedance spectrum by curve fitting [17, 24-26]. A simplified analytical model relating an ECIS impedance spectrum to the properties of a monolayer of adherent cells was described and evaluated in the literature [17, 26-28]. The reader can review Xiao and Sato for an extensive list of articles on research applications of the conventional ECIS for studying a monolayer of adherent cells [18, 29].

The effective and simple nature of this impedance-based technology leads to a variety of products to be used in typical cell culture impedance measurements. Some of the products developed by different companies are listed in Table 4.1 [15]. The first commercialized product is known as ECIS by Applied BioPhysics. Another electronic-based biosensor is represented by the "Real-Time Cell Electronic Sensing" (RT-CES supplied by ACEA Bioscience). To improve the sensitivity and reproducibility of the signal, an array of interdigitated electrodes (IDEs) is use. Another label-free cellular dielectric spectroscopy analyzer called CellKey was developed by MDS (supplied by MDS Sciex). There are also IDEs in a 96-well plate. They are used to measure fast changes in impedance within the radio-wave range to monitor cellular consequences of ligand-receptor interaction. Finally, the Bionas 2500 analyzing system incorporates IDEs structure with other microsensors to monitor acidification rate, oxygen consumption, and adhesion (cell impedance) of cells.

Table 4.5. Commercial products to perform ECIS measurements

Company	Product	Cell-Based Assay	Reference
Applied BioPhysics	ECIS	Cell adhesion, proliferation, barrier function, receptor-mediated signaling, and wound healing	[25]
ACEA Biosciences and Roche	xCELLingence (RT-CES)	Cell adhesion, proliferation, cytotoxicity, receptor-mediated signaling, barrier function, immune-cell signaling, cell migration, and invasion	[10]
Bionas	Bionas 2500	Cell adhesion, proliferation, metabolism, and cytotoxicity	[30]
MDS Sciex	CellKey	Cell adhesion, proliferation, receptor-mediated signaling	[9]

4.3 Microelectrodes Used in ECIS Measurements

The ECIS cell based biosensor requires a cell culture substrate containing microelectrodes. As described in Chapter 3, the electrode must provide a low impedance electrical connection to the cell. The adhesion of cells to the passivation layer utilized is very important since a loosely coupled

cell provides a shunt path for current which decreases the signal strength for impedance. According Wang [15] the measurement mechanism, the planar electrodes used for impedance sensing can be classified into two prototypes as follows:

1. *The monopolar system.* A small electrode is used as the working electrode and the larger electrode functions as the counter electrode. The area ratio of these two electrodes is < 1/100, which provides the ability to differentiate electrode reactions due to high impedance. Also, current density and the voltage drop are much higher at the small electrode, which results in dominating the total impedance changes.
   Giaever and Keese first presented ECIS (a & b from Figure 4.4) that small thin film electrodes with a diameter of 250 µm were located at the bottom of the 1 cm^2 cell culture well. The commercial electrodes are packed in arrays that contain eight wells. Each well has a large counter electrode and either a single or decade of electrodes (c & d from Figure 4.4). The simple layout and relative scale dispense the necessity of high-resolution and high-quality microfabrication technology.

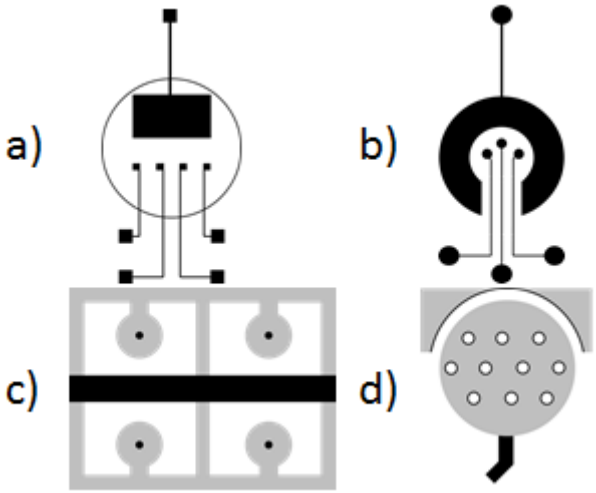

Figure 4.17. Monopolar system electrode architectures

2. *The interdigitated system (IDE). A set* of independently operating IDE units connects to a terminal strip to form one branch of an electrode. A second branch is identical and located on the other side with and interdigitated (alternation of finger derivation) fashion. Figure 4.5 illustrates the diverse schemes of the interdigitated microelectrode structure. Two facing branches weigh equally in measurement because they have identical dimensions. As the cells cover one of the two branches, impedance changes are uniform across the electrode. However there are situations in which this symmetrical behavior does not always hold true. The parameters involving the electrode width, the distance between two neighboring electrodes, the length of the finger, and the total number of fingers deserve attention for optimal performance in impedance sensing of cells. However, Ehret, et al. [6] reported comprehensive experiments on monitoring cellular behavior using IDE structures. The IDE structure exploits advantages of the changed conditions for the

current flow in the vicinity of the electrode surface. It demonstrates a much higher sensitivity toward surface changes compared with the conventional monopolar design.

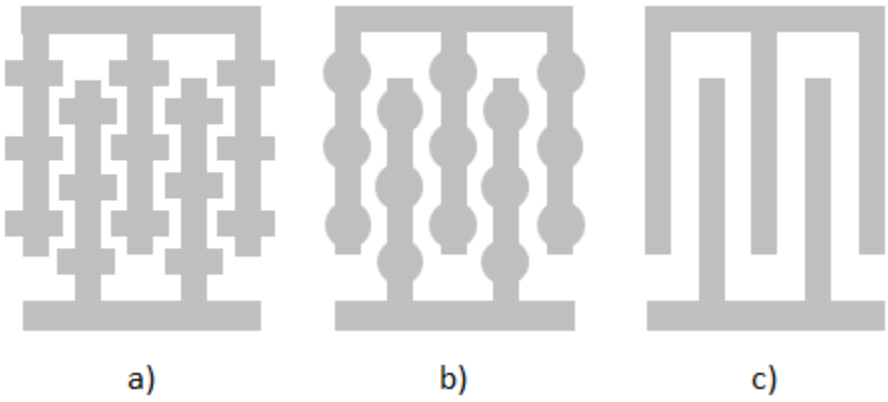

Figure 4.18. Interdigitated system electrode architectures

The two planar electrode types have advantages and disadvantages and the specific application is needed to select a particular system. In drug screening industry, the IDE system is more pervasive and perhaps a preferred device. The large counter electrode in the monopolar system restricts a further miniaturization, which is essential in a high-throughput drug-screening system. Because the area excluding the working electrode is relatively large, only a few cells on the working electrode contribute to the whole impedance measured, which results in fluctuation among experiments. Furthermore, a large number of cells are required to be initially seeded on the electrode to obtain sufficient number on the working electrode. The overall area of the IDEs commonly covers up to about 50% of the area of each well, lowering the well-to-well distribution of responses. Construction of these microelectrodes is presented in references [15, 31-32].

4.3.1 AC Frequency and Sensitivity Characteristics of Interdigitated Electrodes

ECIS techniques still have fundamental unresolved problems. These problems involve first, the frequency and sensitivity characteristics of the sensors and second, the dimension's design for optimizing its operation. The technical research literature is still waiting for publications which could thoroughly address these problems. This section provides a systemic analysis of frequency and sensitivity characteristics of IDEs.

As stated in the third chapter, as soon as the metal is wetted an electric double layer is created; such layer can be treated as a function of the distance perpendicular to the surface. The charge distribution is described by the Gouy-Chapman model [33], which divides the charge distribution into two layers, a Stern layer (adsorbed layer) and a diffusive layer. The Stern layer can be modeled as a regular capacitor, C_{stern}. The capacitance is about 20 µF/cm^2, and this value is independent of the ion concentrations. The diffusive layer capacitance, C_{diff}, depends on the total thickness of this layer, which is a function of the electrolyte concentration [34-35]. In physiological electrolyte solutions, it is about 10 nm. The thinner the diffusive layer is, the higher the electrolyte concentration will be. Thus, the total capacitance of the double layer (C_{DI}) is made up of C_{stern} and C_{diff} in series. If the electrolyte is very dilute, $C_{stern} >> C_{diff}$. On the contrary, when the solution is

concentrated, C_{stern}<<C_{diff}. The constant phase element (CPE) is a better model for the interfacial response to *AC* signals as an imperfect capacitor, where phase difference is given by –(90n)°, 0 ≤ n ≤ 1. This is because the capacitance system tends to equilibrium in practical applications. Its phase difference is remaining constant over frequency. The impedance CPE is given by the empirical formula:

$$Z_{CPE} = \frac{1}{Q_0(j\omega)^n} \tag{4.1}$$

Where Q_0 and n are parameters that depend on the properties of the electrolytes and the electrodes. More detailed descriptions are available in the literature [34]. Equivalent circuits are described in Figure 4.6.

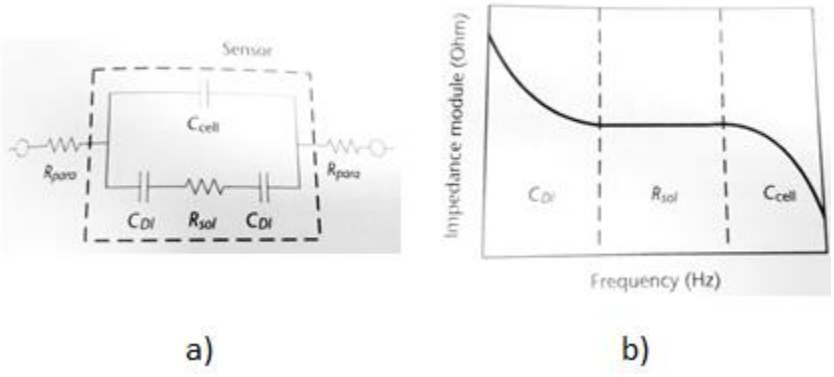

Figure 4.19. (a) Equivalent circuit of IDEs in electrolyte. (b) Schematic diagram of impedance frequency plots divided into domain components [15]

Based on the equivalent circuit shown in Figure 4.6(a), the total impedance can be expressed as a function of the known values of the components and frequencies [35]:

$$Z(j\omega) = 2R_{para} + \frac{x}{j\omega C_{cell}+1}, x = R_{sol} + \frac{2}{j\omega C_{Dl}} \tag{4.2}$$

At lower frequencies, the impedance will be dominated by the C_{Dl} until the impedance of this capacitor becomes lower than R_{sol}. Then the sensor impedance becomes frequency-independent. The low cutoff frequency can be expressed as (4.3) and is a function of the solution resistance and the double layer capacitance:

$$f_{low} \approx \frac{1}{2\pi\left(R_{para}C_{Dl}+2R_{para}C_{cell}+\frac{1}{2}R_{sol}C_{Dl}\right)} \approx \frac{1}{R_{sol}C_{Dl}} \tag{4.3}$$

However, at a certain frequency the impedance of the C_{cell} is lower than the one of R_{sol}. Then the impedance will decrease with an increase of frequency. The high cutoff frequency can be expressed as (4.4) and is a function of the solution resistance and the cell capacitance:

$$f_{high} \approx \frac{1}{2\pi R_{sol}\left(\frac{C_{Dl}C_{cell}}{C_{Dl}+2C_{cell}}\right)} \approx \frac{1}{R_{sol}C_{cell}} \tag{4.4}$$

A schematic diagram of total impedance is shown in Figure 4.7(F). There are three regions in the impedance spectrum, which correspond to the three types of components in equivalent circuit. As shown in Figure 4.7(B), there are paralleling branches. When the frequency is not lower than f_{high}, the current cannot flow through the C_{cell}; thus, the C_{DI} and R_{sol} in series are accounting for the total impedance. When the frequency increases from zero, C_{DI} decreases buy mainly contributes to the total decreasing impedance until f_{low} and f_{high}, the total impedance only depends on R_{sol}. Since f_{high} is beyond the commonly used frequency range and the cell membrane becomes invisible in the radio frequency range, C_{cell} can be neglected in the following cell impedance modeling. The R_{para} is also negligible in frequency characteristic analysis, because it is frequency independent and very small compared to other elements.

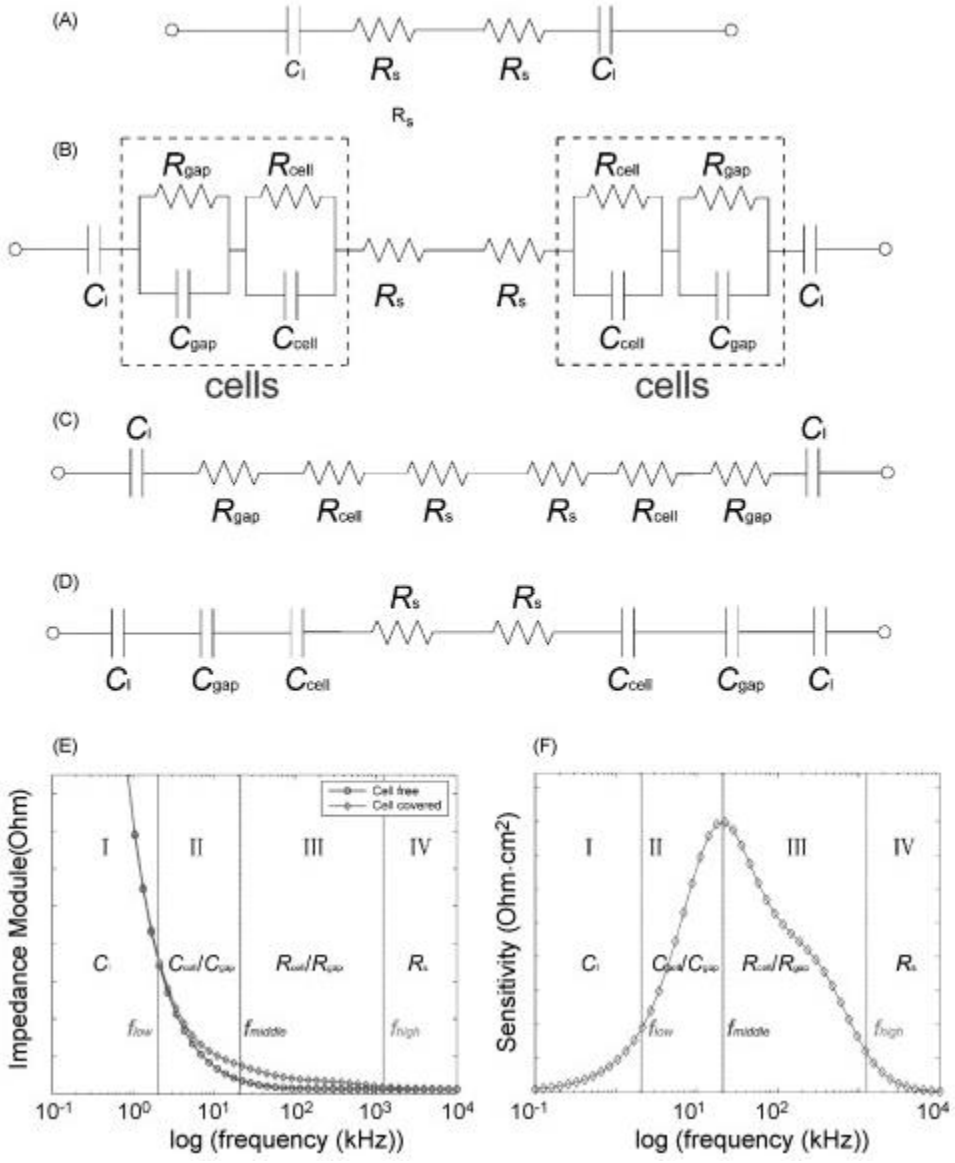

Figure 4.20. Equivalent circuit models for IDA structured coplanar ECIS sensors. (A) Equivalent circuit model for two-branch cell-free ECIS sensors. (B) The equivalent circuit model of two-branch cell-covered ECIS sensors. (C and D) Simplified equivalent circuits m

Cells attached on electrodes can be modeled as a capacitance (C_{cells}), which represents the dielectric property of the insulating cell membrane. The electrical resistance of the gaps between growing cells can be defined as R_{cells}. R_{gap} and C_{gap} stand for the capacitive property of the small gap between the underside of the attached cells and the substrate surface. Based on the equivalent circuit of cell-free electrodes in Figure 4.7(A), the cell-covered model is shown in Figure 4.7(B). Wang defined the $f_{cutoff\text{-}low}$ and $f_{cutoff\text{-}high}$ by simplifying the circuit to classical high pass circuits in a different frequency range [16]. And the f_{low} was defined to be lower than one-fifth of $f_{cutoff\text{-}low}$, f_{high} to be five times of $f_{cutoff\text{-}high}$.

$$f_{low} = \frac{1}{5} \times \frac{1}{2\pi(R_{sol}+R_{cells}+R_{gap})C_{Dl}}, f_{high} = 5 \times \frac{1}{2\pi R_{sol}\left(C_{Dl}^{-1}+C_{cells}^{-1}+C_{gap}^{-1}\right)^{-1}} \quad (4.5)$$

The most appropriate frequency for cell impedance sensing is the one with the highest sensitivity, which is defined to be f_{middle}, the root of (4.6).

$$\frac{d(Sensitivity(f))}{df} = \frac{d(|Z_{cell-covered}(f)|-|Z_{cell-free}(f)|)}{df} \quad (4.6)$$

Based on experimental results and theoretical analysis, some rules are generated from optimization of ECIS sensor designs. The parameters of sensors based on IDEs include electrode width, gap, length, number, and total area. These parameters influence the sensitivity and effective cell number in different ways [36-39]. The sensitivity increases with the reduction of electrode width and length, namely, minimizing the total area of the electrodes should increase the sensitivity. More cells are needed to respond to the same percentage of change in a large area compared to a small electrode area, in accordance with the analysis of the monopolar system. However, if the electrode width and length are reduced to increase the sensitivity, the number of effective cells would be reduced, which is not desirable. Therefore, a tradeoff of the sensitivity and the effective cell number has to be made in sensor design. Additionally, as the electrode width and length reduces, the impedance of each electrode branch will increase, which would cause a large electrical potential difference along the electrode. Cells adhered at different position would contribute differently to the total impedance [40]. Because cells attached to the electrode at any position contribute similar impedance signals, the electrode width should not be too narrow and the electrode length should not be too long. The fringe effect cannot be avoided in planner electrode, which would cause particularly large impedance when a cell attaches on the edge of an electrode. The equivalent circuit model mentioned earlier is based on the premise that one cell cannot simultaneously adhere to two adjacent electrodes, which is also not desirable in sensor design. Summarizing, shot electrode branch length and high branch number can provide a more uniform electric field and higher sensitivity.

4.4 Device and System

Based on the ECIS measuring technique and IDEs architecture for the microelectrodes, there has been reported several solutions for impedance measurements. The classical ECIS study applies a 4,000-Hz AC signal with amplitude of 1.0 V from a wave generator through a large resistor and measures the in-phase and out-phases voltage values by a lock-in amplifier in order to obtain the

electrical characteristic of the analyte [12, 17, 41]. Ehret performed impedance spectroscopy with a Solatron MTC 1260A impedance/gain-phase analyzer and long-term measurement with a Stanford Research System SR 715 or SR 720 LCR meter [6]. In other work, an Agilent 4294A impedance analyzer was used for impedance spectroscopy [42] at a frequency range between 40 Hz - 100 MHz. However, traditional impedance measurement instruments pose some problems, such as bulk mass, high costs, and lack of flexibility. As digital signal processing develops the methods of impedance measurement change accordingly. Not so long ago, Geisler et al. proposed and established a digital sensing processing based integration system for simultaneously detecting cell impedance, pH, and O_2 of 24 wells [43]. Although the new integration of hardware is highly automatic and flexible, the development period of these new systems may be a problem. As a partial solution to this problem, Wang's group provided a solution based on virtual instruments [16]; where measurements were carried out using a multifunctional data acquisition card NI DAQ PCI-6110 (National Instruments) program. The development time using predesigned multifunctional systems cut the development time considerably, as the impedance was calculated, recorded, and displayed automatically in real time as it would be in any other previously mentioned system. The application and viability of these systems has already been proved and stands as a good option to obtain the desired impedance measurements.

Two considerations are important in the design of an ECIS impedance data acquisition system. First, the design of the biosensor and second the technique that would be used to collect the impedance data. The criteria to design the biosensor consider the following:

- Biocompatibility.
- Maintenance of the physiochemical environment and sterility.
- Methods of sample introduction.
- Transducer for monitoring the desired electrical signal.
- Low signal path parasitic.
- Packaging.

Once the biosensor is selected, the data acquisition and processing technique are defined. Some of the traditional techniques which can be used are:

1. Phase sensitive detection (PSD)
2. Frequency response analysis (FRA)
3. Fast forward Fourier transform (FFT)

The FFT-based method is used in this research work. To study other techniques the reader may refer to Wang [15]. This method applies the Fast Fourier Transform to transfer the time domain signal into the frequency domain. Thus, a complex value can be presented as amplitude and phase, which corresponds to the impedance. In order to obtain this data array, a wideband white noise is applied on the sensor to get a response signal. Then, the sensor output is converted to a digital signal by ADC block for FFT calculation in a PC or a digital signal processor (DSP). The schematic diagram of this system is shown in Figure 4.8. The main advantage of these systems is that all the impedances at all interested frequencies can be obtained simultaneously, if the noise source is ideal; however, as in this research, it is also possible to obtain the impedance when only

a single or several frequencies are of interest using a series of sinusoidal signals as the stimulus. The FFT-based method provides a speed boost in comparison with both the PSD and FRA techniques. Nevertheless, the disadvantage is the requirements of high-speed ADC and mass data process for which a processing computer is used with this system.

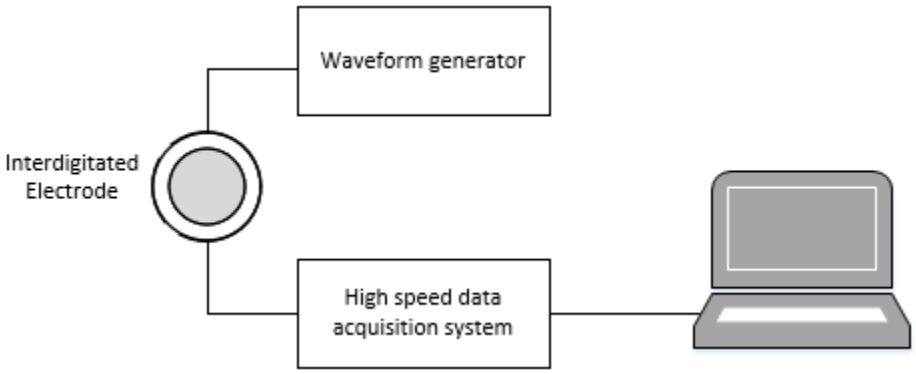

Figure 4.21. Schematic diagram of impedance measurement system based on FFT technique

4.5 Theoretical Analysis

One of the main drawbacks of the ECIS technique is the need to use efficient models to decode the electrical results obtained. To efficiently manage bio-impedance data, reliable electrical models of the full system comprising electrodes, medium and cells are required. Several studies have been carried out in this field [17, 31, 44-46]. Once the data has been obtained from the cell culture, a model has to be applied; these models are the key for matching the electrical impedance spectral response of the cell monolayer to real system performances and hence for correctly decoding the results obtained in experiments. The current models for the interpretation of these responses can be divided into two distinct approaches: the lumped model or distributed circuit model, and the analytical model based on microscopic characteristics of the monolayer.

4.5.1 Lumped Model

The lumped model is given based on the assumptions that the microscopic characteristic of the system, such as the properties of cell membranes, tight junctions, and different morphologies crate global electrical properties for the ensemble of cells. Many publications have presented the lumped models for data analysis [47-48]. However, there is no optimal one for every application. Complicated models give more comprehensive descriptions of true properties of cells, whereas redundant parameters retard the data fit in practical use. Upon the knowledge of some general rules, we can develop specific suitable models for particular applications.

Mostly, cell impedance is measured in cell culture media, which only contains electrolyte such as K^+, Na^+, Cl^-, PO_4^{3-}, and dome biomolecules, as suggested in [15]. Thus, the equivalent circuit and explanation of measured data can be simplified by dismissing faradic current. In the range of 1 Hz-100 kHz, C_{DI} and R_{sol} mainly dominate the impedance if there is no adsorption and desorption of species at the electrode surface. We consider the equivalent circuit of electrodes in electrolytes without redox couple to be a series connection of double layer and solution resistance as shown in

Figure 4.6(a) and Figure 4.7. Cell membrane (5-10 nm) has been reported to have a capacitance of 0.5-2.5 μF/cm^2 and a resistance of 10^2-10^5 Ωcm^2. Either specific or nonspecific cell attachments on electrodes do not directly affect the double layer for that cell scale beyond the order of several Angstroms. Cells adhere to adjacent cells with a gap of 10-20 nm, and the aqueous gap between cells and the electrode surface prevents the direct effect of the cell membrane on the impedance of electrodes. Contact area can be viewed as an aqueous compartment spanned by the polycationic segments of membrane macromolecules [49].

4.5.2 Analytical Model

By now it is clear that when the cells grow over the electrode, the measured impedance keeps increasing due to the increase of cell number and the growth of the cell-covered electrode area. Even when the cell layers become confluent, the impedance continues to slightly fluctuate. That happens because the monolayer is more complicated than the single cell, as it includes the cell-cell interactions and cell micromotion. Giaever and Keese proposed a model previously reviewed for the monolayer to understand the mechanism involved [34], and Goda [39] proposed a simplified method of the same model. This model has three adjustable parameters: R_b, α, and C_b. The curves of normalized resistance share a common trend where the resistance value increases with frequency until a turning point called middle frequency; then, it decreases as the frequency increase. Specifically, these three parameters contribute in different ways to the total impedance. The junction resistance R_b significantly affects the resistance and capacitance in the range near middle frequency, while α does so below the middle frequency, and C_b does so above the middle frequency. Additionally, the shift in peak results from the changes in these parameters. These distinct differences create an opportunity for extracting lots of information from the impedance measurements, such as junction resistance and space between cells and substratum, as well as the morphology of apical membrane and basal membrane.

4.5.3 Data Calculation and Presentation

Measured data and model data supplement each other. It is necessary to distinguish measured *"raw"* data, calculated measured data, and derived data. The measuring setup determines what data is raw data, which can be present in some chosen form (Figure 4.9). The data can be acquired as a function of time or frequency. When the data is related to frequency and time, a three dimensional presentation is required. Calculated data is based on a simple mathematical operation that contains no additional information with respect to any disturbing influence like temperature, atmospheric pressure and so on. Therefore, impedance and admittance are just two different ways to present the measured data. The derived data may contain some nonelectrical variable derived from electrical variables. For example, cell number, cell viability, tightness of cell-substrate adhesion, and cell-cell tight connection all have some interior relations with measured data. The interpretation of the measured data always relies on some of the already described models.

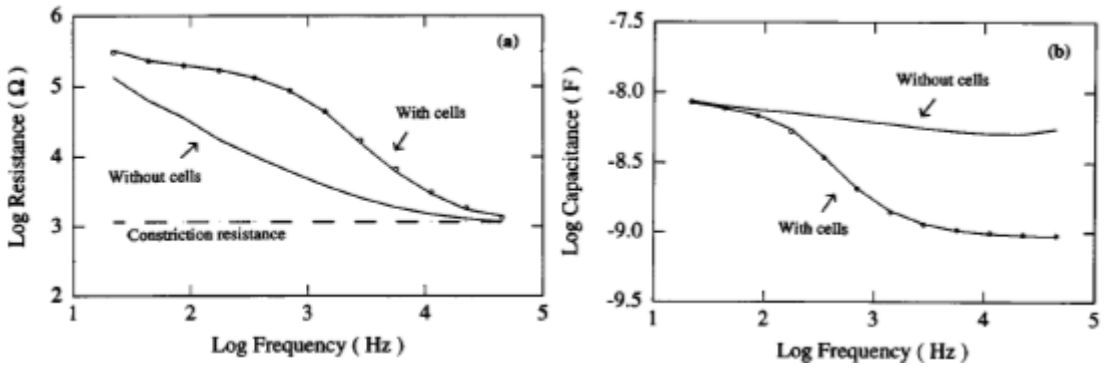

Figure 4.22. Raw data obtained for impedance measurements taken from [25]

References

[1] Giaever I, and Keese CR. **"Use of Electric Fields to Monitor the Dynamical Aspect of Cell Behavior in Tissue Culture,"** *IEEE Trans. Biomed.Eng.* 33, pp. 242-247, 1986.

[2] Xiao C, Lachance B, Sunahara G, Luong JHT. **"An In-Depth Analysis of Electric Cell-Substrate Impedance Sensing to Study the Attachment and Spreading of Mammalian Cells,"** *Anal. Chem.* 74, pp. 1333-1339, 2002.

[3] Seriburi P (2008) *Using Electric Cell-Substrate Sensing (ECIS) to Measure Properties of an Individual Adherent Cell.* ProQuest Dissertations and Theses. Doctoral Dissertation

[4] Park HE, Kin D, Koh HS, Cho S, Sung JS, Kim JY. **"Real-Time Monitoring of Neural Differentiation of Human Mesenchymal Stem Cells by Electric Cell-Substrate Impedance Sensing,"** *Journal of Biomedicine and Biotechnology 2011*, 1-8, 2011.

[5] Bagnaninchi P, Drummond N. **"Real-time label-free monitoring of adipose-derived stem cell differentiation with electric cell-substrate impedance sensing,"** *PNAS*, vol. 108, no. 16, pp. 6462-6467, 2011.

[6] Ehret R, et al. **"Monitoring of cellular behavior by impedance measurements on interdigitated electrode structures,"** *Biosensors & Biolectronics*, vol. 12, no. 1, pp. 29 – 41, 1997.

[7] Baumann WH, et al. **"Microelectronic Sensor System for Microphysiological Applications on Living Cells,"** *Sens. Actuators B: Chem.*, vol. 55, no. 1, pp. 77-89, 1999.

[8] Wegener J, Keese CR, Giaever I, **"Electric Cell-Substrate Impedance Measurements on Interdigitated Electrodes as a Noninvasive Means to Monitor the Kinetics of Cell Spreading to Artificial Surfaces,"** *Exp. Cell Res.*, vol. 259, no. 1, pp. 158-166, 2000.

[9] Ciambrone GJ, et al. **"Cellular Dielectric Spectroscopy: A powerful New Approach to Label-Free Cellular Analysis,"** *J. Biomol. Screen.*, vol. 9, no. 6, pp. 467-480, 2004.

[10] Solly K, et al. **"Application of Real-Time Cell Electronic Sensing (RT-CES) Technology to Cell-Based Assays,"** *Assay Drug Dev. Technol.*, vol. 2, no. 4, pp. 363-372, 2004.

[11] Pänke O, et al. **"Impedance Spectroscopy and Biosensing,"** *Biosensing for the 21st Century*, pp. 195-237, 2008.

[12] Giaever I, Keese CR. "**Monitoring Fibroblast Behavior with an Applied Electric Field,"** *PNAS*, 81, pp. 3761-3764, 1984.

[13] Grimmes S, Martin ØG. *Bioimpedance and Bioelectricity Basic*, San Francisco, CA: Academic Press, 2005.

[14] Gheorghiu E, Asami K. **"Monitoring Cell Cycle by Impedance Spectroscopy: Experimental and Theoretical Aspects,"** *Bioelectrochem. Bioenerg.*, vol. 45, no. 2, pp. 139-143, 1998.

[15] Wang P, Liu Q (editors), *Cell-Based Biosensors; Principles and Applications*. Norwood, MA: Artech House. 2010.

[16] Wang L, et al. **"Analysis of the Sensitivity and Frequency Characteristics of Coplanar Electrical Cell-Substrate Imepdance Sensors,"** *Biosens. Bioelectron.*, vol 24, no. 1, pp. 14-21, 2008.

[17] Giaever I, and Keese CR. **"Micromotion of Mammalian Cells Measured Electrically,"** *PNAS USA*, 88, pp. 7896-7900, 1991.

[18] AppliedBioPhysics, Applied Biophysics, Consulted on: http://biophysics.com

[19] Sapper A, Wegener J, Janshoff A. **"Biological activity of cells probed by noise analysis of thickness shear mode resonators: a new means to measure vertical cell motility,"** *Anal. Chem.* 78, pp. 5184-5191, 2006.

[20] Xiao C, Luong J, "**On-Line Monitoring of Cell Growth and Cytotoxicity Using Electric cell-substrate Impedance Sensing (ECIS),**" *Biotechnal Prog*., 19, pp. 1000-2005, 2003.

[21] Xiao C, Lachance B, Sunahara G, Luong J, "**Assessment of Cytotoxicity Using Electric Cell-Substrate Impedance Sensing: Concentration and Time Response Function Approach,**" *Anal. Chem.*, vol. 74, no. 22, pp. 5748-5753, 2002.

[22] McCoy MH, Wang E. *Journal of Virological Methods*, 130, pp. 157-161, 2005.

[23] Hartmann C, Zozulya A, Wegener J, Galla HJ. "**The impact of glia-derived extracellular matrices on the barrier function of cerebral endothelial cells: An in vitro study,"** *Experimental Cell Research*, 2007.

[24] Kataoka N, Iwaki K, Hashimoto K, Mochizuki S, Ogasawara Y, Sato M, Tsujioka K, Kajiya F. *Proceedings of the National Academy of Sciences*, 99, pp. 15638-15643, 2002.

[25] Lo CM, Keese CR, Giaever I. **"Impedance Analysis of MDCK Cells Measured by Electric Cell-Substrate Impedance Sensing,"** *J. Biophys.*, vol. 69, no. 6, pp. 2800-2807, 1995.

[26] Lo CM and Ferrier J. **"Impedance analysis of fibroblastic cell layers measured by electric cell-substrate impedance sensing,"** *Phys. Rev. E.*, 57, pp. 6982-6987, 1998.

[27] Bodmer JE, English A, Brady M, Blackwell K, Haxhinasto K, Fotedar S, Borgman K, Bai EW, Moy AB. *Am J Physiol Cell Physiol*, vol. 289, pp. 735-747, 2005.

[28] Giaever I, Keese CR.**"A morphological biosensor for mammalian cells,"** *Nature,* 366, pp. 591–592, 1993.

[29] Patskovsky S, Kabashin AV, Meunier M, Luong JHT. **"Multilayer Si-Based Surface Plasmon Resonance Structure for Absorption Sensing,"** *Analytical Letters,* vol. 36, no. 15, pp. 3261-3270, 2003.

[30] Thedinga E, et al. **"Online Monitoring of Cell Metabolism for Studying Pharmocolodynamic Effects,"** *Toxicol. Appl. Pharmacol.*, vol. 220, no. 1, pp. 33-44, 2007.

[31] Borkholder DA (1998) *Cell Based Biosensors Using Microelectrodes.* Doctoral Dissertation.

[32] Radke SM, Alocilja EC. **"Design and Fabrication of a Microimpedance Biosensor for Bacterial Detection,"** *IEEE Sesors Journal*, vol. 4, no. 4, pp. 434-440, 2004.

[33] Sato N., *Electrochemistry at Metal and Semiconductor Electrodes*, New York: Elsevier, 1998.

[34] Bard AJ, *Electrochemical Methods: Fundamentals and Applications*, New York: John Wiley & Sons, 1980.

[35] Timmer B, et al. **"Optimization of an Electrolyte Conductivity Detector for Measuring Low Ion Concentrations,"** *Lab Chip*, vol. 2, pp. 121-124, 2002.

[36] Ibrahim M, Claudel J, Kourtiche D, Nadi M. **"Geometric parameters optimization of planar interdigitated electrodes for bioimpedance spectroscopy,"** *J. Electr. Bioimp.*, vol. 4, pp. 13-22, 2013.

[37] Paschero A, McLoughlin E, Moore EJ. **"Continuous non-destructive monitoring of cell health using impedance based interdigitated electrode structured sensors,"** *Proceedings of the 5th BioNanoTox and Applications International Research Conference*, Little Rock, Arkansas 2010, AIP, pp. 100-105, 2011.

[38] Min J, Baeumner AJ. **"Characterization and Optimization of Interdigitated Ultramicroelectrode Arrays as Electrochemical Biosensor Transducer,"** *Electroanalysis*, vol. 16, no. 9, pp. 724-729, 2004.

[39] Goda N, Kataoka N, Yamamoto Y, Okuda H, Kajiya F. **"Evaluation of the electrical cell-substrate impedance sensing system (ECIS) method using a mathematical model,"** *The 47th IEEE International Midwest Symposium on Circuits and Systems,* vol. 3, pp. 223-226, 2004.

[40] Xu X, Wang XB. **"Impedance Based Devices and Methods for Use in Assays,"** U.S. patent, 2005/0112544, 2005.

[41] Urdapilleta EM, Bellotti M, Bonetto FJ. **"Impedance Analysis of Cultured Cells: A Mean-Field Electrical Response Model for Electric Cell-Substrate Impedance Sensing Technique,"** *Phys. Rev. E.*, vol. 74, no. 4, p. 041908-11, 2006.

[42] Abdar Rahman AR, Prince DT, Bhansali S. **"Effect of Electrode Geometry on the Impedance Evaluation of Tissue and Cell Culture,"** *Sens. Actuators B: Chem.*, vol. 127, no. 1, pp. 89-96, 2007.

[43] Geisler T, et al. **"Automated Multiparametric Platform for High-Content and High Throughput Analytical Screening on Living Cells,"** *IEEE Trans. Autom. Sect. Eng.*, vol. 3, no. 2, pp. 169-176, 2006.

[44] Huang X, et al. **"Simulation of Microelectrode Impedance Changes Due to Cell Growth,"** *IEEE Sensors Journal*, vol 4, no. 5, pp. 576-583, 2004.

[45] Joye N, et al. **"An Electrical Model of the Cell-Electrode Interface for High-density Microelectrode Arrays,"** *30th Annual International IEEE EMBS Conference*, pp. 559-562, 2004.

[46] Olmo A, Yúfera A. **"Computer Simulation of Microelectrode Based Bio-Impedance Measurements with COMSOL,"** *Third International Conference on Biomedical Electronics and Devices, BIODEVICES 2010,* pp. 178-182. Valencia, Spain.

[47] Wegener J, Sieber M, Galla HJ. **"Impedance Analysis of Epithelial and Endothelial Cell Monolayers Cultured on Gold Surfaces,"** *J. Biochem. Bioph. Methods,* vol. 32, no. 3, pp. 151-170, 1996.

[48] Paunescu TG, Helman SI. **"cAMP Activation of Apical Membrane Cl^- Channels: Theoretical Considerations for Impedance Analysis,"** *J. Biophys.*, vol. 81, no. 2, pp. 838-851, 2001.

[49] Gingell D. **"Cell Contact with Solid Surfaces,"** *Biophys. Cell Surf.*, pp. 263-268, 1990.

Chapter 5 – MEASUREMENT METHODOLOGY AND DATA ACQUISITION SYSTEM

5.1 Experimental Set-up

The platform developed in this thesis is used to detect the impedance changes in a rat stem cells culture (rSCs) while growing and during the process of differentiation to motor and dopaminergic cells. This sensing platform consists of microelectrodes, an impedance acquisition card, and a multiplexing control system. The chapter presents: the microelectrode selection, the data acquisition specifications, the design and functionability of the control system, and the basic information of the stem cell culture.

The electrical monitoring of the tissue culture is based on the well-established ECIS technology [1]. Experimental set-up based in Wang design [2] is depicted in Figure 5.1. The measurement chamber consists of a commercial set of 8-well cell culture dish with interdigitated gold electrodes deposited on the bottom of each well (Applied BioPhysics Inc., (USA); type 8W10E+) [3].

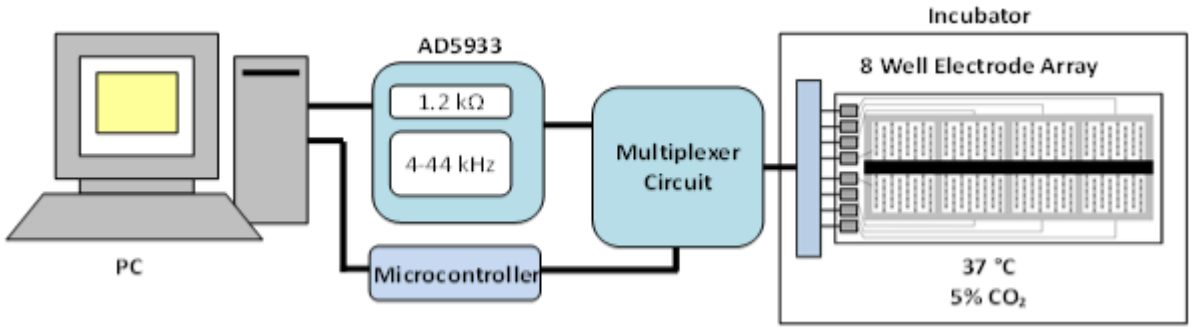

Figure 5.23. Experimental set-up based in Wang design

Each well contains an array of small working electrodes and a large counter electrode. Data collected from each ECIS well will describe the behavior of the cells cultured (growing and differentiation) on the small working electrodes. These 8-well electrode arrays are placed in a humidified cell culture incubator at 37°C with 5% CO_2. Electrodes are interfaced to the electronics equipment located outside the incubator by an electrode holder and a ribbon cable connected to the multiplexing circuit. The multiplexing circuit allows switching between the different electrodes and it's used to separate each sample in the array. The control of the switches is implemented using a synchronic connection with an ATMEGA328 microcontroller. This control circuit is connected to an AD5933 (Analog Devices, (USA)) impedance analyzer/frequency generator card controlled through an ordinary PC.

To acquire ECIS data, the impedance analyzer applies an AC signal at a sampling frequency between 4 and 44 kHz with an amplitude of 40mV (rms) to the electrodes every minute (16 min per cycle). The associated current is measured and using the Ohm's law, the impedance of the system can be calculated. The selection of frequencies is selected according to the frequency map illustrated in Chapter 4's Figure 4.7 which shows the appropriate frequencies to detect changes in

confluent layers of most cell types, and Figure 5.2 which shows the suggested range of variables to perform the measurements [4-5]. Moreover, at this range of frequency the impedance contains contributions from trans- and paracellular current pathways so that changes in cell-cell-contacts, cell-matrix-contacts and the cell membranes are mirrored in the impedance signal [6]. The impedance magnitude |Z| at any time will be normalized for its final presentation as suggested by Lo, et al. [7].

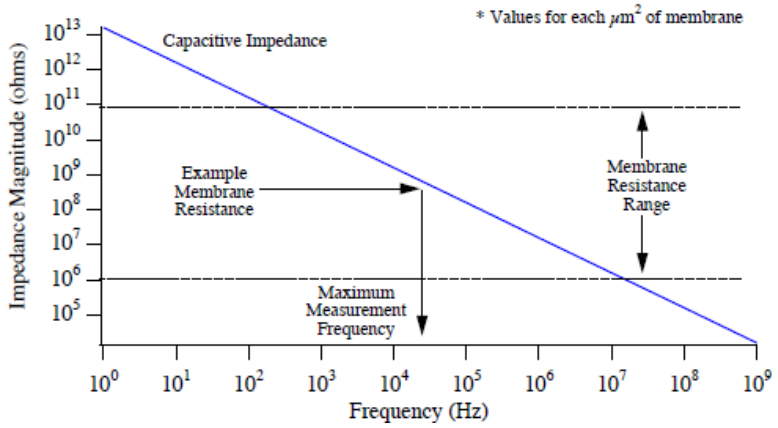

Figure 5.24. Estimate of the maximum measurement frequencies which should be used during ECIS technique [5]

5.2 Cell Culture

Cell culture and induction processes are based in the work of Bagnaninchi [8]; however, the cells used in this thesis are rat stem cells (RSCs) instead of human adipose-derived stem cells. RSCs were obtained from a ***X*** kind of rat, cultured in DMEM-F12 10% SFB medium and used at a passage between 5-7. According to the recommendations of the ECIS Handbook [9], the electrodes were first treated with cysteine in order to clean the electrodes. Once cleaned, ECIS arrays were first coated with 200 µl polylysine solution to promote cell adhesion and growth of cells during 1 hr, then rinsed and incubated with cell culture medium (DMEM-F12 10% SFB) 2 hr before cell inoculation to condition the gold film electrodes. After the conditioning period, each well was seeded with 200 µl of cell suspension for a resulting cell density of ≈50,000 cells per cm^2. The culture has a media change in the second day prior the inoculation of 200 µl of new media. At the time of induction (day 4), the medium was switched to a motor or dopaminergic differentiation medium. Noninduced controls were kept in complete DMEM F-12 10% SFB media. When the media has to be changed every 2, the ECIS system is to be paused and the arrays unplugged to perform microscopic analysis using a simple inverted microscope. After the cell culture media is replaced, the arrays must be plugged back to the system and the acquisition resumed. At the end of the experiment the wells are stained using fluorescent marker nestin. Once added the protection of the cultureware has to be removed in order to visualize the cultured cells under the fluorescence microscope (Zeiss Axio Imager Zi). Protocols used and process are described in Appendix A.

5.3 Selected Components

5.3.1 Microelectrodes

The microelectrode array consists of 8 wells which are the denomination model 8W10E+ from Applied BioPhysics Inc. [3]. They provide data obtained from the prototype of planar electrodes used in ECIS measurements. Each well array includes a small working electrodes set (20 small electrodes), and an array of counter electrodes (20 small electrodes). The area of the working and counter electrodes is approximately ≈$2x10^{-4}$ cm^2 in the 8W10E+. In this case the assumption that the working electrode has to be much smaller than the counter electrode is not met. That is why the working electrode does not become the bottle neck for current flow, and the model to be used has to change as described by Borkholder [5].

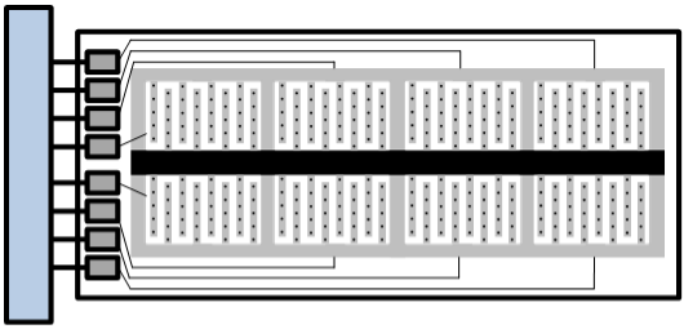

Figure 5.25. Applied BioPhysics 8W10E+ Cultureware

This ECIS cultureware consists of disposable electrode arrays containing gold film electrodes delineated with an insulating photoresist film mounted on a 20 mil optically clear Lexan* polycarbonate substrate. The well top assembly is made of polystyrene. The gold layer is thin enough to allow microscopic observation of the cells using a standard inverted tissue culture microscope. Each well has a gold electrode at the base, which is 250 µm in diameter and has a surface area for cell attachment and growth of 0.8 cm^2. The distance between electrode fingers is ≈1.2 mm (gap between electrodes ≈300 µm and interdigitated finger ≈550 µm), and the distance between electrodes in the same finger is ≈850 µm. The well holds a maximum volume of about 600 µL. The ECIS electrode array is placed in the holder located in the incubator.

During the manufacturing process there is an exposure to oxygen plasma that both cleans the electrodes and sterilizes the chamber and lids (which also renders both the substrate and the polystyrene walls of the well very hydrophilic). However, in order to ensure cleaning and stabilization of the electrodes, a cysteine treatment is applied before cell inoculation as suggested by the ECIS Handbook [9].

5.3.2 Impedance Reader: AD5933 Evaluation Board Overview

There are several commercially available electronic devices, such as USB-6281 made by National Instruments or the Agilent 4294A, which can be used as a single point impedance reader. In this thesis, the AD5933 from Analog Devices was used because of its low cost and user friendliness. The AD5933 has already been widely used for health monitoring and single cell

analysis [10-11], as well as design of real-time sensing platforms [12-15]. This evaluation board uses the FFT method to extract the data from the analyte. Figure 5.4 illustrates the friendly and intuitive interface let the user program visually the starting frequency, increment frequency, number of increments, range of output excitation, settling times cycles, DDS settling time cycles, PGA gain factor and select a desired clock. Also, the Figure 5.4 shows calibration options, graphs to the impedance measurements and the option to program cycles of measurements.

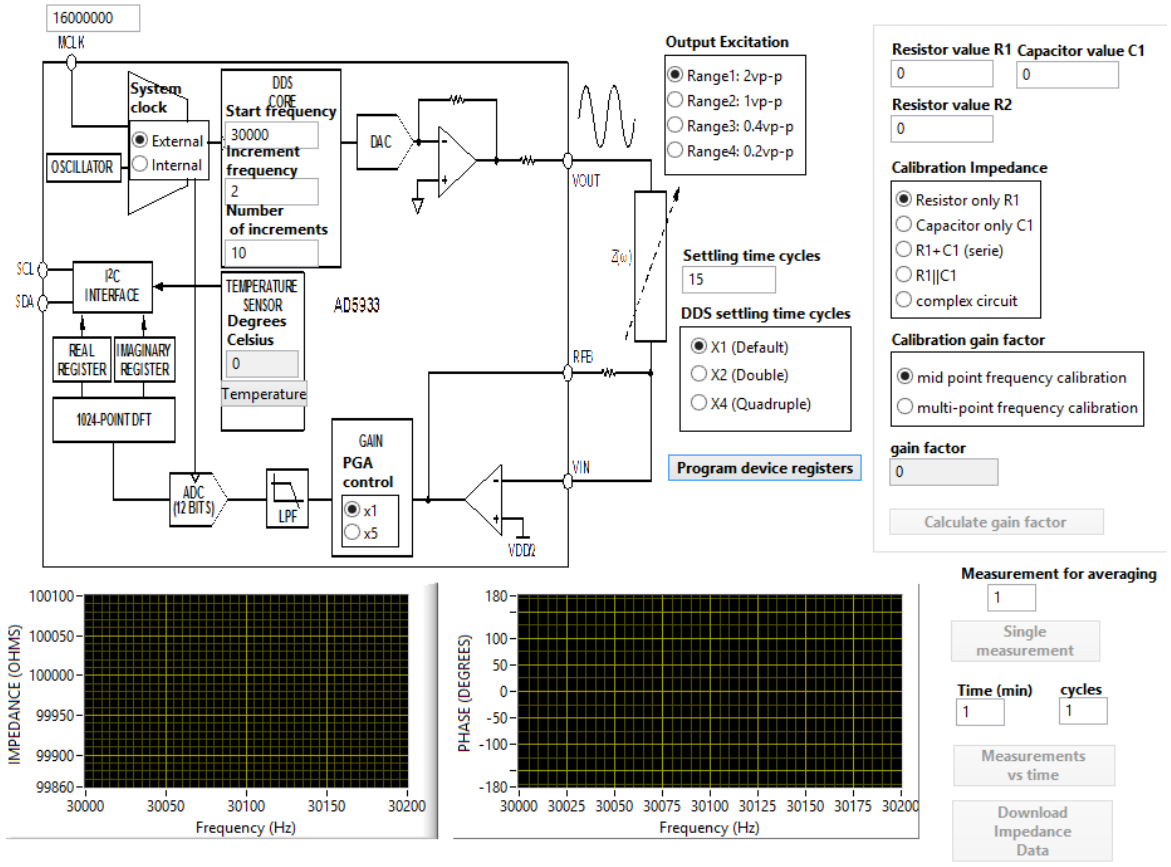

Figure 5.26. AD5933 evaluation software main dialog box

The AD5933, developed by Analog Devices [16], is a two electrode high precision impedance measurement device composed of several blocks including a wave generator, an Analog-to-Digital Converter (ADC), an output voltage source, and a Fourier Transform based impedance estimator. It has a dynamic range of 1KΩ to 1MΩ which according to AD5933 datasheet is determined by a variable resistor connected to the input Feedback Resistor (R_{FB}). AD5933 has a maximum frequency of 100 kHz. The internal functional block diagram of AD5933 is shown in Figure 5.5.

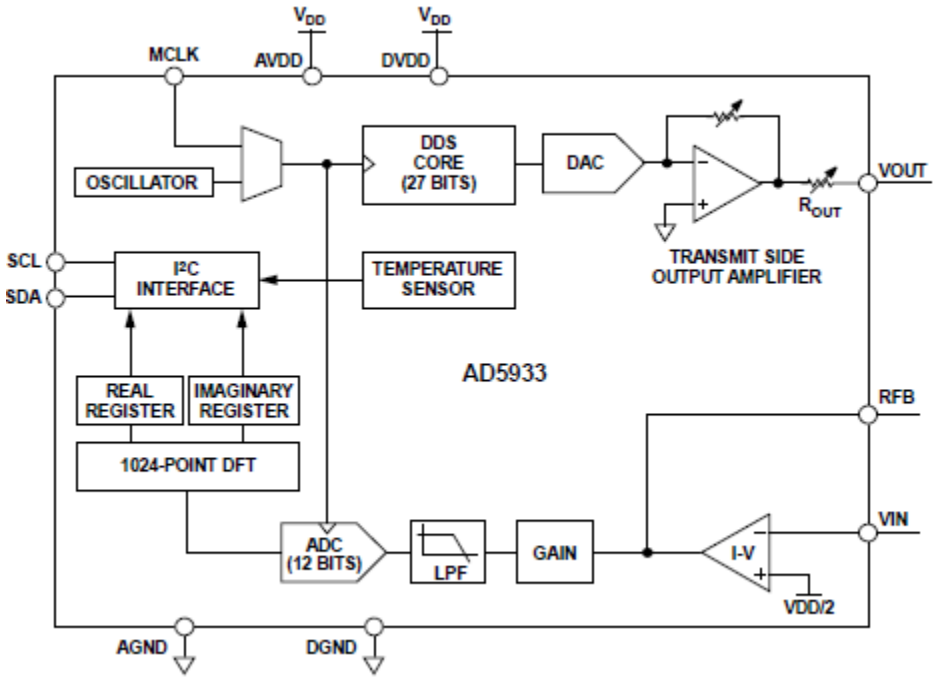

Figure 5.27. AD5933 evaluation board functional block diagram

To measure an unknown impedance *Z(ω)* which is connected between V_{out} and V_{IN} terminal of AD5933, a sinusoidal voltage is first used to excite the cell culture. The sine wave is digitally generated by a 27-bit Direct Digital Synthesizer (DDS) with the clock input of the synthesizer provided either by an external clock through a USB connection or internal clock. The generated waveform is then amplified through a programmable gain amplifier. Four output excitation voltages are generated through this method: 0.2, 0.4, 1.0 and 2.0 V. The output voltages are generated by setting the control register of programmable gain stage. The peak-to-peak and DC bias estimates of output voltages are shown in Table 5.1.

Table 5.6. Output Bias DC Voltage dependent of excitation voltage

Amplitude of excitation voltage	Output DC bias
2 V_{p-p}	1.5 V
1 V_{p-p}	0.75 V
0.4 V_{p-p}	0.3 V
0.2 V_{p-p}	0.18 V

In order to correct those output bias, and standardize them, a pair of op-amps is used as shown in Figure 5.6. The final bias voltage will be a DC voltage of $V_{DD}/2$.

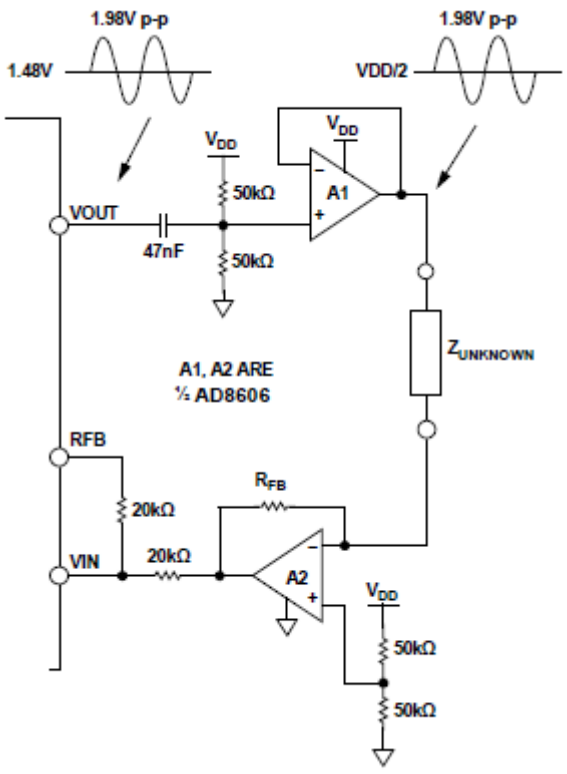

Figure 5.28. Unknown impedance interrogation stage

The block responsible for generating and applying the excitation voltage to the load is known as transmission block and is shown in Figure 5.7. The system offers a frequency resolution programmable by the user down to 0.1 Hz.

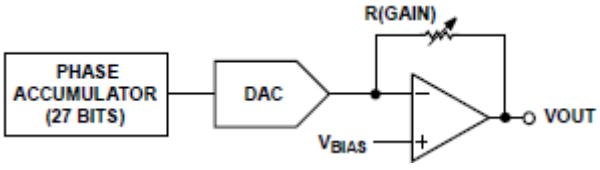

Figure 5.29. Transmit Stage

After the output excitation is generated and applied to the cell culture (unknown impedance), the resulting current is acquired and measured. The current is measured by using a current-to-voltage converter. The gain of current-to-voltage converter can be changed by varying the R_{FB} resistance. The resulting voltage is amplified using a programmable gain amplifier (PGA) by setting the gain to either 5 or 1. Figure 5.8 shows how the PGA output signal feeds the analog to digital converter device (ADC).

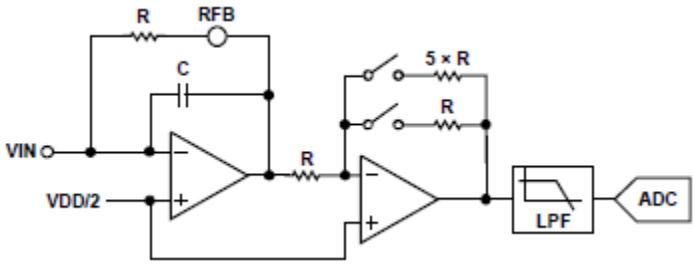

Figure 5.30. Receive Stage

Since the maximum sampling voltage of the ADC is V_{DD}, any voltage input greater than V_{DD} will cause saturation and the resulting measurement will be inaccurate. The final PGA output voltage is calculated as follows:

$$V_{out} = \left(V_{in}x\left(1+\frac{Rf}{Rg}\right) - V_{ref}x\left(\frac{Rf}{Rg}\right)\right)\cdot K_{PGA} = \left(\left(\frac{V_{DD}}{2}+V_p\right)x\left(1+\frac{RFB}{Z}\right) - \frac{V_{DD}}{2}x\left(\frac{RFB}{Z}\right)\right)\cdot K_{PGA} \quad (5.1)$$

Making some simplifications in the system and according to AD5933 datasheet, the value of the voltage that enters the ADC can be calculated by:

$$V_{out} = Output\ Excitation\ Voltage\ x\frac{RFB}{Z_{unknown}}\ x\ PGA\ Gain \quad (5.2)$$

Parameters, R_{FB} and PGA gain, have to be set correctly to schedule the expected impedance and the output excitation voltage such that ADC saturation is avoided. Knowing from literature that impedance of cell culture will range at 1-13kΩ [17-18], RFB can be selected in order to avoid problems of saturation.

In the final stage of impedance calculation, the digital data provided by the ADC are processed by an on-board DSP. The impedance can be calculated by using Ohm's law. The applied voltage (reference signal) is divided by the corresponding current generated by the unknown impedance (measured signal).

$$\frac{Signal_{ref}}{Signal_{meas}} = \frac{V_{out}(\omega)}{I_{in}(\omega)} = Z(\omega) \quad (5.3)$$

Digital Fourier Transform (DFT) is performed on the ADC data and the real and imaginary components of the impedance measured are stored in the chip data registers. The magnitude and phase of the measured impedance is calculated by:

$$Magnitude = \sqrt{R^2+I^2} \quad (5.4)$$

$$Phase = \tan^{-1}(I/R) \quad (5.5)$$

Phase and magnitude of impedance are transferred to computer for further processing. The final value of magnitude is multiplied by a gain factor. Before measuring any impedance, the

AD5933 must be calibrated and the gain factor has to be calculated. The calibration and gain factor calculation is performed to compensate for errors caused by the device electronic components such as time delay, attenuation, etc. The calibration and gain factor calculation is performed by connecting and measuring known impedance between V_{IN} and V_{OUT}. The impedance magnitude is measured by the device and the gain factor is calculated by using the following formula:

$$GF = \frac{\frac{1}{Z_{known}}}{Magnitude} \tag{5.6}$$

Finally, the value of the unknown impedance magnitude under measurement is calculated according to the following equation:

$$Z_{unknown} = \frac{1}{Magnitude \cdot GF} \tag{5.7}$$

The AD5933 desktop software (Figure 5.4) is used to calculate the GF and the final value of magnitude. The real and imaginary values from the data register are transferred to the software and processed to acquire the final results. Configuration of the AD5933 can be consulted in Appendix B.

5.4 Multiplexing Circuit Design

To make the switch between samples, the circuit in Figure 5.9 has been designed and assembled on a PCB. As can be seen from this Figure, some form of multiplexing is needed to connect the array of electrodes with the measurement system (switch array). In order to activate the switches and therefore be capable of differentiate between samples; a microcontroller is used to activate the switches s_1, s_2… in a specific sequence. When a switch is activated a specific electrode is connected. The pre coded program of the AD5933 makes possible to easily differentiate between E_1, E_2… E_N.

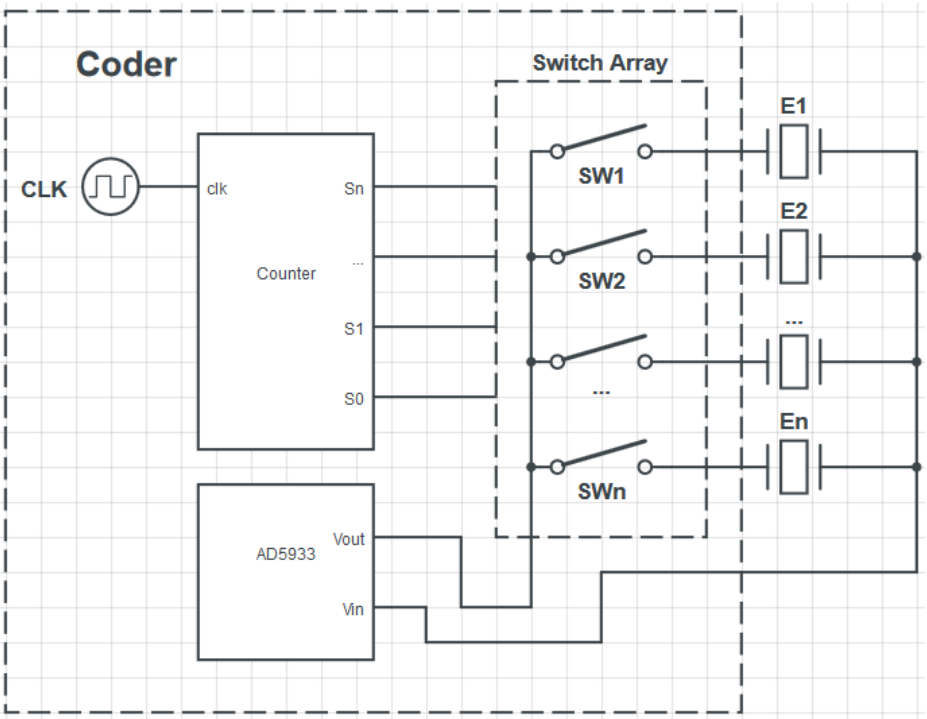

Figure 5.31. Proposed circuit of impedance coder

5.4.1 Circuit Components

The proposed solution for a 16 electrode array consists on a set of microcontroller signals, a push button, a standard FC20P output port, and a 16 channel analog multiplexer connected to the Analog Devices AD5933 (S1 and S2). This system is shown in Figure 5.10. The microcontroller controls the ON time for each switch (sets A, B, C and D), which in turn establish the connection with each electrode. The chips used in the design are 4 MC14066B quad bilateral CMOS switches connected to the electrodes. In order to demonstrate functionability of the setup, a PCB board was designed and printed to mount the chips (Figure 5.11 & 5.12). The fully assembled circuit (10 x 11 cm) is shown in Figure 5.13.

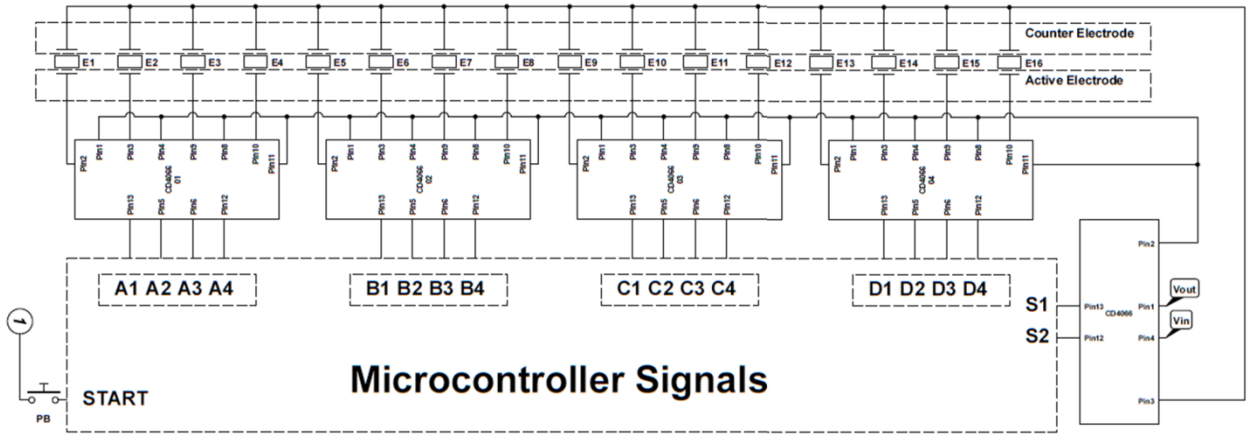

Figure 5.32. Block diagram of multiplexing system using MC14066B

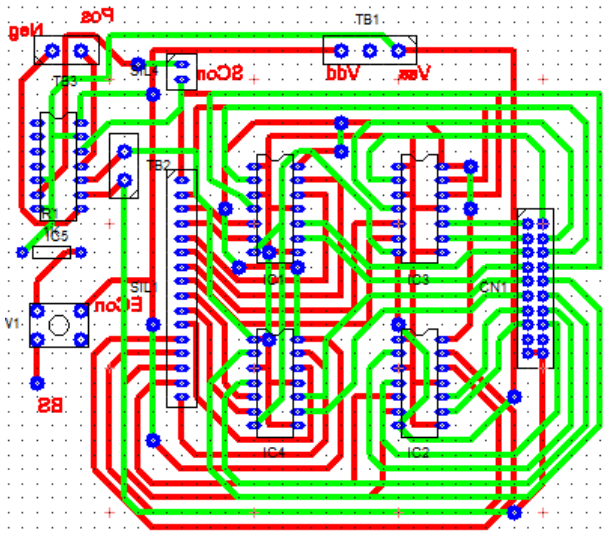

Figure 5.33. Designed board for multiplexing system using MC4066B

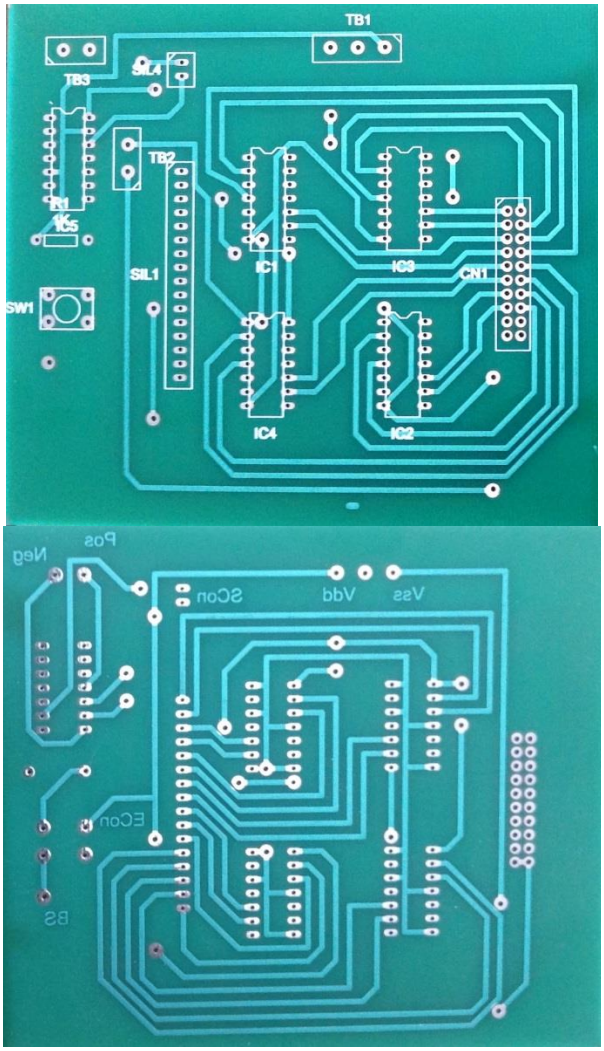

Figure 5.34. Printed PCB multiplexing system using MC4066B

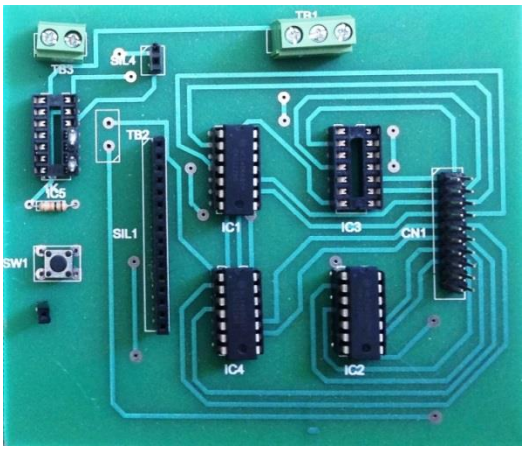

Figure 5.35. Assambled PCB multiplexing system using MC4066B

A simplification of the previously proposed system is also presented (even when not printed in a PCB). Such simplification uses a 74HC4067, 16 channels analog multiplexer IC instead of the 5 quad bilateral switches, and is presented due unexpected problems with the first design. This approach reduces the quantity of integrated systems and the probability of errors depending upon the activation each one of the bilateral switches. This option also reduces the quantity of signals and uses the already present V_{dd} and V_{ss} signals coming from the microcontroller. The V_{in} signal coming from the AD5933 is the signal that is connected to the 74HC4067 *Z* reference signal, letting pass the desired sinusoidal signal only to one electrode at a time. This new system is shown in Figure 5.14, and the full design of the PCB is shown in Figure 5.15.

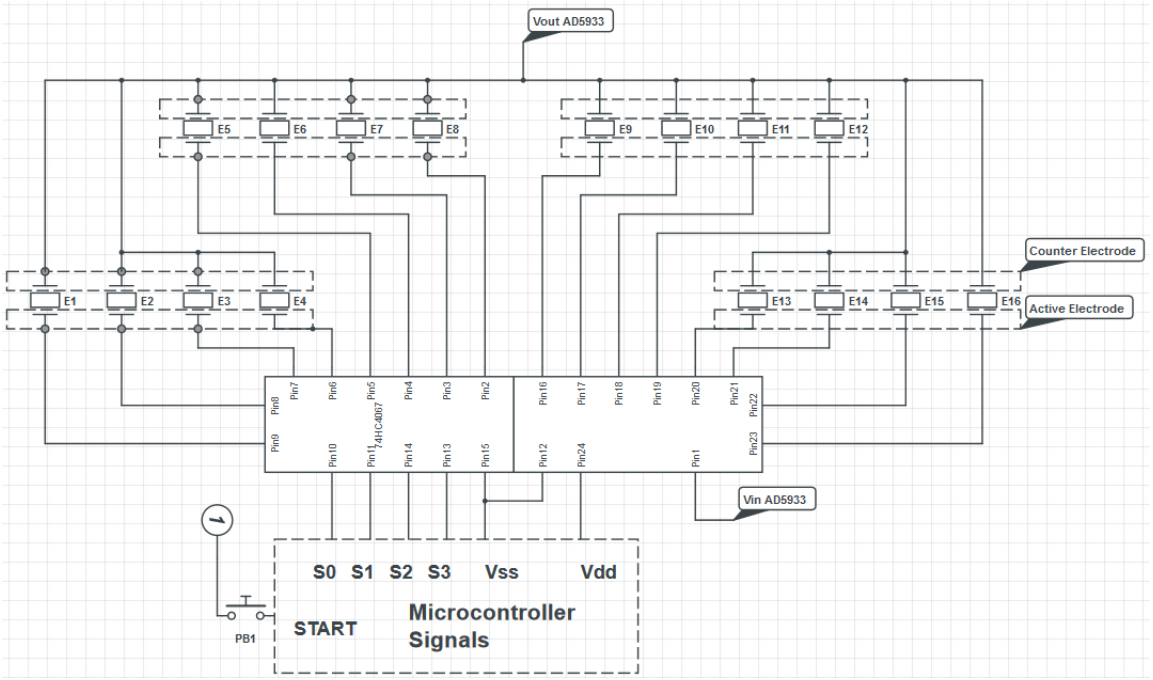

Figure 5.36. Block diagram of multiplexing system using 74HC4067

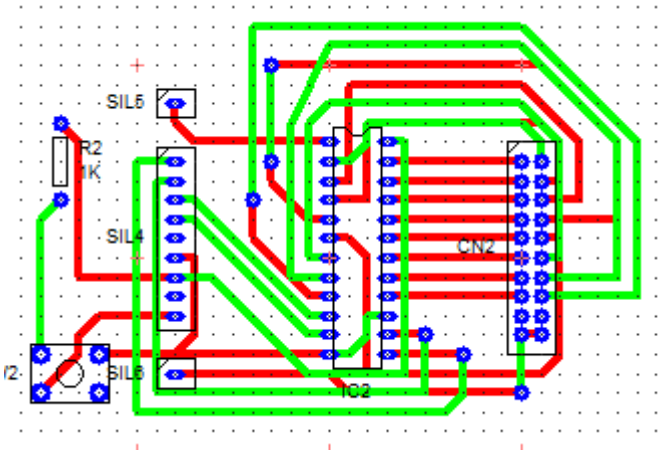

Figure 5.37. Designed board for multiplexing system using 74HC4067

5.4.2 Control System

The control system signals mentioned before (circuit using the 74HC4067) are implemented using a program developed in an Arduino microcontroller. The switching is controlled through a pre-established value of time that has to be actualized in every configuration of impedance sweep and that is obtained during the calibration of the system (for the experiments done, t_{ON} = 25 s). In the simplified system the application uses 6 output control signals, 4 of which are control signals for the multiplexer coder and 2 connecting ground and V_{dd}, and 1 input signal for a push button that start the control program. Definition of the connections of the pins in shown in Table 5.2.

Table 5.7. Port and signal configuration of the Arduino board

Port	Type	Signal
D0	-	-
D1	-	-
D2	-	-
D3	-	-
D4	-	-
D5	-	-
D6	-	-
D7	-	-
D8	-	-
D9	-	-

Port	Type	Signal
D10	-	-
D11	-	-
D12	-	-
D13	-	-
A0	Output	S0
A1	Output	S1
A2	Output	S2
A3	Output	S3
A4	-	-
A5	Input	PB

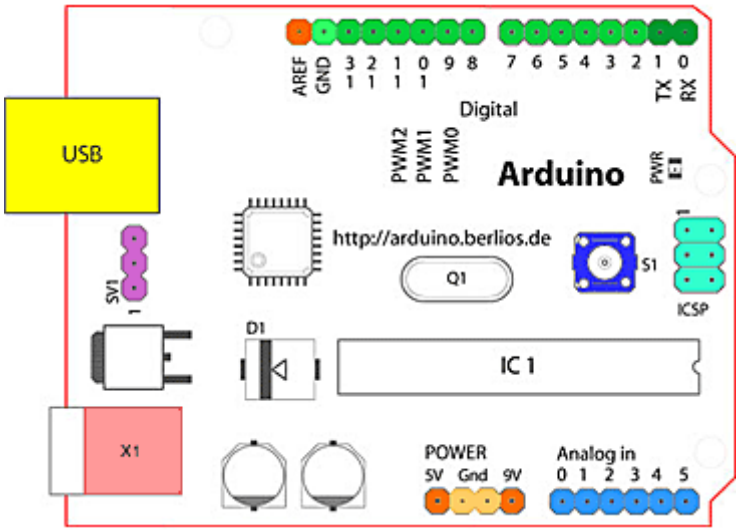

Figure 5.38. Arduino board architecture

5.5 Experimental Result

As reviewed in Chapter 1, the change in impedance is due the change of pathway of the electrical fields over the electrode due to the presence of an analyte. As suggested in [19] and taken as an example for the EIS experiment in [20], the first measurement to be done is the initial impedance of cell culture medium. Electrodes will be immersed in an ionic cell culture medium with high conductivity (DMEM-12 10% SFB), which form a resistor $R_{med}/R_{sol}/R_s$. The cell culture medium also creates an electrectrified double layer or a capacitance representating the electric behavior of the medium or C_{med}. The series network of R_{sol} and C_{med} forms the equivalent circuit without cells shown in Figure 5.17.

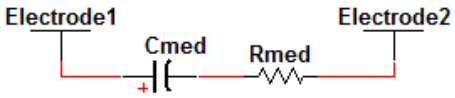

Figure 5.39. Cole model for culture medium

After all the presented models in Chapter 3 and 4, the final used models are the ones of Wang [4] and Yúfera [21]. Wang [4] proposes the model in Figure 5.18, where the only components of the impedance are the solution resistance (R_{sol}) and the double layer capacitance created between the electrode and the media (C_l/C_{DL}). In accordance with Yúfera model in Figure 5.19, a visual "simplification" of Figure 5.18, for the two-electrode sensor the variables are: A as the sensing area of e_1 and $Z(w)$ as the impedance by unit area of the empty electrode (without cells on top). In this model, the capacitance and media resistance are modeled as impedance per area unit dependent upon the frequency; and at high frequencies, R_S/R_{sol} would turn dominant.

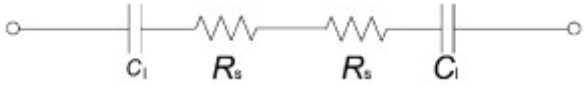

Figure 5.40. Electrical model of wells filled only with media

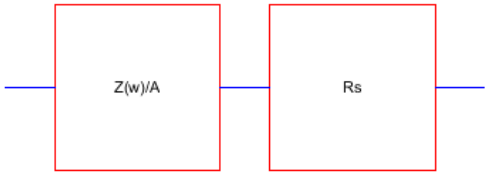

Figure 5.41. Simplification for Figure 5.18 electrical model by Yúfera [21]

According to Van Gerwen [22], R_{sol} can be approximated with the following formula using physical variables of the electrodes (Figure 5.20) and the electrolyte:

$$R_{sol} = \frac{1}{nl} \cdot \frac{1}{\kappa} \cdot \frac{2K\left(\sin\frac{\pi w_{sp}}{2L}\right)}{K\left(\cos\frac{\pi w_{sp}}{2L}\right)} \tag{5.8}$$

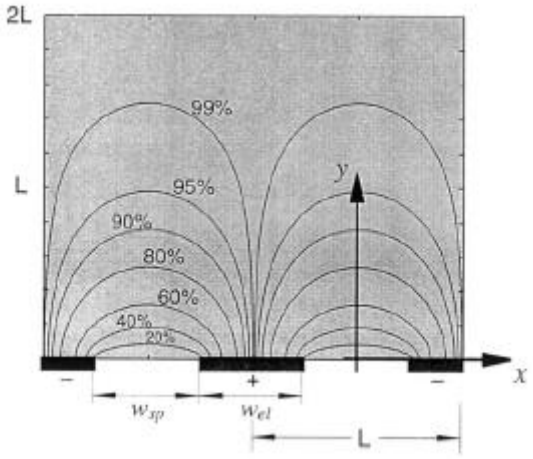

Figure 5.42. Electrode physical characteristics and calculated current comprisement of interdigitated electrodes [22]

Where κ is the conductivity of the solution and n the number and l the length of the fingers of the interdigitated electrodes. Based in R_{sol}, is possible to determine the changing value of capacitance over the frequency range having the impedance measurements:

$$C_{med} = \frac{1}{w \cdot \left(Z^2 - R_{sol}^2\right)^{\frac{1}{2}}} \tag{5.9}$$

In the same manner than the electrode electrolyte model, the model used when cells are inoculated over the electrode, the used models are from Wang and Yúfera [4, 21], where the given impedance comes per area unit and as a difference between the measured value and the electrode electrolyte model. According to Wang [3] the cell culture over planar electrode could be modeled as the circuit in Figure 5.21 (c), due to the fact that interdigitated electrodes are used two cells have to be modeled. The system could be divided in two parts, at high frequencies Figure 5.21 (a) will dominate and at low frequencies the series resistances shown Figure 5.21 (b) will become dominant. According to Yúfera model [21], when the electrode is partially covered by cells in a surface A_c, $Z(w)/(A-A_c)$ is the electrode impedance associated with the area not covered by cells, and $Z(w)/A_c$ is the impedance of the area covered. R_{gap} models the current flowing laterally in

the electrode-cell interface, which depends on the electrode-cell distance at the interface (in the range of 15-150 nm) as showed in the previous sections. R_s is the spreading resistance through the conductive solution. Due to be complicated to determine the specific coverage of each electrode, it is implied according to the hyperboelastic growth model the coverage of the electrodes by cells. Parameter *ff*, called the fill factor, can be zero for $A_c=0$ (e_1 electrode empty), and 1 for $A_c=A$ (e_1 electrode full); and is used to study the difference between impedances while different percentages of the active area is covered. Presented impedance will be the division between the measured impedance and the active electrode area.

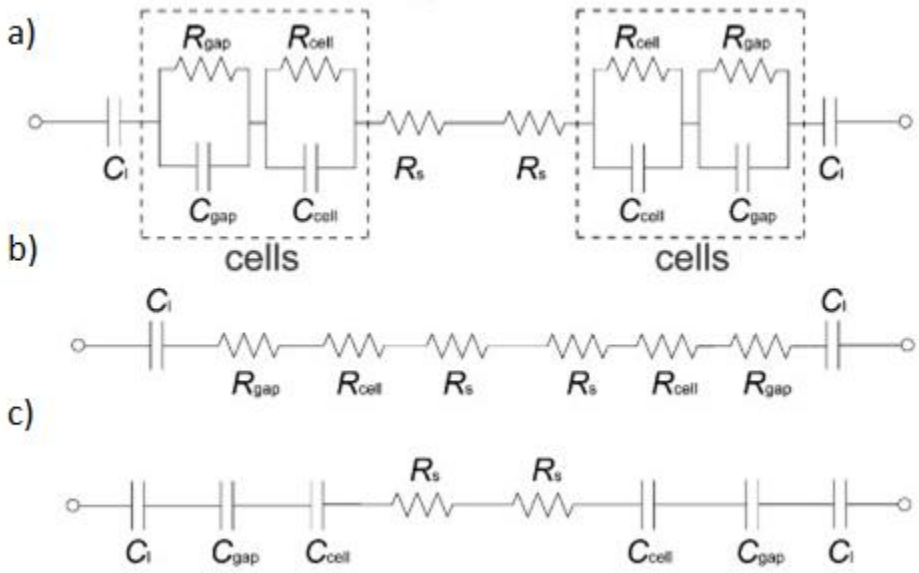

Figure 5.43. Electrical model of wells with cultured tissue over them [4]

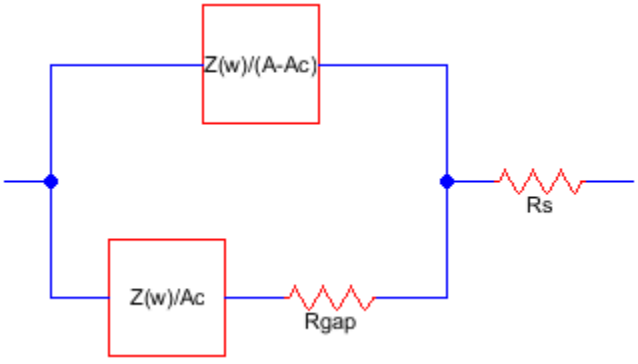

Figure 5.44. Electrical model for cell covered microelectrodes used by Yúfera [21]

When both systems had been obtained, the simple covered electrode by media, the presence of cells in the holder and its growth changes of electrode impedance, it is possible to model the final form. As suggested by Siddiquei [19], the impedance changes due to cell growth can be described in a normalized form as in (5.10) and in its capacitive and resistive components as suggested in (5.11).

$$\mathrm{Z_{cell}} = \frac{\mathrm{Z - Z_{initial}}}{\mathrm{Z_{initial}}} \tag{5.10}$$

$$Z_{cell} = Z - Z_{initial} = R_{cell} + jX_{C_{cell}} \tag{5.11}$$

Where $Z_{initial} = R_{med} + jX_{C_{med}}$ and $Z = R + jX$. The dielectric membrane of rSCs exhibits a capacitance still to be determined in order to achieve an approximation using this method. The total impedance of the system is a combination of the cells capacitance C_{cell} and the resistance of the rSCs, R_{cell}. Change in impedance values will be observed when addition, movement or growth of cells takes place. The total impedance, Z_{tot} can be also be described using (5.12).

$$\mathrm{Z_{tot}} = \mathrm{R_{med}} + \frac{(\mathrm{x_{C_{cell}} + R_{cell}})\mathrm{x_{C_{med}}}}{\mathrm{x_{C_{cell}} + x_{C_{med}} + R_{cell}}} \tag{5.12}$$

References

[1] Giaever I, Keese CR. **"A morphological biosensor for mammalian cells,"** *Nature*, 366, 1993.

[2] Wang P, Liu Q. (Eds.) (2010) *Cell-Based Biosensors Principles and Applications: Electric Cell-Substrate Impedance Sensor (ECIS) as Cell-Based Biosensor.* Norwood, MA: Artech House. pp. 155-156.

[3] Applied BioPhysics Inc. 2013. Consulted on: www.biophysics.com

[4] Wang L, et al. **"Analysis of the Sensitivity and Frequency Characteristics of Coplanar Electrical Cell-Substrate Impedance Sensors,"** *Biosens. Bioelectron,* vol. 24, no. 1, pp. 14-21, 2008.

[5] Borkholder DA (1998) *Cell Based Biosensors Using Microelectrodes.* Doctoral Dissertation.

[6] Arndt S, Seebach J, Psathaki K, Galla HJ, Wegener J. **"Bioelectrical impedance assay to monitor changes in cell shape during apoptosis,"** *Biosens. Bioelectron*. 19, pp. 583-594, 2004.

[7] Lo CM, Keese CR, Giaever I. **"Impedance Analysis of MDCK Cells Measured by Electric Cell-Substrate Impedance Sensing,"** *J. Biophys.*, vol. 69, no. 6, pp. 2800-2807, 1995.

[8] Bagnaninchi P, Drummond N. **"Real-time label-free monitoring of adipose-derived stem cell differentiation with electric cell-substrate impedance sensing,"** *PNAS,* vol. 108, no. 26, pp. 6462-6467, 2011.

[9] Applied BioPhysics, Inc. (2009) *ECIS® Handbook.* Retrieved from http://www.biophysics.com/publications/ECIS%20Handbook.pdf

[10] Giaever I, Keese CR. **"Micromotion of mammalian cells measured electrically,"** *Proc Natl Acad Sci USA*, 88, pp. 7896-7900, 1991.

[11] McKee T. *Biochemistry: An Introduction.* McGraw-Hill Education, 1999.

[12] Marquette CA, Lawrence MF, Blum LJ. **"DNA covalent immobilization onto screen-printed electrode networks for direct label-free hybridization detection of p53 sequences,"** *Anal. Chem.,* vol. 78, no. 3, pp. 959-964, 2006.

[13] Ansede A (2010) *A Feasibility Study of the Suitability of an AD5933-based Spectrometer for EBI Applications.* Master Thesis.

[14] Ibáñez D (2008) *Implementation of an Electric Bioimpedance Monitoring System and a Tool for Bioimpedance Vector Analysis*. Master Thesis.

[15] Rösner A, Frank T, Tobehn I, Steinke A. **"Bio Instrumentation for Determining the Viability of Cells on the Basis of the Impedance Measurement,"** *MME 2012*, 2012

[16] Analog Devices AD5933 Data Sheet. Retrieved from http://www.analog.com/en/rfif-components/direct-digital-synthesis-dds/ad5933/products/product.html

[17] Keese CR, Giaever I. **"A biosensor that monitors cell morphology with electrical fields,"** *Engineering in Medicine and Biology Magazine*, vol. 13, no. 3, pp. 402-408, 1994.

[18] Cole KS. *Membranes, ions, and impulses.* Berkeley: University of California, 1968.

[19] Yiling Q (2010) *Impedance sensing for cellular response studies*. Master Thesis, Boston University, Boston, MA.

[20] Siddiquei H, et al. **"Electrical cell-substrate impedance sensing (ECIS) based biosensor for characterization of DF-1 Cells,"** in *IEEE International Conference on Computer and Communication Engineering, 2010*, pp. 1 – 4, 2010.

[21] Yufera A, Olmo A, Daza P, Cañete D (2011). *Cell Biometrics Based on Bio-Impedance Measurements. Advanced Biometric Technologies*, Dr. Girija Chetty (Ed.) Retrieved from: http://intechopen.com/books/advanced-biometric-technologies/cell-bioemetrics-based-on-bio-impedance-measurements

[22] Van Gerwen, P, Laureyn W, et al. **"Nanoscaled interdigitated electrode arrays for biochemical sensors,"** *Sensors and Actuators B Chemical*, vol. 49, no. 2, pp. 73-80, 1998.

CHAPTER 6 – BIOLOGICAL TEST RESULTS

This chapter describes the experiments and results performed with the cell cultures. The first section covers the description of the experiments and some problems that arose during this experimentation phase. Following section analyses the obtained data to determine the cell and media parameters utilizing electrical models. The third section compares the cell growth model with the experiment results to determine if the behavior of the impedance matches with the expected population of cells through time. The fourth section analyzes the differentiated stem cells obtained after the experiment. Finally, a comparison between induced and non-induced cells is presented to characterize differentiation and observations through impedance curves.

6.1 Experiments and Observations

During the biological tests, the proposed methodology was implemented. Four experiments using 2 well arrays were undertaken under a month of experimentation. Every experiment lasted around 7 days as suggested by Bagnaninchi [1] with the objective of observe if there is a relevant change of impedance that can be used to monitor cell growth and differentiation in real-time. The first 4 days, the cells were expanded in culture using DMEM-12 SFB 10% as culture media, and the last 3 days induction media was used to promote differentiation into dopaminergic or motor cells. Selection of wells to be differentiated or used as control, were not selected until the 4 day. Each experiment consisted in taking real time and impedance measurements of the 8 8W10E+ Applied BioPhysics culture wells. Once finished the experiments, and during the following 2-3 days, the wells were prepared to and analyzed using fluorescent microscopy. Figure 6.1 shows the culture distribution after and before induction in both experiments.

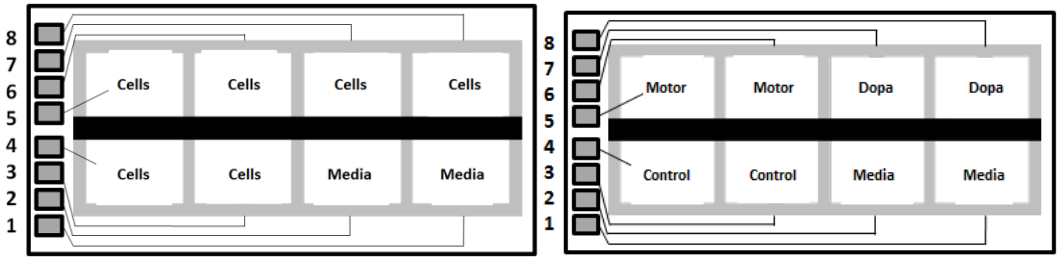

Figure 6.45. Culture distribution before (left) and after induction (right)

***X stands for non-usable wells, Dopa for dopaminergic cells, Motor for motor cells, and Control and Cells for undifferentiated stem cells**

Measurements were performed each minute, which translates to around 10080 individual sweep measurements and approximately 1260 per well, it is important to mention that a lot of treatment of data is needed to present results as raw total data contains more than 12 million data cells of information per experiment. Post processing of data was performed using MATLAB functions and GraphPad Prism analysis. Appendix C contains those MATLAB functions and GraphPad Prism analysis used to process raw data.

Additionally and in order to determine the proper health of the culture, a parallel tissue culture was maintained in BD™ 25 cm^2 flasks during the experiment in the culture arrays. This parallel

culture was the reference or control as in previous experiments the culture did not grow due to an inefficient freezing process. Inverted microscope analysis was used to determine if the culture was growing properly over the flasks; it was determined that if the cultures were growing in the flasks they should also be growing properly in the culture wells. Figure 6.2 shows the expected evolution of a culture in a BD™ 25 cm^2 flask; Figure 6.2(a) shows the culture after inoculation and Figure 6.2(b) the state of it at the seventh day in culture.

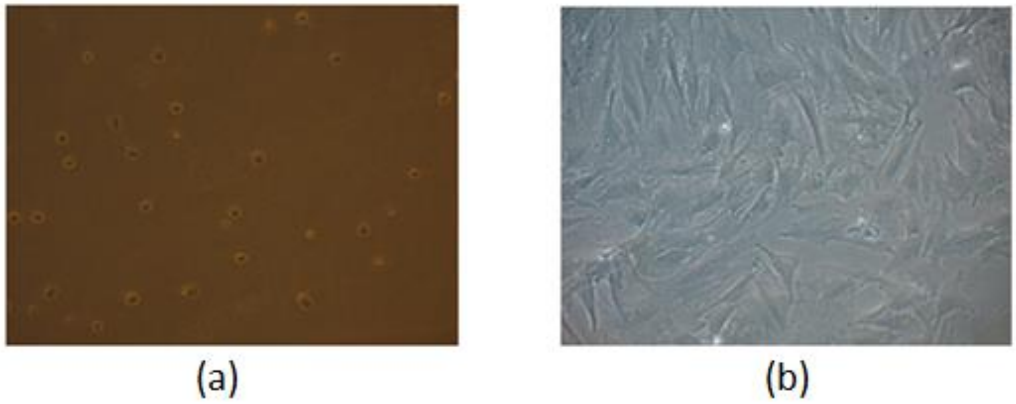

Figure 6.46. Expected evolution of control tissue culture after inoculation (a) and at the seventh day (b)

6.2 Problems during Experimentation

Some problems were obtained during the experiment phase. One of the problems had to do with the first version of the proposed circuit to measure the impedance change (first two experiments). The circuit was not measuring in real time the change of impedance in the culture. This is, the only measurement obtained during the first three experiments were open circuits (Figure 6.3). A simplified solution was to use a 74HC4052 4 channels multiplexer instead of the 74HC4067 16 channel multiplexer.

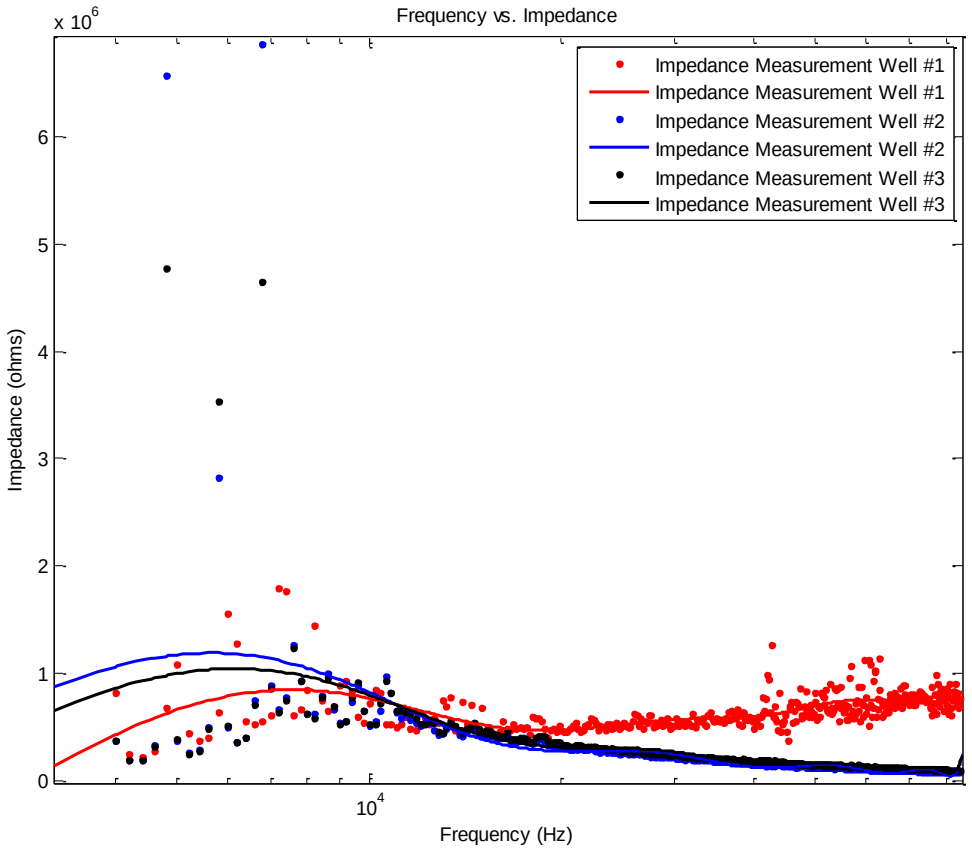

Figure 6.47. Impedance measurements (open circuits) using proposed solution

Nevertheless and due to the initial characteristics of the first proposed system, the necessity of lots of post processing of the data, and persistent problems with the used computer, this change was not made until the last stages of the last experiment. The modification also reduced the quantity of information to be gathered to only 4 wells per experiment. Figure 6.4 shows the configuration of the final system. Another problem surged when the data from day 0-2 was lost due to misconfiguration of the new simplified system and problems with the computer controlling the microcontroller and the acquisition card. However, this last problem did not represent a problem; because cell's differentiation could still be analyzed as it started until day 4. Cell growth was monitored as the impedance kept changing in the 5 days the measurements took place.

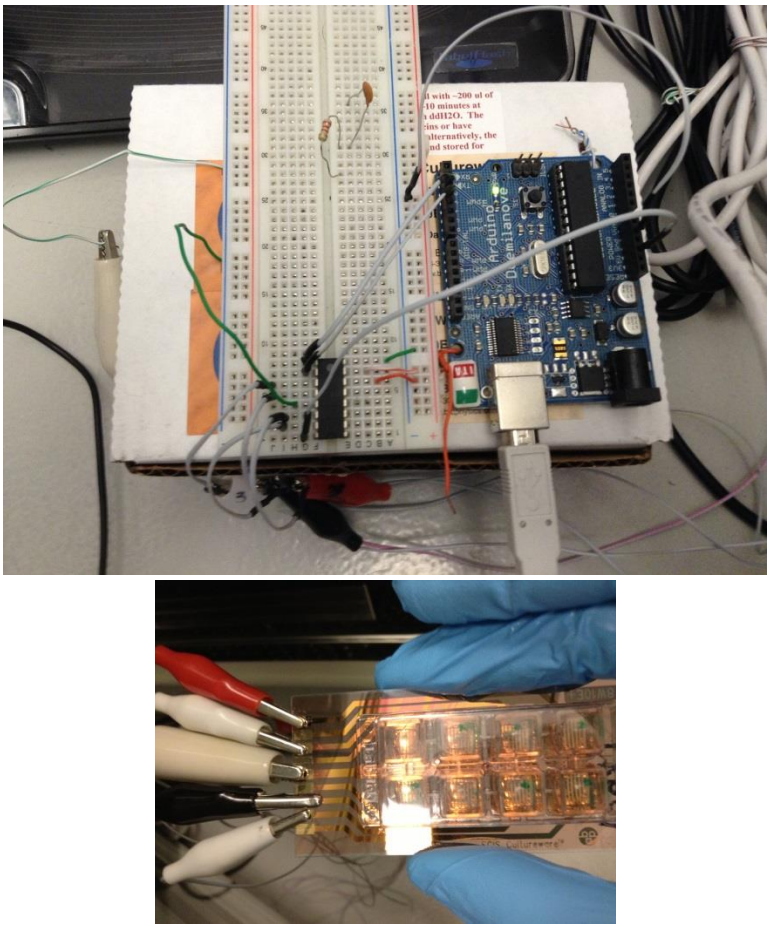

Figure 6.48. Simplified solution configuration: circuit connection (upper) and electrode connection (lower)

Before conducting the experiments two cell cultures were made in the 8W10E+ culture wells, one with a cell anchoring solution and one without a cell anchoring solution. This test was done in order to determine if the cells used could attach to the wells without a specific protein. The results gave the expected information. It was discovered that prior cell inoculation wells must be coated with a cell anchoring solution; otherwise, the cells would not properly anchor to the bottom as it happens in the pre-coated culture flasks and wells with anchoring solution. Figure 6.5 shows the anchored and not anchored cells in the wells.

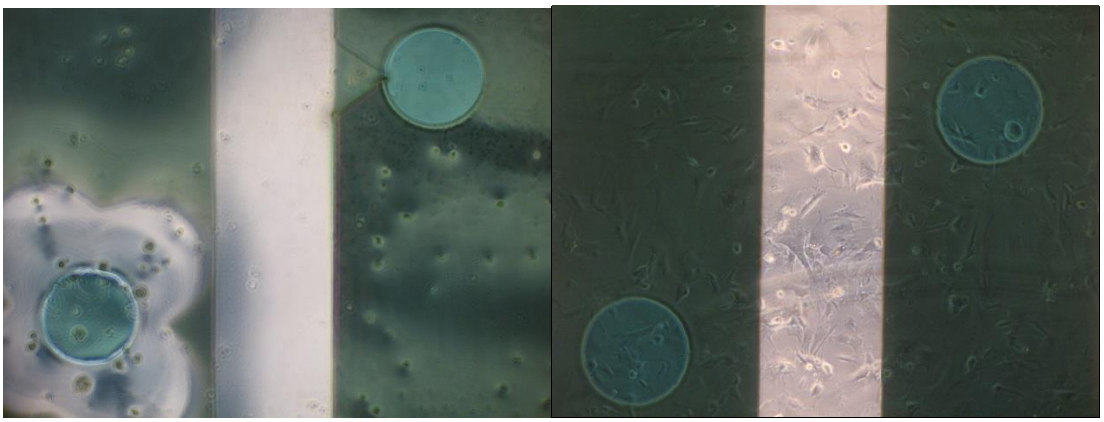

Figure 6.49. Non anchored cells in a well with burnt electrode (left) and anchored cells (right)

By simple inspection after using various culture arrays, it was also found that the microelectrodes and the arrays presented anomalies; Figure 6.6 and 6.7 show these anomalies. Figure 6.6 illustrates how the array is not standardized, even when the separation between the gold connectors is standard. This made difficult the interconnection using the FC20P connector. The original design took into account that the array connections, including the thin layer of plastic, size and distribution were standard; these small differences in the cutting made impossible for the FC20P to connect properly each and every array.

Figure 6.50. Non-standard array cutting

Figure 6.7 shows the most interesting anomaly, the presence of burnt electrodes. This problem was present during all the experiments, for the complex and simplified design, with a ratio of 1:8 wells in every array (commonly rendering just 7 wells usable per array). This problem could not be pinpointed as it presented some times after and some others before the inoculation of cells.

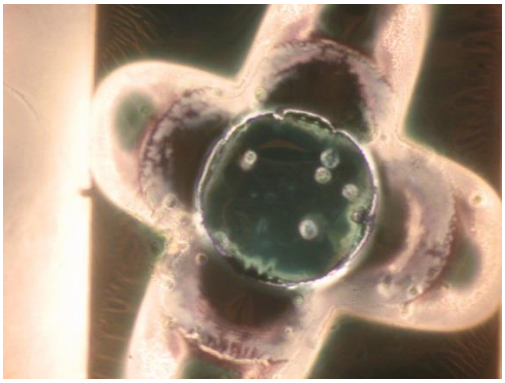

Figure 6.51. Burnt electrode (inverted microscopy x10)

Another important discovery is that the arrays have specific reactions to ethanol. Figure 6.8 shows the two reactions that could be seen during the experiments. In the first, if ethanol touches the upper surface of the array and then is put in incubation, the plastic covering and the gold roads will eventually crack, taking from 2 to 4 days, rendering the array unusable. In the second, if ethanol touches the connection ports in the array and then enters in contact with the FC20P metal connectors, the gold in the connection ports will lift up and get stick to the metal connectors. It is believed that a chemical reaction that is not in the scope of this work takes place; and while it was not further studied, knowing this, it is imperative to avoid the contact between ethanol and the upper surface of the electrode array.

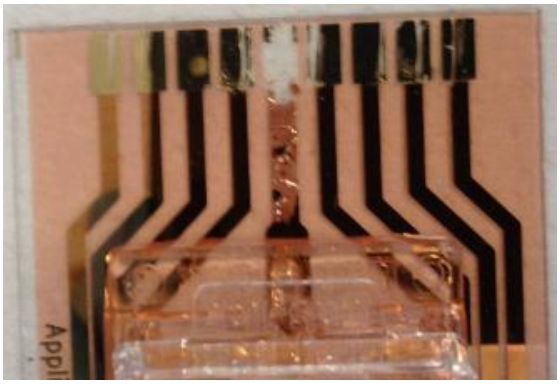

Figure 6.52. Arrays reactions to ethanol

6.3 Parameter Extraction

To obtain the parameters for the media, electrical models presented in Chapter 3 and 4 are used. The first parameters to be obtained are the ones of the wells were only media is present, as the parameters of the cells can be obtained easily if media parameters are known. To determine such parameters, the sets of frequency sweeps over time measured from the without cells is averaged and shown in Figure 6.13. This approximation can be taken because is expected that the impedance measurement over the electrodes covered by only media is constant due that the lack of introduction of another analyte that may change the value. In Figure 6.9- 6.12 is possible to see that the value of impedance of the media changes in time, probably due noise or decay of the media. Thus, the value can be considered constant in time.

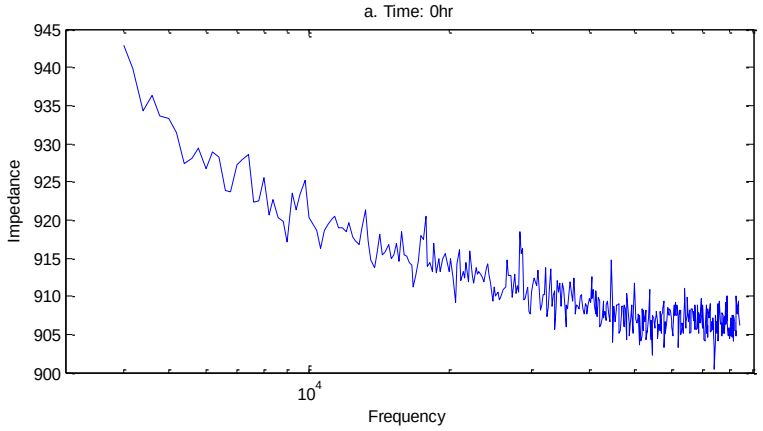

Figure 6.9. Media impedance measurements time 0 hr

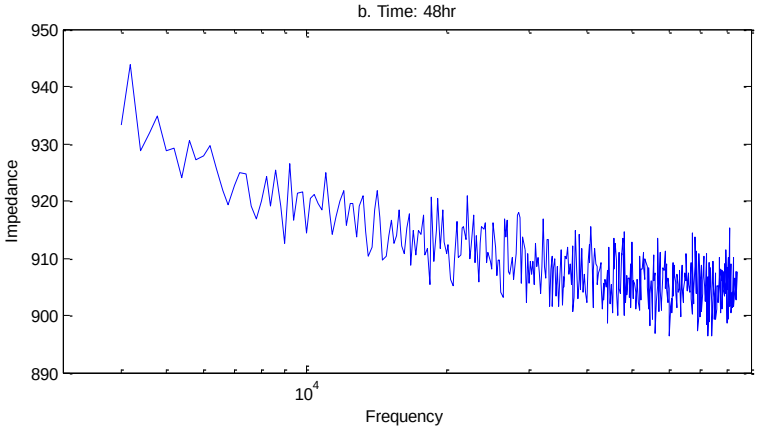

Figure 6.10. Media impedance measurements time 48 hr

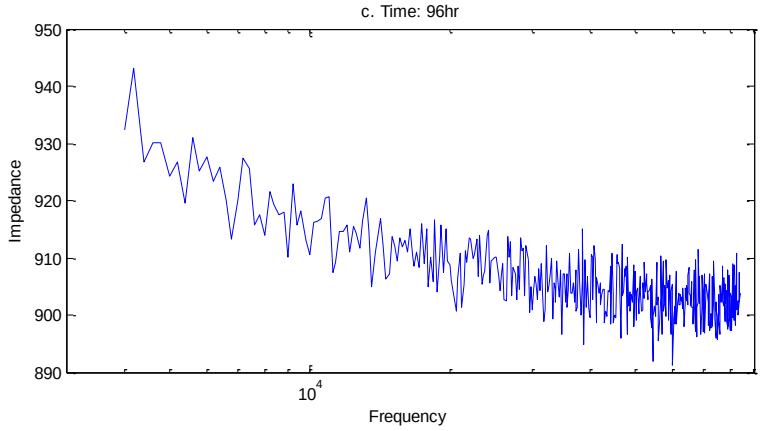

Figure 6.11. Media impedance measurements time 96 hr

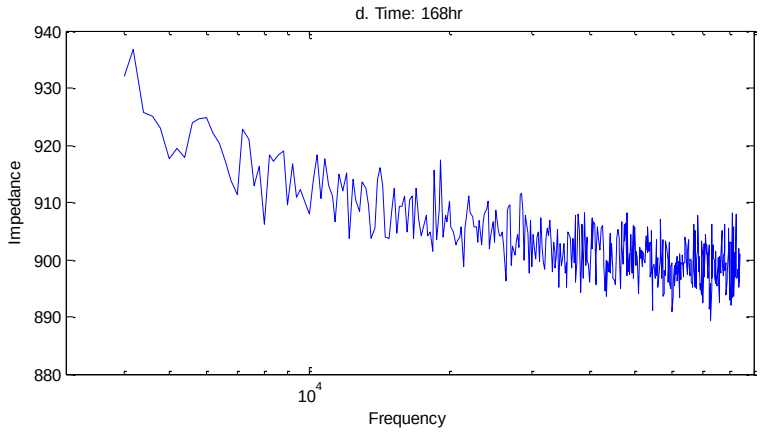

Figure 6.12. Media impedance measurements time 168 hr

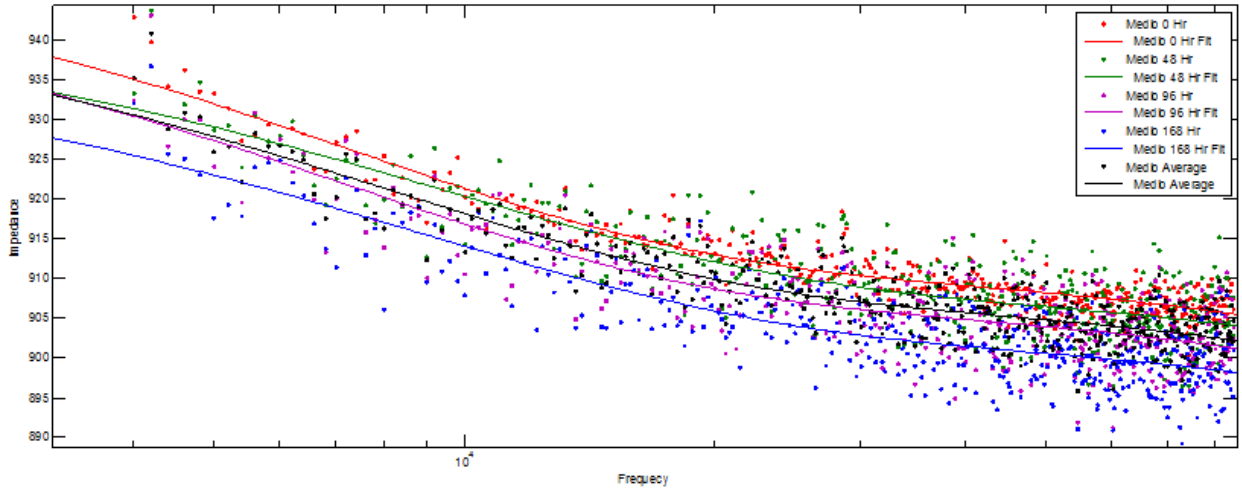

Figure 6.53. Fit of media impedance measurements and average media value in time

Exponential decay equations are used to fit the data using MATLAB and GraphPad Prism. It is of special interest the value of R^2 or *coefficient of determination* that indicates how good is the fit (R^2=1 means a perfect fit). Media average value fit using MATLAB shows a R^2 coefficient of 0.7939 using the equation and parameters (6.1). Figure 6.14 shows the exponential decay equation fit obtained in MATLAB.

$$f(x) = a \cdot \exp(b \cdot x) + c \cdot \exp(d \cdot x) \tag{6.1}$$

a	0.1438
b	-2.928
c	905.2
d	-0.001863

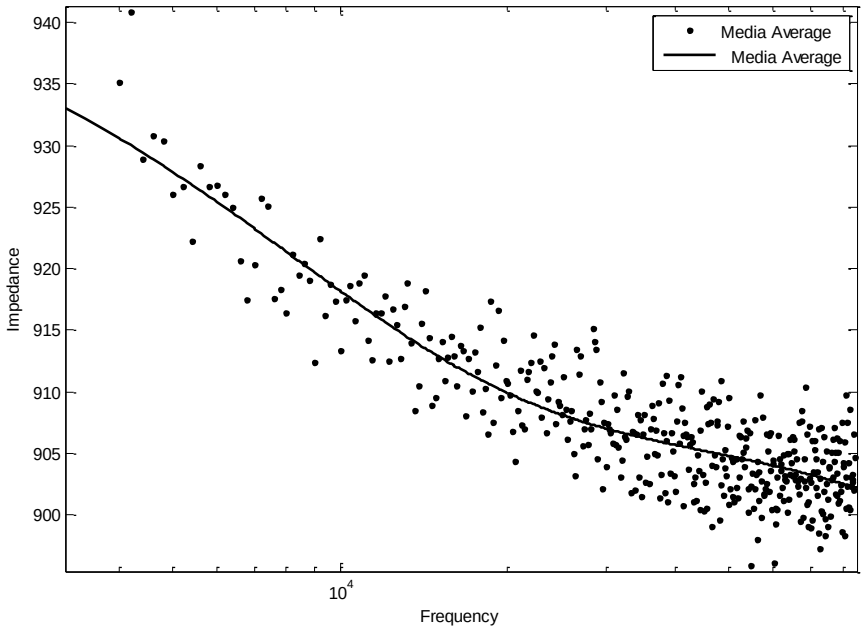

Figure 6.54. MATLAB fit for media average impedance measurements

Using GraphPad Prism fit, R^2 is equal to 0.7871, which is quite similar to the obtained using the MATLAB fitting tool. The equation and parameters (6.2) were used in the GraphPad Prism fit. Figure 6.15 shows the exponential decay equation fit obtained in GraphPad Prism.

$$f(x) = (f(0) - plateau) \cdot \exp(-k \cdot x) + plateau \tag{6.2}$$

f(0)	937.5
plateau	903.5
K	7.912e-5

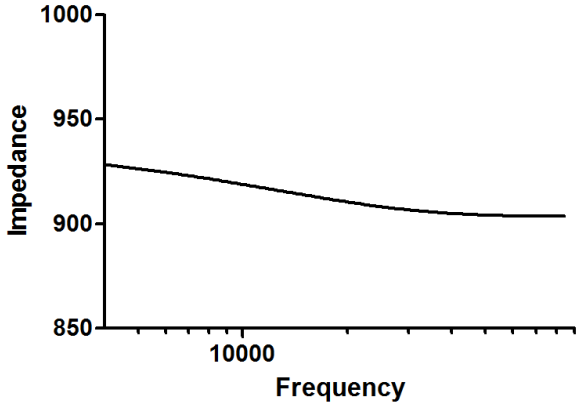

Figure 6.55. Prism fit for media average impedance measurement

Comparing the two graphs, Figure 6.14 shows that the MATLAB fit is clearer, but it never reaches a plateau; MATLAB linearization follows a more *"free"* path and the Prism fit is constricted to the final plateau. The behavior in the MATLAB fit shows that if the frequency increases, the impedance decreases, which would not happen in reality in the window of interest. The similarity

in the R^2 and its value is because the data to be fit has too many noise and is difficult to linearize every point in it. Linearization in Figures 6.14 and 6.15 are quite alike which suggests that both can be used in the parameter extraction.

As mentioned in Chapter 3 and 4, the resistance and capacitance could be found using a combination of the models proposed by Wang and Aliakbar based in either of these exponential equations [2-3]. Such models propose R_{sol} can be considered dominant at the highest frequency; and that one, is a point that is possible to find with the presented fits. R_{sol} value can be obtained inspecting the average final point of both fits (the plateau). As can be seen, obtaining such value is easier in the Prism fit as it already takes into account such value. Knowing R_{sol} and the impedance used to graph Figure 6.10, is possible to calculate an approximation to the medium capacitance using Equation 6.3.

$$R_{sol} \approx 903.5\Omega$$

$$Z^2 = R_{sol}^2 + \left(\frac{1}{j\omega C_{med}}\right)^2 \therefore C_{med}^2 = \frac{1}{(Z^2 - R_{sol}^2)*\omega^2} \tag{6.3}$$

$$C_{medprom} = 0.45888\mu F$$

According to this obtained value, is possible to graph the actual expected curve of impedance for the simplified electrical model shown in Figure 6.16. Curve in Figure 6.17 is congruent with the values and shape reported by Seriburi for gold electrodes covered with media and without cells using ECIS technology [4].

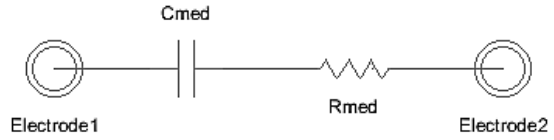

Figure 6.56. Simplified electrical model with Cmed=0.45888µF and Rsol=903.5Ω

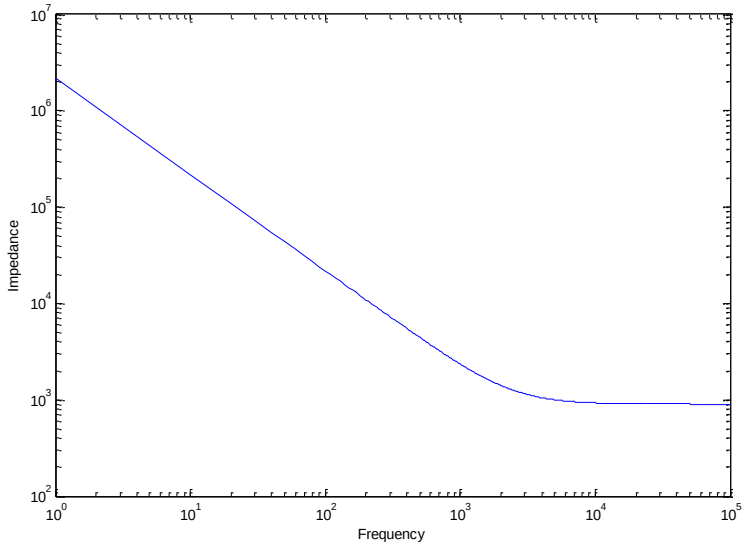

Figure 6.57. Expected impedance curve with electrical model

6.4 Detection of Cellular Growth through Bioimpedance

Due to the previously mentioned problems, the analysis of growth is made in the span of time from day 2 to day 7 of the experiment. According to Bagnaninchi [1] it should be the most interesting span of time because it's the moment when the population of cells over the electrodes starts growing significantly. Initially seeded with 50,000 cells, by this moment each seeded well should hold an average cell population of approx. 200,000 cells, by the end of day four approx. 800,000 cells, and it should stay stable at around $1.6X10^6$ cells per well according to Yúfera [5]; however, such values may not reflect the real quantity of cells in the wells as the percentage of anchored cells is not the 100% of the seeded cells.

Analysis of impedance vs. time and impedance vs. frequency are made to obtain both the curve of impedance change that comes with the change of frequency over the electrode and to characterize the growing cell monolayer. Figure 6.18, 6.19 and 6.20, show the obtained surfaces in well 1, 2 and 3 respectively during a span of 45 hr. These graphs are the combination of previously mentioned parameters in order to obtain surfaces that characterize the impedance growth. Two major analyses can be made in each graph, impedance vs. time and impedance vs. frequency. Using impedance and frequency is possible to analyze the response of the culture at a sweep of frequencies at a given time; and using Impedance and Time is possible to analyze the response of the culture at a specific frequency. As a whole it is possible to see in these surfaces that the changes in impedance are more visible at frequencies under the 10k and that as time pass the impedance in the culture grows which is expected and a direct representation of cellular growth.

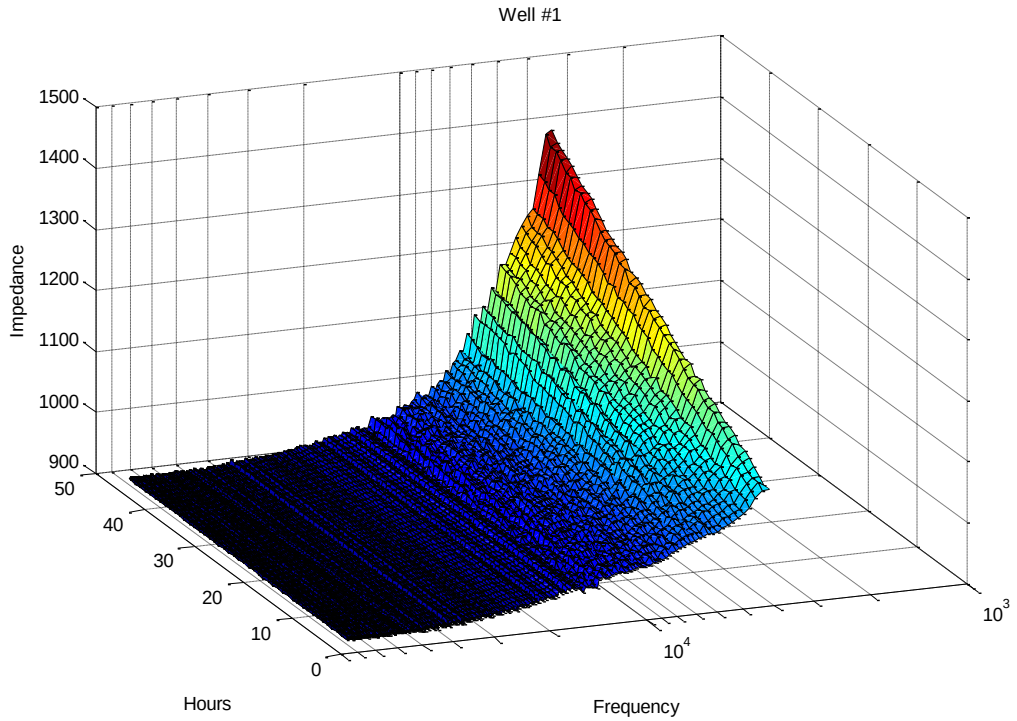

Figure 6.58. Surface of impedance change in time and frequency in well #1

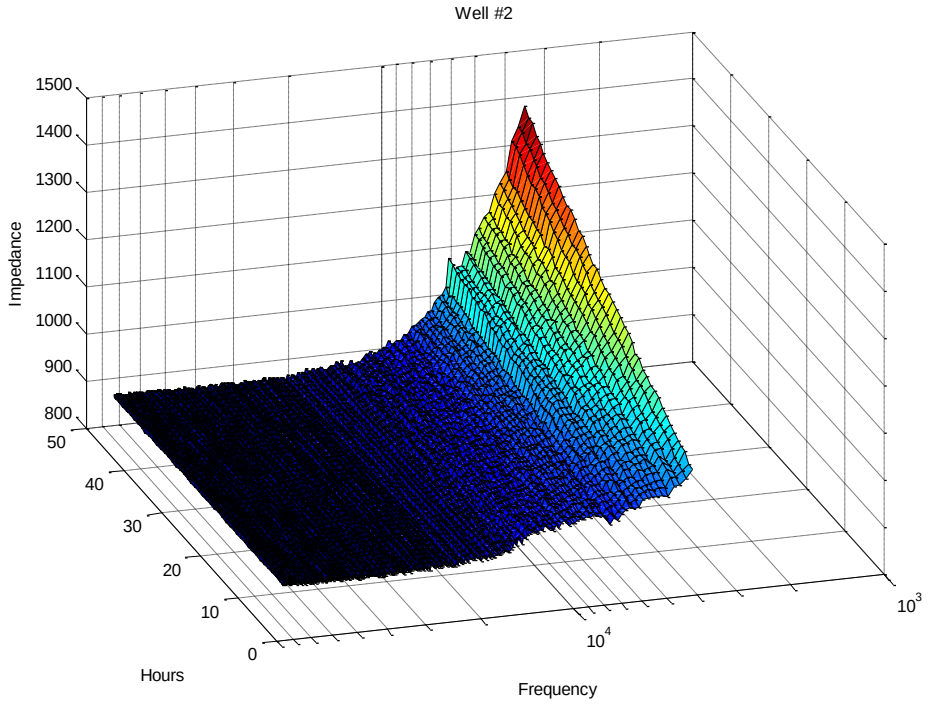

Figure 6.59. Surface of impedance change in time and frequency in well #2

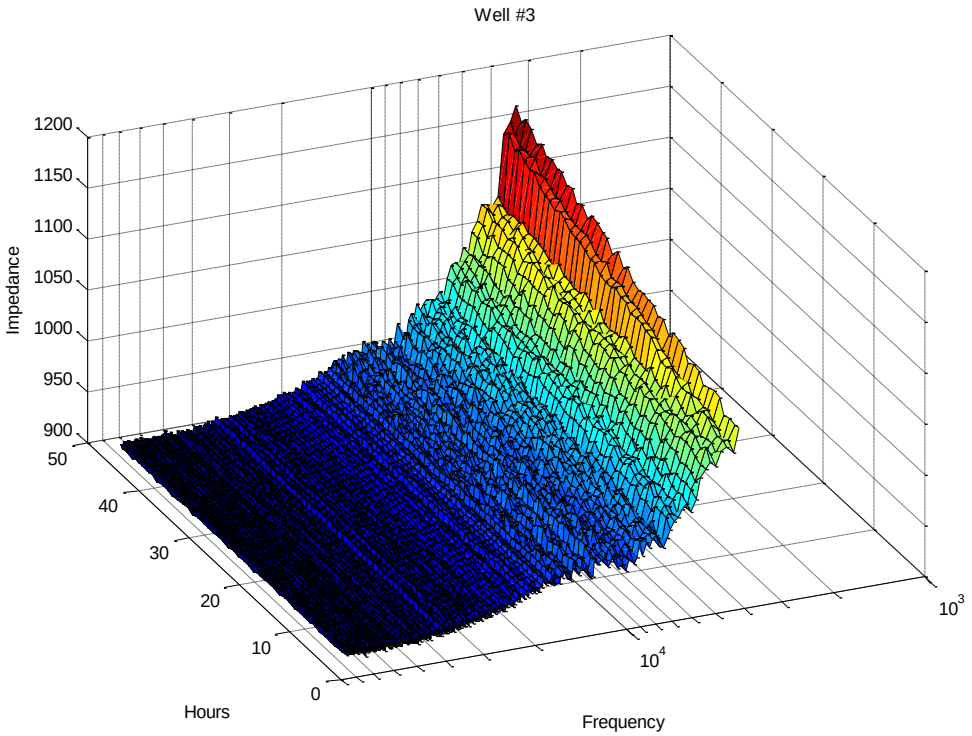

Figure 6.60. Surface of impedance change in time and frequency in well #3

The impedance acquisition card AD5933 provides measurements of both the impedance (Z) and the phase angle (θ). Impedance measurements between the two gold electrodes were taken continuously during 48 hr over a frequency range from 4-84 kHz. Figures 6.21, 6.22 and 6.23 illustrate the change in impedance measurements (Z) over this frequency range for each one of the wells; three measurements are illustrated in each of these Figures, namely impedance of the cells at 24 hours, 48 hours and 72 hours of incubation respectively. We conclude that the change in impedance were due to the growth of stem cells. The noise in the impedance is produced by the acquisition card, the interconnections and environmental changes inside the incubator.

Using MATLAB fit equation (6.1), impedance measurements fit of well #1 show R^2 coefficients of 0.9788, 0.9833 and 0.9892, respectively using the parameters in Table 6.1.

Table 6.1. Parameters using MATLAB fit for well #1

Parameter	After 24 Hrs	After 48 Hrs	After 72 Hrs
A	0.593	0.004815	0.0006486
B	-3.119	-6.368	-7.81
C	923.8	927.7	928.3
D	-0.004297	-0.009116	-0.01002

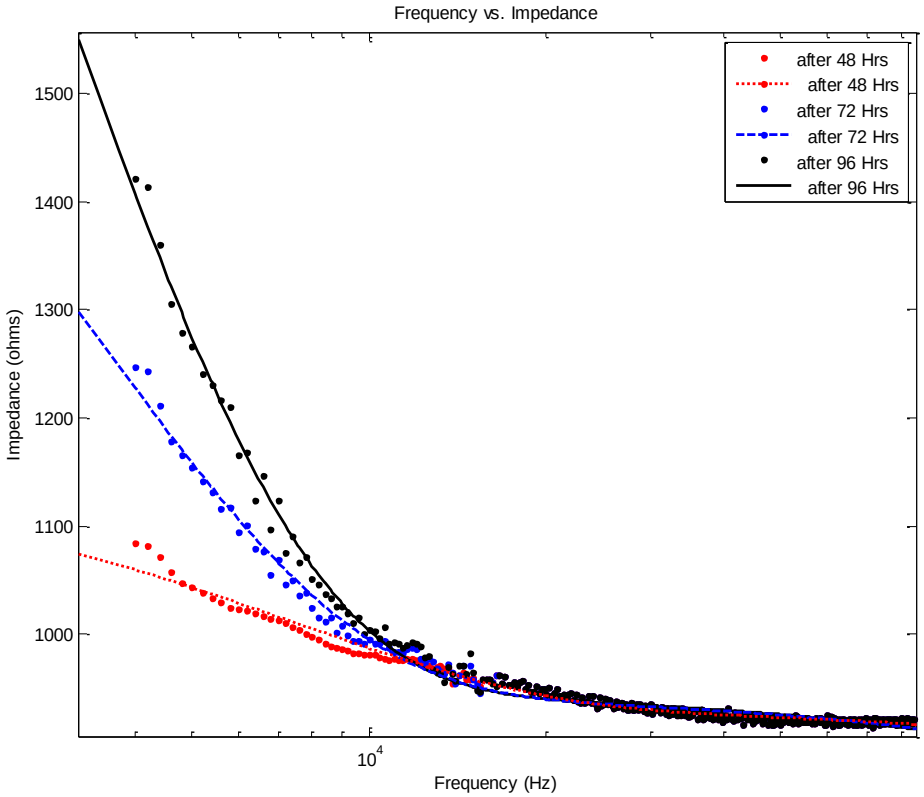

Figure 6.21. Impedance measurement with growth of cells in well #1

Using MATLAB fit equation (6.1), impedance measurements fit of well #2 show R^2 coefficients of 0.9457, 0.9855 and 0.9928, respectively using the parameters in Table 6.2.

Table 6.2. Parameters using MATLAB fit for well #2

Parameter	After 24 Hrs	After 48 Hrs	After 72 Hrs
A	1.246	0.004512	0.0001813
B	-2.692	-6.44	-8.611
C	905.1	909.7	910.1
D	-0.004299	-0.001053	-0.001551

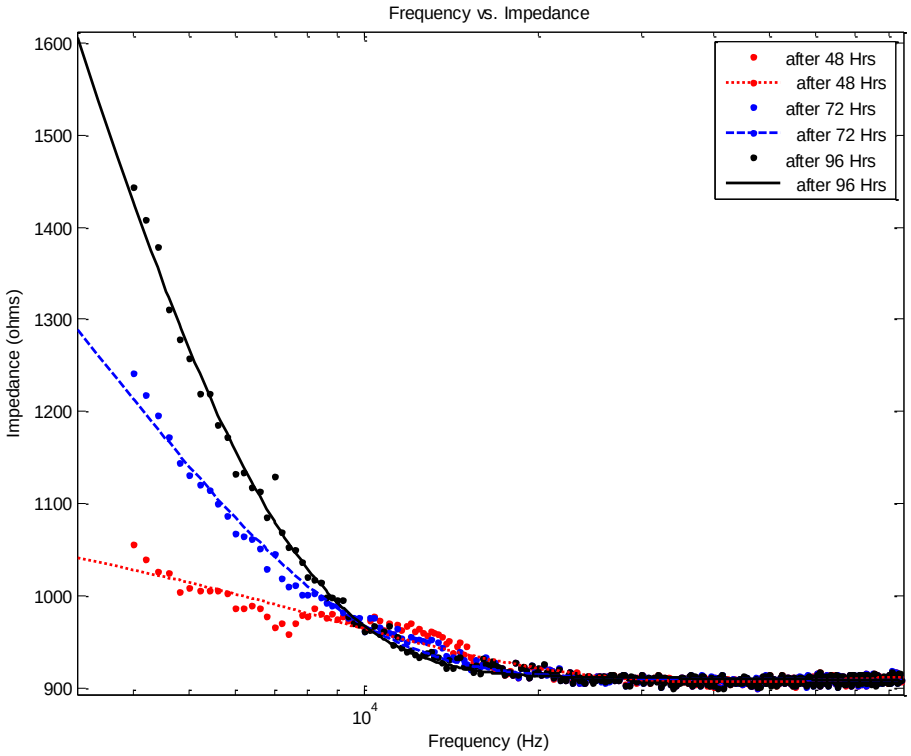

Figure 6.22. Impedance measurement with growth of cells in well #2

Using MATLAB fit equation (6.1), impedance measurements fit of well #3 show R^2 coefficients of 0.9191, 0.9516 and 0.9606, respectively using the parameters in Table 6.3.

Table 6.3. Parameters using MATLAB fit for well #3

Parameter	After 24 Hrs	After 48 Hrs	After 72 Hrs
A	0.03293	0.00813	0.005446
B	-4.68	-5.716	-6.105
C	927.1	927.9	928
D	-0.008165	-0.009269	-0.009577

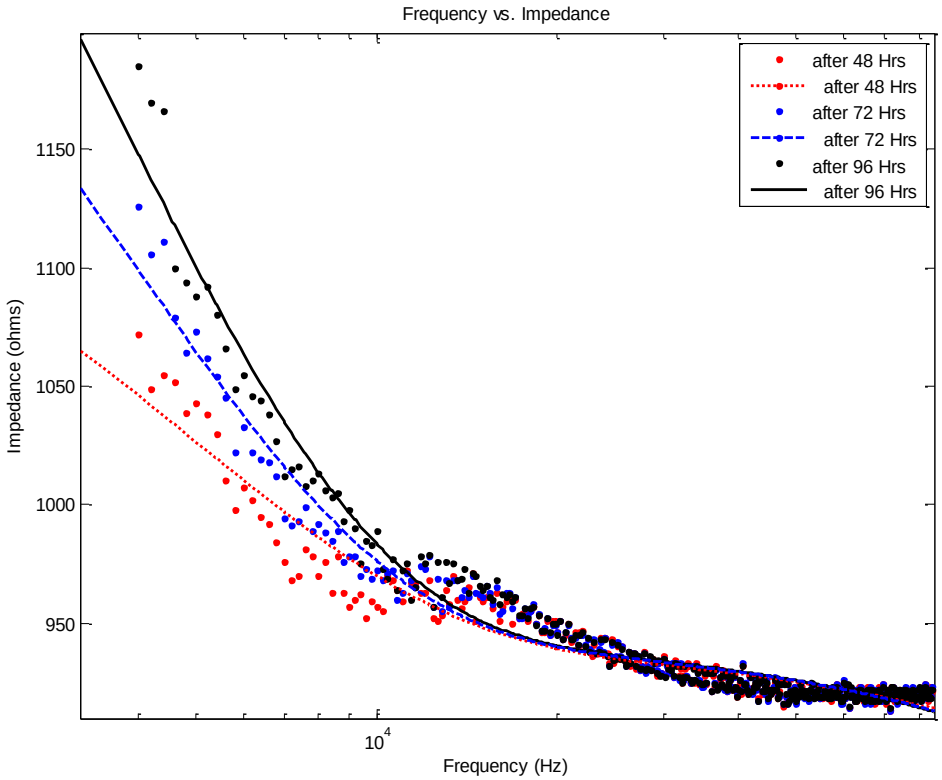

Figure 6.61. Impedance measurement with growth of cells in well #3

As mentioned in Chapter 5 a marked change in impedance will occur at low frequencies (4-10 kHz), as higher frequencies will not show relevant information. Figures 6.24-6.26 show the change in impedance at three different frequencies (4.4 kHz, 8.4 khz and 12.4 kHz) in the full span of time ($48\ Hrs$). These images help to decide which one of the selected frequencies is more useful to perform the parameter extraction of the cell culture. Lower frequencies than 4.4 kHz where not selected due a problem with the acquisition card where it didn't worked properly in the measurements at the smallest frequency. This problem persisted in the measurements using the first and second frequency, reason for which the measurements using low end frequency were not selected to be analyzed. It is possible to see that measurements at 4.4 kHz frequency is the more useful, as 8.4 kHz and 12.4 kHz measurements over time are neither sufficient nor relevant to be analyzed.

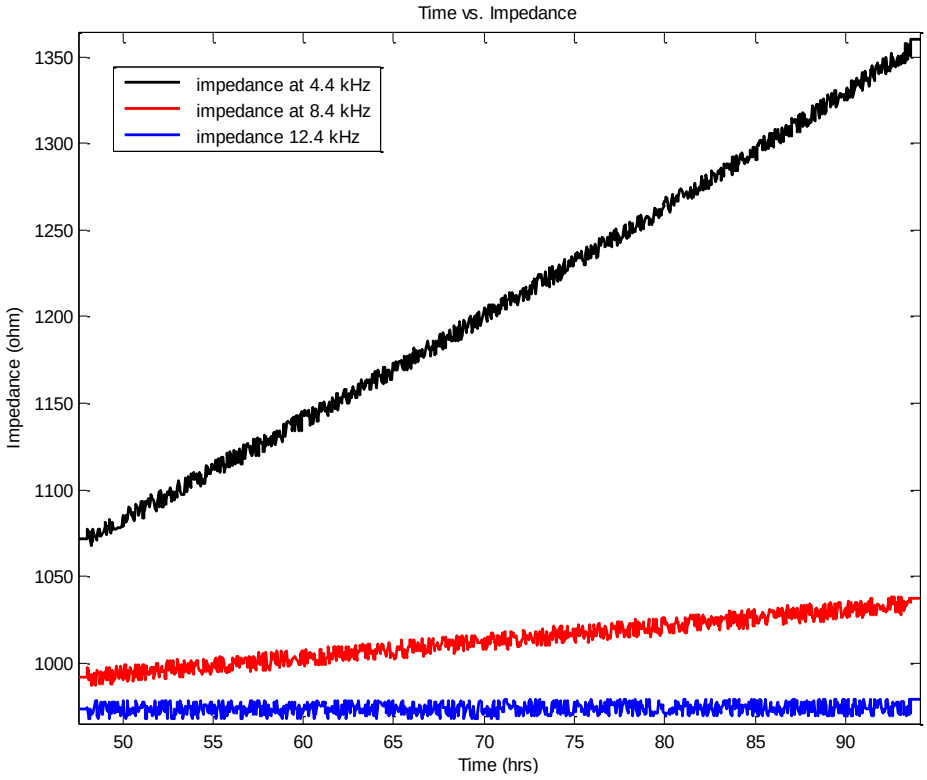

Figure 6.62. Time vs. impedances at different frequencies well #1

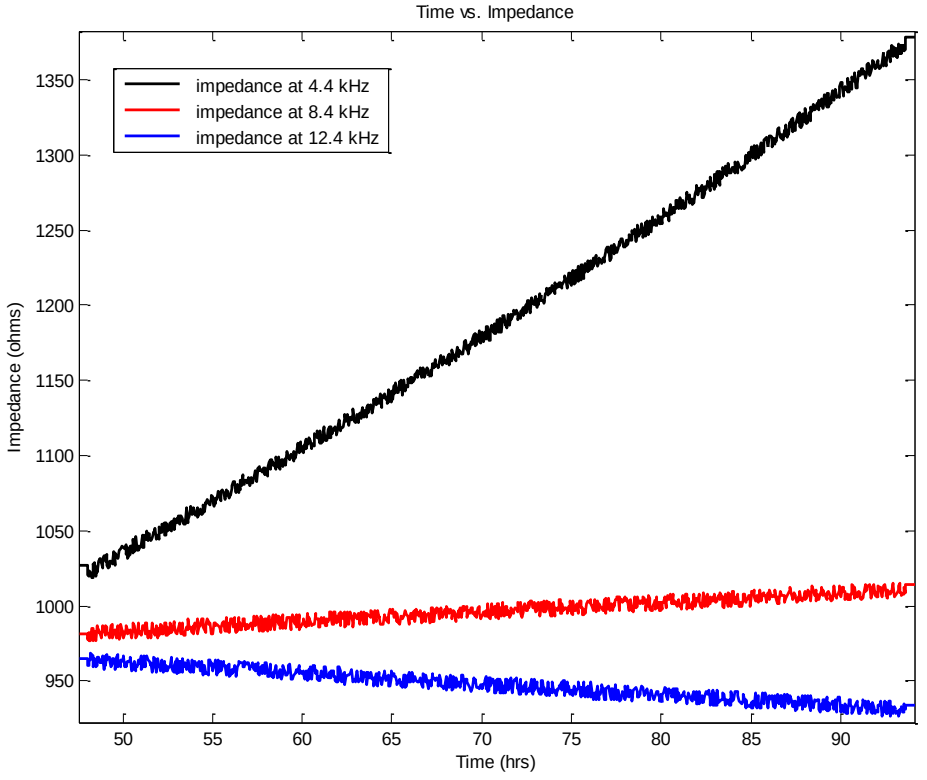

Figure 6.63. Time vs. impedance at different frequencies well #2

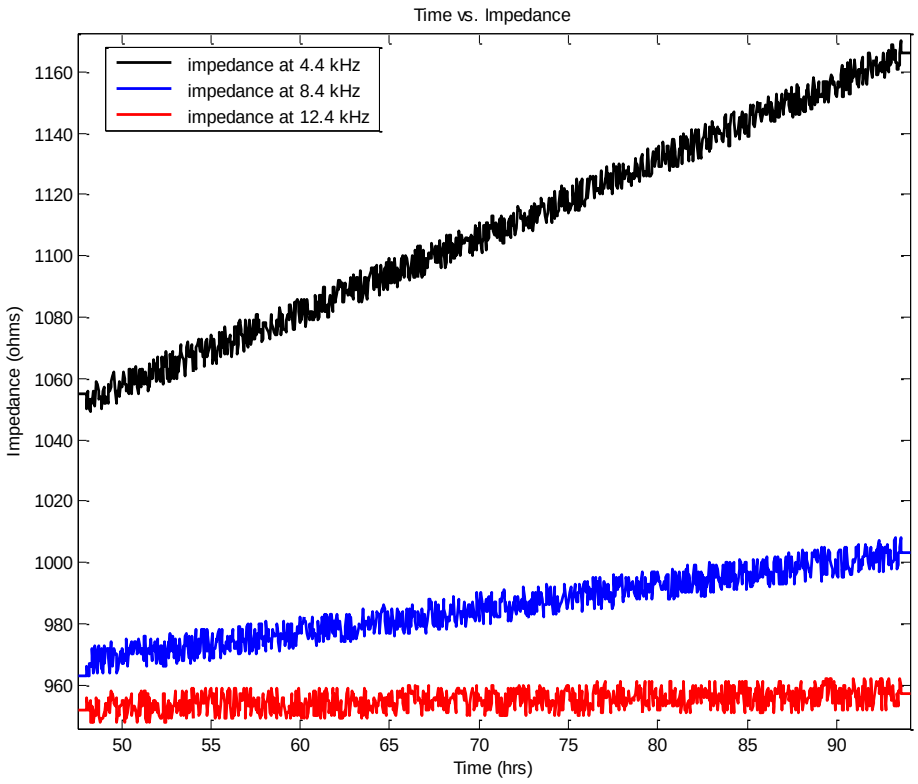

Figure 6.64. Time vs. impedance at different frequencies well #3

According to Siddiquei [6], the components of the impedance of the cell can be obtained from the impedance measurement and the media resistance and capacitance using the following formulas:

$$R_{cell} = R - R_{med} \tag{6.4}$$

$$X_{C\,cell} = \frac{(Z - R_{med})\left(X_{C_{med}} + R_{cell}\right) - X_{C_{med}} \cdot R_{cell}}{X_{C_{med}} - Z + R_{med}} \tag{6.5}$$

In order to calculate R_{cell} and C_{cell} for every well at certain times, the measurements at 4.4 kHz are used. Such selection follows Chapter 5 literature review, Giaever research [7] and is sustained in concordance with the information obtained from Figures 6.24-6.26 as it is the only frequency in which a change in impedance can be clearly appreciated. Following Equations (6.4) and (6.5), Tables 6.4-6.6 show the overall cell resistances and impedances in various times (it must be considered that this experiment starts at time 48 Hrs).

Table 6.4. Overall and cell resistances and impedances well #1

Time (Hrs)	R(Ω)	X(Ω)	C(μF)	R_{cell}(Ω)	X_{Ccell}(Ω)
0	903.5	78.8258	0.45888	0	0
48	1055.7139	186.1508	0.19431	152.2139	-300.3295

54	1089.1974	192.0549	0.18834	185.6974	-314.7641
60	1127.6049	198.8272	0.18192	224.1049	-341.1267
66	1152.2251	203.1684	0.17804	248.7251	-360.6588
72	1192.6022	210.2879	0.17201	289.1022	-395.0998
78	1230.0249	216.8866	0.16677	326.5249	-428.6507
84	1273.3564	224.5271	0.1611	369.8564	-468.6823
90	1304.8703	230.4311	0.15697	401.3703	-498.3285
96	1339.3385	236.1615	0.15316	435.8385	-531.1164

Table 6.5. Overall and cell resistances and impedances well #2

Time (Hrs)	R(Ω)	X(Ω)	C(μF)	R_{cell}(Ω)	X_{Ccell}(Ω)
0	903.5	78.8258	0.45888	0	0
48	1011.3976	178.3367	0.20283	107.8976	-325.8082
54	1048.8202	184.9353	0.19559	145.3203	-299.3026
60	1087.2277	191.7076	0.18868	183.7278	-313.6203
66	1130.5593	199.3481	0.18145	227.0593	-343.3894
72	1177.8301	207.6832	0.17416	274.3301	-382.2352
78	1222.1464	215.4974	0.16785	318.6464	-421.4928
84	1272.3716	224.3534	0.16122	368.8716	-467.7621
90	1325.5512	233.7304	0.15476	422.0512	-517.9624
96	1357.0651	239.2872	0.15116	453.5651	-548.0945

Table 6.6. Overall and cell resistances and impedances well #3

Time (Hrs)	R(Ω)	X(Ω)	C(μF)	R_{cell}(Ω)	X_{Ccell}(Ω)
0	903.5	78.8258	0.45888	0	0
48	1038.9721	183.1988	0.19744	135.4722	-299.796

54	1053.7443	185.8036	0.19467	150.2443	-299.9405
60	1065.562	187.8873	0.19251	162.062	-303.2259
66	1082.2304	190.8393	0.18954	178.8037	-310.8847
72	1094.1214	192.9231	0.18749	190.6214	-317.7359
78	1104.9543	194.8333	0.18565	201.4543	-324.7658
84	1125.6352	198.4799	0.18224	222.1353	-339.6325
90	1135.4834	200.2163	0.18066	231.9833	-347.2148
96	1148.2858	202.4738	0.17865	244.7858	-357.4406

From Tables 6.4-6.6, it can be seen that the overall resistance between electrodes increases from the previously obtained $R(0) = 903.5\Omega$ to $R(96) = 1339.3385\Omega$ $(well\ 1)$, $, 1357.0651\Omega$ $(well\ 2), 1148.2858\Omega$ $(well\ 3)$ respectively. The difference in resistance due to the growth of cells can be calculated as $R(96) - R(0) = 435.8385\Omega$ $(\text{well } 1), 453.5651\Omega$ $(\text{well } 2)$, 244.7858Ω $(\text{well } 3)$ respectively. Hourly change of resistance only due to cell growth and death is shown in the 5th column of the above tables. Based on these measurements, it can be concluded that the highest cell growth occurs in the second 48 hours, which is consistent whit Siddiquei [6] and Bagnaninchi [1] observations.

This observation is also supported by a plot of overall capacitance versus time, which is shown in Figures 6.27-6.29. The Figures show that when the stem cells attach and grow into the surface of the electrodes, impedance increases and capacitance decreases. The increase in the number of cells, directly contributes to the total impedance. If analyzed as an electric circuit, the attachment and arrangement of cells at the surface can be visualized as a series connection of these small resistances. In contrast, a series connection of the capacitances due to each cell decreases the overall capacitance. After a certain time the growth and attachment rate to the electrode surface reduces and ultimately saturates, which subsequently stops the impedance grow as it reaches a peak and then starts falling due to cell apoptosis.

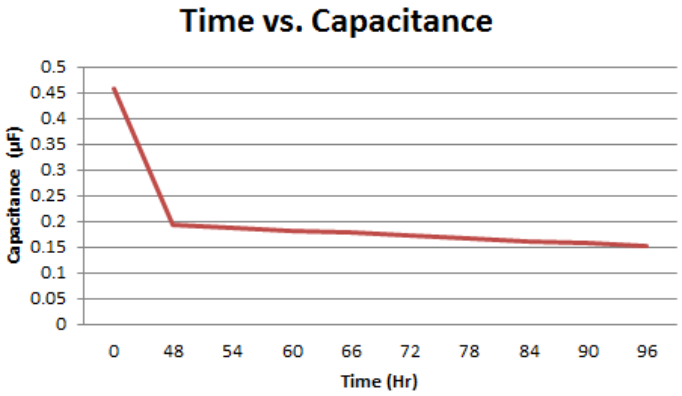

Figure 6.65. Time course of overall capacitance in well #1 at 4.4 kHz

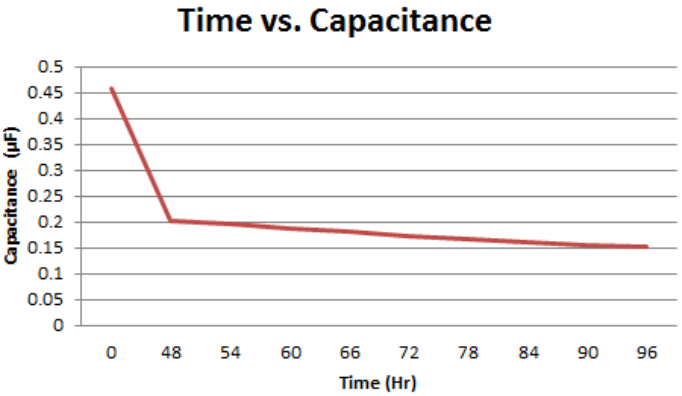

Figure 6.66. Time course of overall capacitance in well #2 at 4.4 kHz

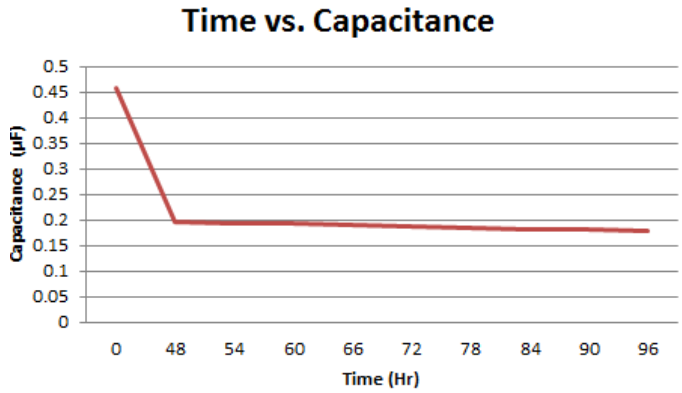

Figure 6.67. Time course of overall capacitance in well #3 at 4.4 kHz

To observe the cell culture attachment and arrangement behavior, pictures were taken using the inverted microscope. The area in the culture well (from where the images area taken) is very important to make those observations. Figure 6.30 shows in a square the area from which the images were taken. This area was selected due an interesting observation over the first experiments. It became a tendency in cultures a high concentration of cell adhesion, and therefore

growth, in the center and near the walls of the culture well (between dotted and continuous lines). This situation was indeed addressed following ECIS Handbook suggestions [8]; even then, the phenomenon continued, with less degree of concentration it kept taking place in the previously mentioned areas.

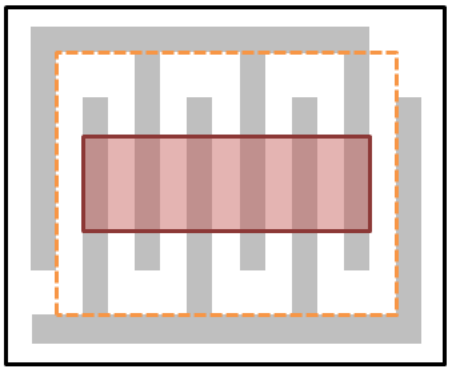

Figure 6.68. Cell concentration areas

Figure 6.31-6.33 presents 10x microscopic images of the development of the cell culture in the three wells every time the cell media was changed (48 hrs, 96 hrs and 168 hrs); images after inoculation were not taken as they were not considered relevant to show the cellular growth.

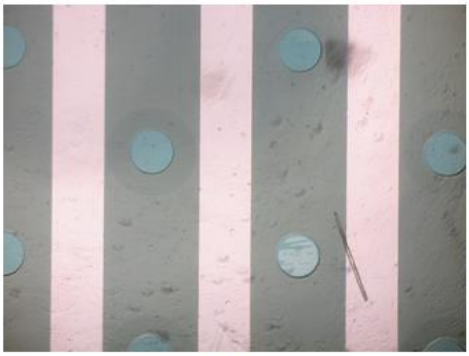

(a)

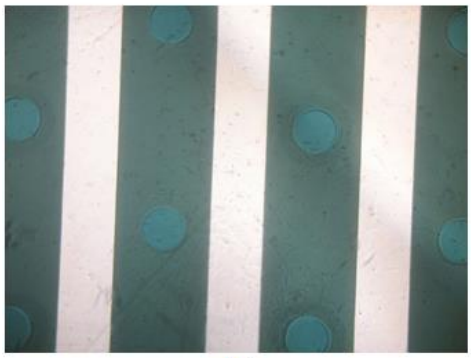

(b)

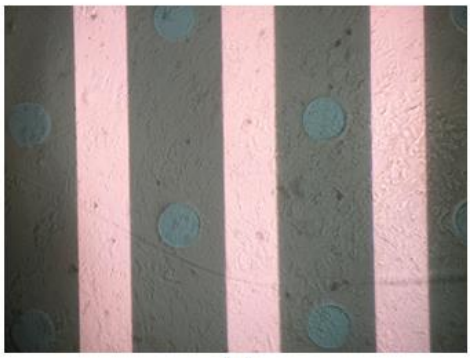

(c)

Figure 6.69. Evolution of cellular growth in well #1 (10x - Control)

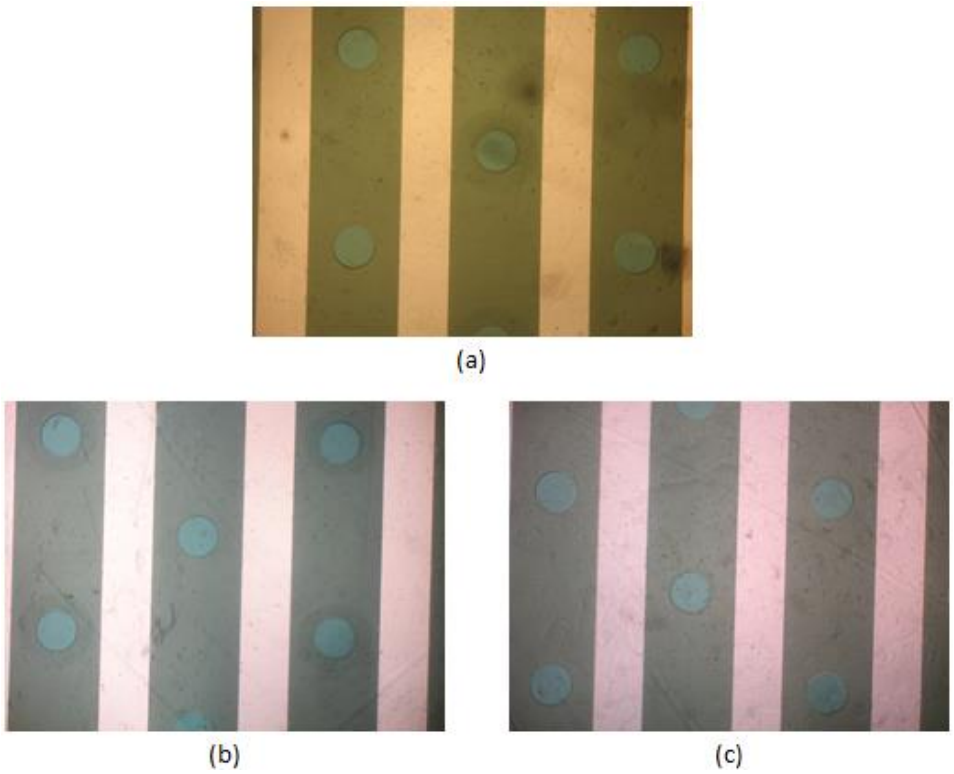

Figure 6.70. Evolution of cellular growth in well #2 (10x - Motor)

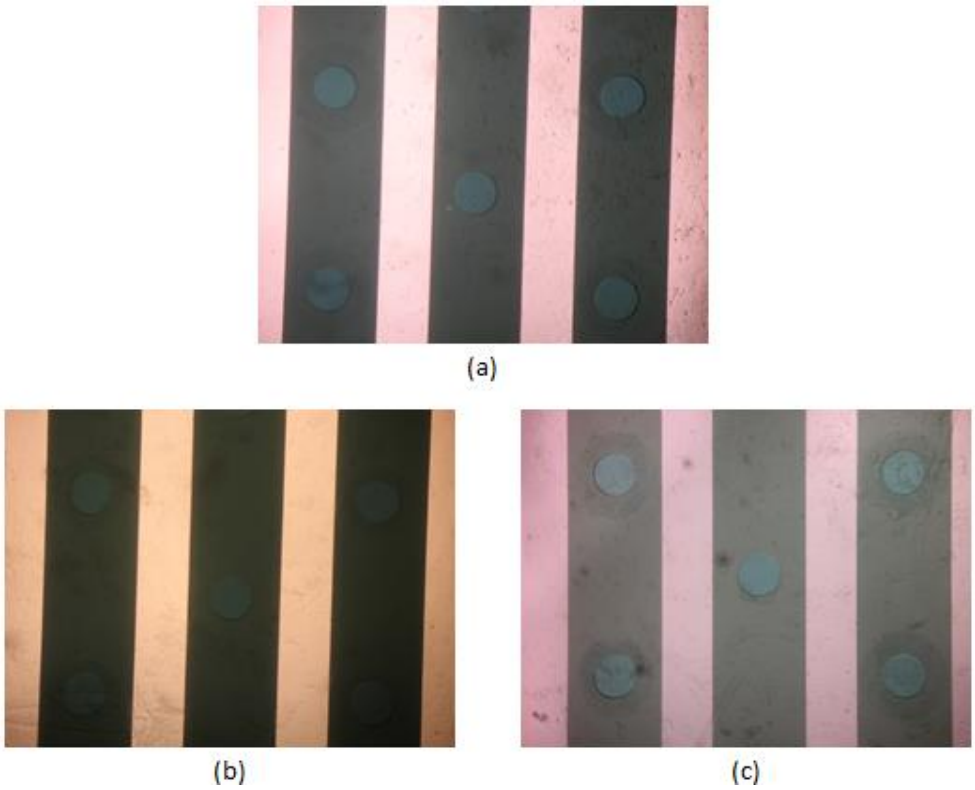

Figure 6.71. Evolution of cellular growth in well #3 (10x - Dopaminergic)

In order to show more clearly the growth of cells over the electrodes, images were taken using the 20x lenses. Images of the well #1 are presented in order to show the growth of cells over specific electrodes during the 120 hrs the experiment took place. Figure 6.34 show these images, in them it's possible to appreciate the steady grow of the cell culture during time. Essentially, images from all electrodes should have been taken to map the grow of cells over every point of the culture well; however, and as the process was time consuming it was decided just to use it as a tool to show the actual growth with more detail than the 10x images shown in Figures 6.31-6.33.

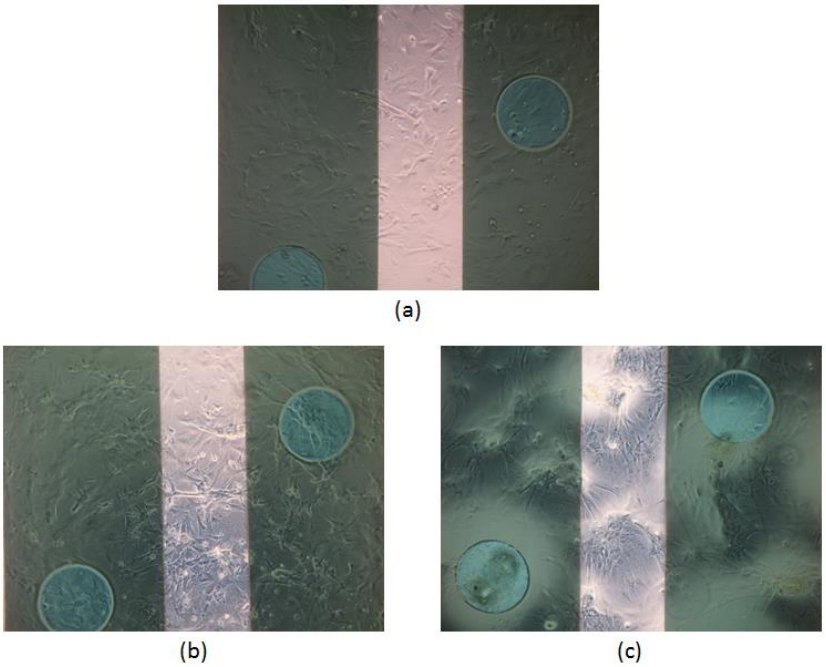

Figure 6.72. Evolution of cell growth in well #1 (20x - Control)

Finally, a comparison between the growth model and the actual impedance measured change is made. The comparison between both graphs is done based in the already corroborated assumption that as the cellular culture grows, the impedance measured also grows. Two models were used to represent the cellular growth. The first shown in Figure 6.35 uses only the doubling time of approximately 24 hours; in this first case the unrestricted growth of the cell culture suggest a steady grow in the cell culture if the 100% of cell adhesion to the well and no major death of cells are considered. While the second, shown in Figure 6.36, uses the hyperboelastic model (H3) by Tabatabai [9] to characterize the growth of stem cells considering cell death and confluence. The measured impedance (Figure 6.37) behaves in a similar way to the behavior depicted in the first approximation, at least during the first 5 days; from this moment on the measured impedance suggest that there is a decrease in the number of cells, probably due cell apoptosis at confluence. The H3 model by Tabatabai [9] adjusts a little better to the impedance measurement obtained curve as it also considers the maximum quantity of cells the well can house according to Yúfera [5] ($\approx 1.2 \times 10^6$ cells). This approximation reaches the maximum quantity of cells predicted by Yúfera and then the number stay steady over this; however, in reality, the number would decrease due apoptosis while reaching confluence.

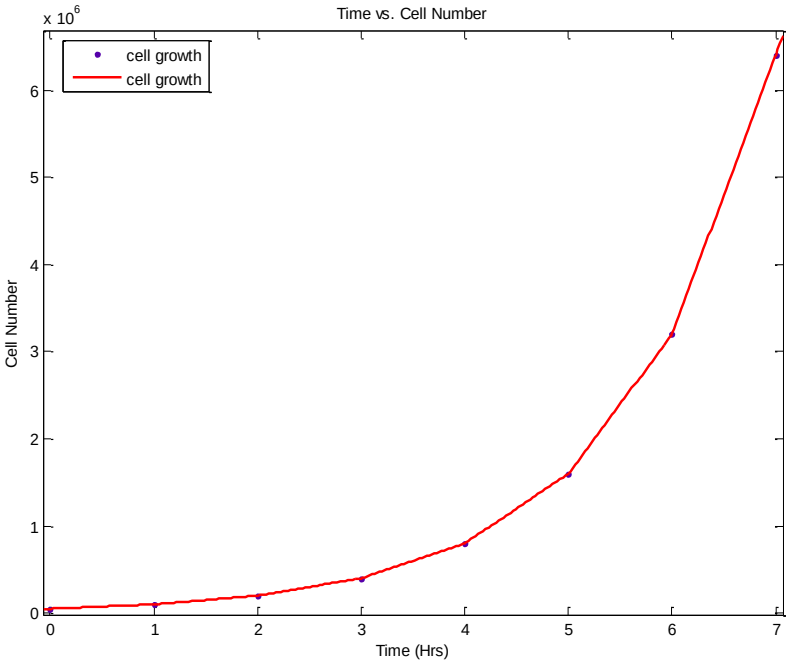

Figure 6.73. Cell population growth based in doubling time

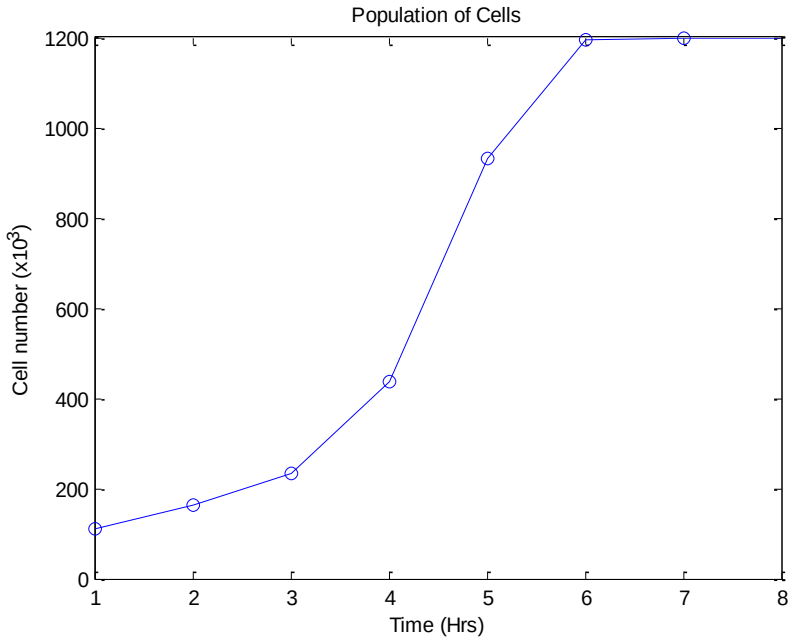

Figure 6.74. Cell population growth using Tabatabai model

Experiment results suggest that the study and observation of cellular growth using the designed system based in ECIS measurements is possible. In concordance, the experiments show the evolution of impedance and the microscopic images of the cell culture evolution through time. However, further work is needed to assure that the designed system is capable of correctly track the cellular growth. It is also needed to determine a direct correlation of the measurements obtained with a specific mathematical model. To fully assure that the system is a capable tool to

study cell growth it is necessary to keep on the testing over the designed system and the experiments running.

6.5 Differentiation of Cells through Bioimpedance

The analysis of cell differentiation (cell induction) is made in the span of time from day 4 to 7 of the experiment. During this span of time cells were induced to dopaminergic and motor cells, while a well was left with traditional media to have them as control group. It is expected that every lineage behaves different according to Bagnaninchi [1]. Figure 6.37 shows the frequency dependent magnitude of impedance at 4.4 kHz over 120 Hrs for 3 wells: Noninduced, motor induced, and dopaminergic induced.

After induction ($t = 96\ hr$), different trends in the measured impedance of the cultures were identified. In the case of motor induced cells, impedance growth is characterized by a very similar curve to the one of the non-induced cells, only presenting lower impedance during the differentiation process. In the case of dopaminergic induced cells, a really interesting behavior takes place as the curve does not correspond with the expected behavior prior induction. As Figure 6.37 show, while control and motor induced cell culture measured impedance behaves in a similar way before induction, dopaminergic induced culture shows a different impedance curve.

The behavior of these cultures can be explained with more detail. It is possible that the behavior of dopaminergic culture before induction actually represents the expansion but there is an error in the measurements (probably a non-characterized element in the circuit that is changing impedance), as it is possible to appreciate a growth slope in the expansion period even when the tendency is really different from the other cultures. After induction, it is possible to appreciate a steady growth in impedance in the dopaminergic culture which suggests a characteristic curve of differentiation As well, after the induction the separation of the curves representing the motor and control cells suggests that there is actually a change in the impedance in the culture which would also mirror into a differentiation process. These explanations seem to support the hypothesis that the designed systems can in fact capture data that indicates the differentiation pathways of the different types of cell and that such differentiation processes are characterized by a distinct impedance time-course curve.

Another interesting point in the measured impedance of non-induced and motor induced cells appears at $t = 130\ hr$. At this time, the impedance reaches a peak and then starts falling. In concordance with tissue culture theory and Giaever experiments [7] this point probably represents the reaching of the confluence state and the posterior cell apoptosis, which explains the falling of impedance towards the end of the experiment. It is also possible that the impedance fall is due to decay in the media richness. Further studies should be undertaken to determine if this point represents indeed the confluence point.

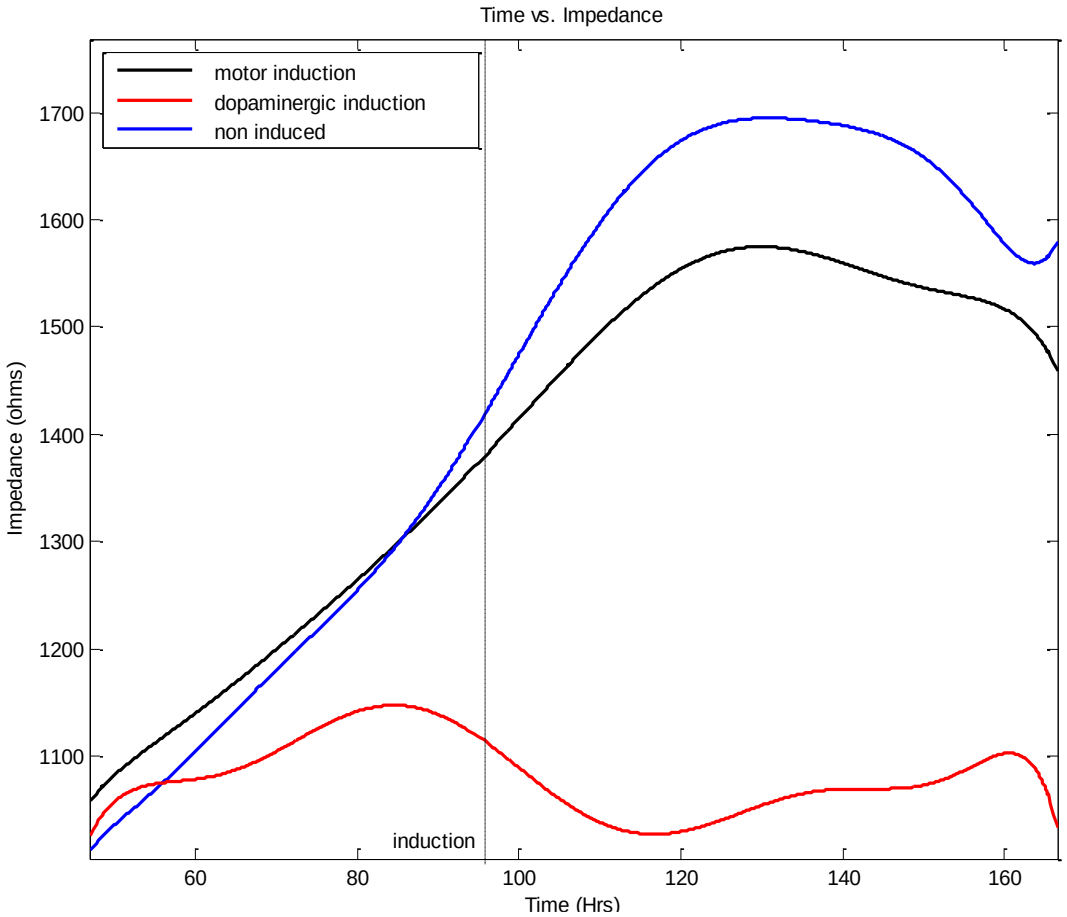

Figure 6.75. Magnitude of Impedance vs. Time (at 4.4 kHz); real time and label free monitoring of RSCs induced toward motor and dopaminergic cells

In the case of non-induced and motor induced cells, as their curves behave in a similar way, it is possible to analyze the real and imaginary component of the cells. As this analysis intend to study the cells real and imaginary component, it can only be made if the media in both cultures is considered to have similar properties; which is supposed as there is no perceptible impedance change once the inductor is added. Figure 6.38 and 6.39 show the comparison between such components in both wells. In concordance with Bagnaninchi [1], the main difference can be appreciated in the resistance, while the reactance is almost equal. However, a big difference between the reported by Bagnaninchi and the results of this research is that a negative reactance appears in this research. The reason for this behavior is that the phase of the impedance changes at every time steps in the sweep, which became a situation that could not be solved. None the less, the difference between the resistance curves suggests a different composition of the cultures.

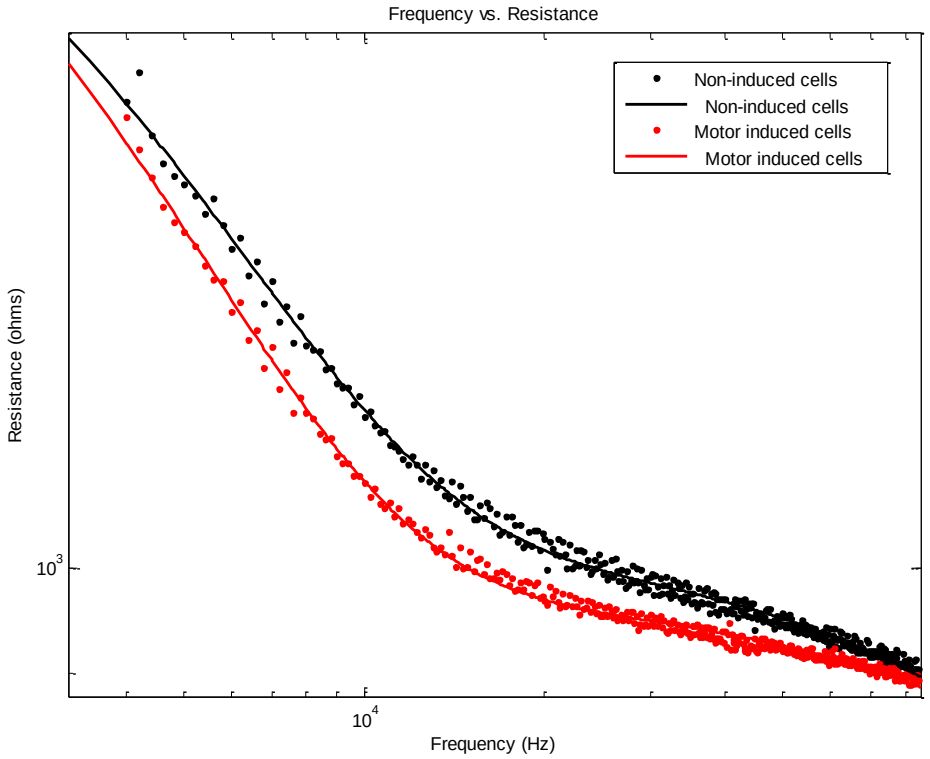

Figure 6.76. Frequency vs. Resistance

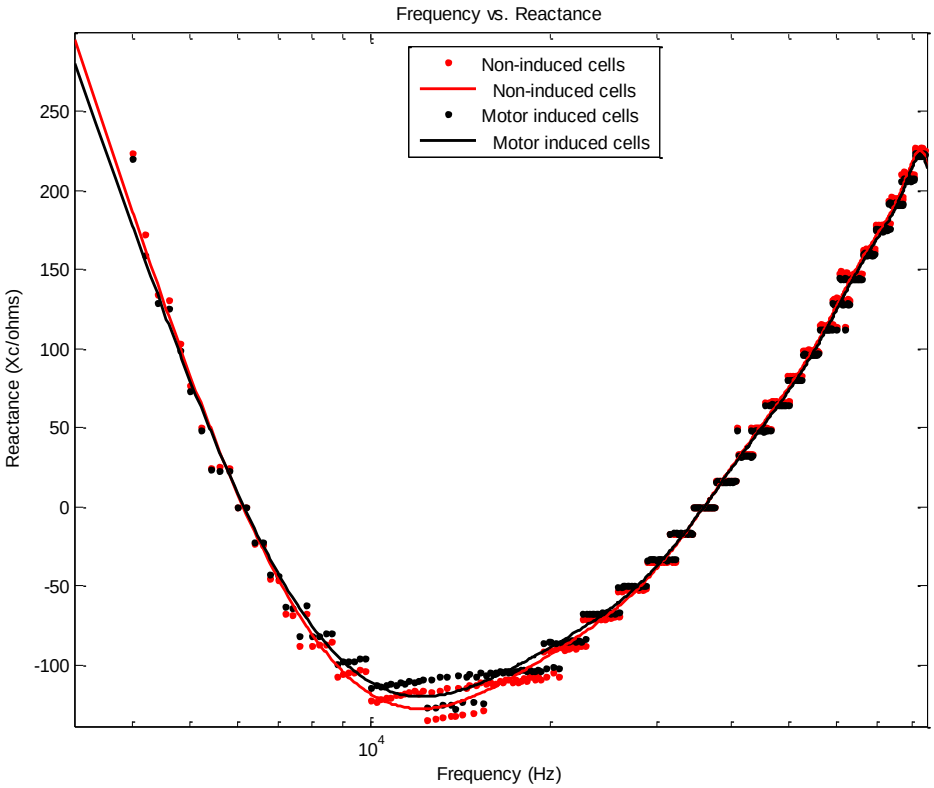

Figure 6.77. Frequency vs. Reactance

In order to corroborate the results, cell staining took place 4 days after induction. The objective was to demonstrate that the RSCs were properly induced toward motor and dopaminergic cells, validating the obtained impedance curves. However, the activity resulted really difficult due to the contrast between the plastic and the interdigitated fingers; making almost impossible to acquire a clean image. Figure 6.40 shows two different images from each culture. After analysis of the images it was determined that only in one picture (Figure 6.40 (a) / Figure 6.41) is possible to conclude that one of the cultures actually differentiates, this observation can be done because in none other image it's possible to clearly see the interconnections and form of cells. None the less, a problem arises, as the only culture that could be determined to undergo differentiation is the only culture (dopaminergic) that presents a strange curve in the impedance measurement. Finally, a conclusive verification of differentiation was not made through comparison because a secondary study to sustain this claim was not performed.

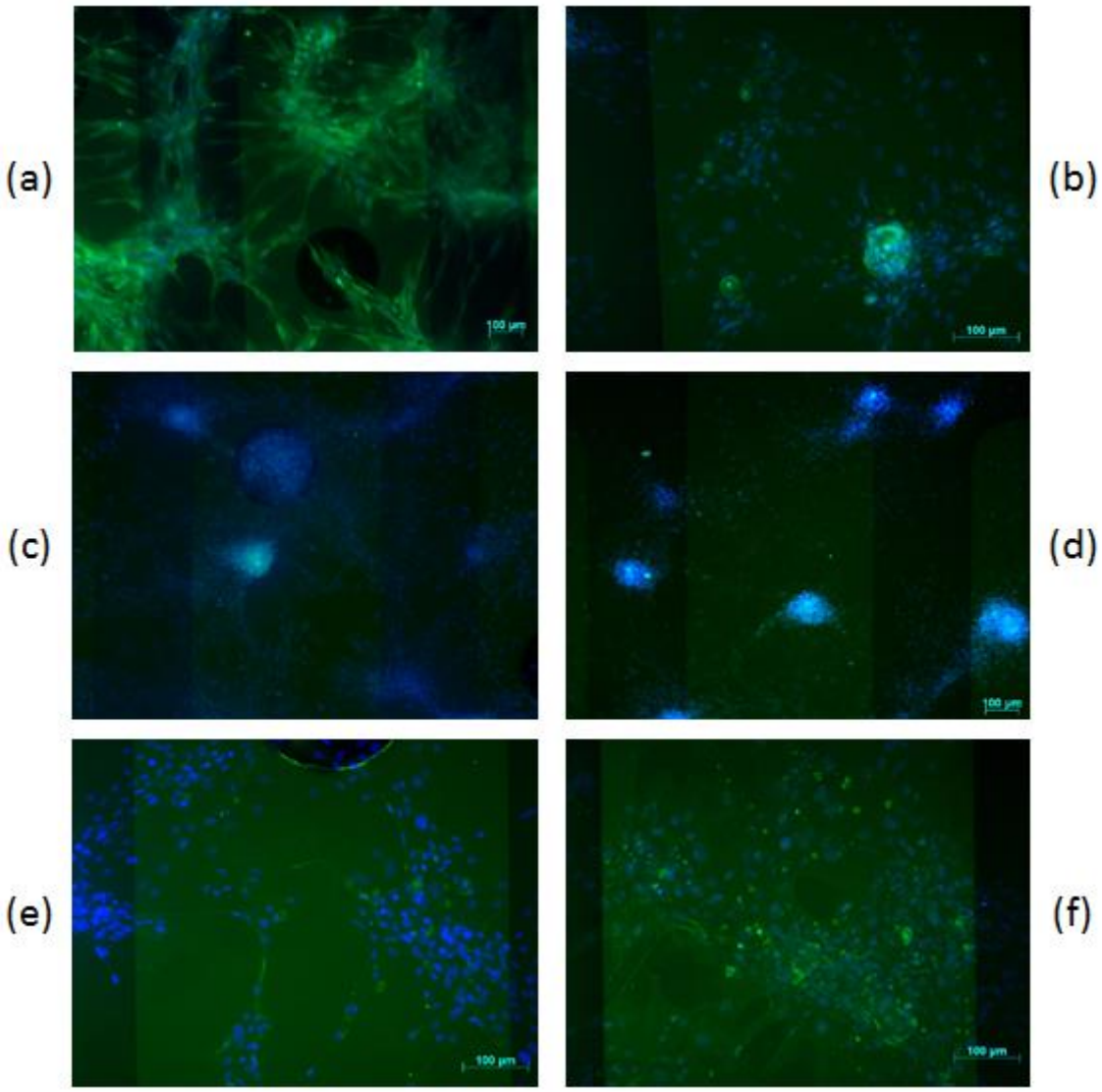

Figure 6.78. Images taken with fluorescent microscope. (a) & (b) – Dopaminergic Induced Culture. (c) & (d) – Motor Induced Culture. (e) & (f) – Non-Induced Culture

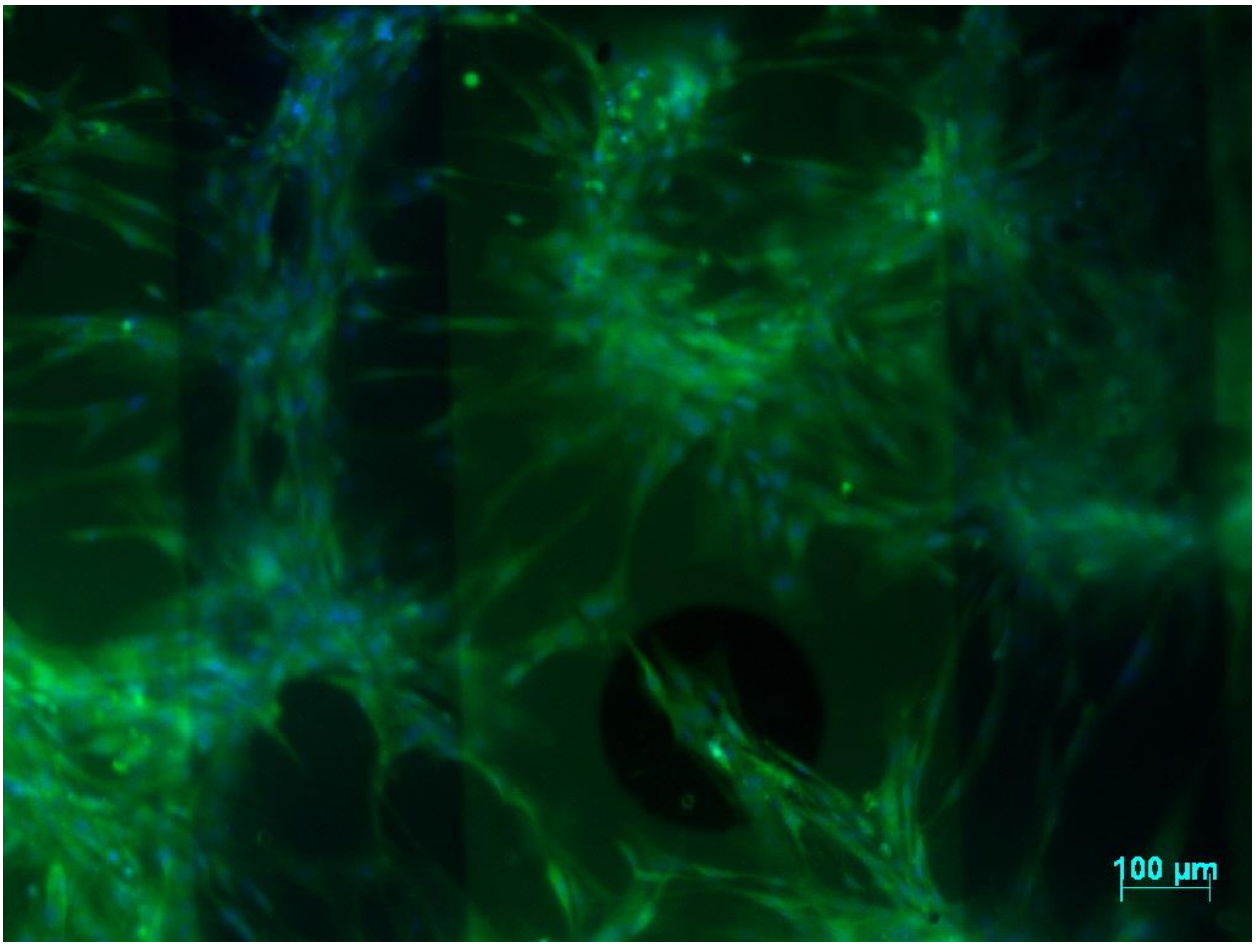

Figure 6.79. Dopaminergic differentiated cell culture

References

[1] Bagnaninchi P, Drummond N. **"Real-time label-free monitoring of adipose-derived stem cell differentiation with electric cell-substrate impedance sensing,"** *PNAS*, vol. 108, no. 16, pp. 6462-6467, 2011.

[2] Wang L, et al. **"Analysis of the Sensitivity and Frequency Characteristics of Coplanar Electrical Cell-Substrate Impedance Sensors,"** *Biosens. Bioelectron,* vol. 24, no. 1, pp. 14-21, 2008.

[3] Aliakbar AM (2009) *Handheld Impedance Based Biosensor System for Glucose Monitoring*. Master Dissertation.

[4] Seriburi P (2008) *Using Electric Cell-Substrate Sensing (ECIS) to Measure Properties of an Individual Adherent Cell.* ProQuest Dissertations and Theses. Doctoral Dissertation

[5] Yúfera A, Cañete D, Daza P. **"A Microelectrode-Cell Sensor for Real time Monitoring,"** *Conference Paper – The Second International Conference on Sensor Device Technologies and Applications, SENSORDEVICES 2011*, 2011.

[6] Siddiquei H, et al., **"Electrical cell-substrate impedance sensing (ECIS) based biosensor for characterization of DF-1 Cells,"** *IEEE International Conference on Computer and Communication Engineering, 2010*, pp. 1 – 4, 2010.

[7] Giaever I, Keese CR.**"A morphological biosensor for mammalian cells,"** *Nature,* 366, pp. 591–592, 1993.

[8] Applied BioPhysics, Inc. (2009) *ECIS® Handbook.* Retrieved from http://www.biophysics.com/publications/ECIS%20Handbook.pdf

[9] Tabatabai MA, et al. **"Mathematical modeling of stem cell proliferation,"** *Med Biol Eng Comput.*, 49, pp. 253-262, 2011.

Chapter 7 – CONCLUSIONS AND FUTURE WORK

This research demonstrated that the designed platform (following ECIS methodology) can be used to measure the impedance of cells cultures. Such impedance measurement can also provide indication of tissue culture growth, differentiation and confluence processes. Relevant data was obtained, providing a continuous non-invasive monitoring of cells in culture in several experiments using dedicated and specialized electrode structures. The experimental work was focused on the development of a low cost cellular measurement system based on the conductometric ECIS technique. The potential uses for a similar system based in bioimpedance measurement include monitoring and detection of chemical and biological agents in the environment, pharmaceutical screening, drug discovery, automatization of cell culture systems, and basic biological knowledge of the cells as pursed in this work.

This work illustrated the design of a system using commercial parts, even when the original idea was to design of each individual part (electrodes, acquisition system, connectors, specific cables, etc.). Such integration limits the system capabilities while giving it an affordable price. Even though the cell culture experimentation may not be as exact as commercial bioimpedance measurement systems, the measurements obtained are consistent with the suggested expected measurements by literature. However, they are a good representation of what happens inside the tissue culture. At the end, the decision to use low cost parts to design the system resulted a success, presenting a final product that cost no more than $200.00 USD against the commercial systems that can go up to $25,000.00 USD.

The objectives to measure cell growth and observe differentiation through impedance measurements ended with mixed results. Experiments of cellular growth using three wells were *conclusive* and the results show a growth that corresponds with the suggested results in literature. However, more experiments are needed to suggest that the system was properly functioning and to consolidate robust measurements. The consistency in the three wells behavior suggest that the system is actually capable of measuring values that in some way reflect the activity of the cell culture. Experiments of differentiation using two different cell types (dopaminergic and motor) were not conclusive due to intrinsic noise, the connectors, the electrodes and other minor problems that limited the generalization of the research work. Therefore, we recommend further experimentation to validate impedance curves and to conclude that the system provided the culture differentiation.

Once this initial platform is developed and ECIS methodology applied, future work can be divided in three major areas: the system area, the analysis area and the biological area.

In the *system area*, alternative methods for impedance measurement must be explored. It is possible that a different technique offer more consistent, clear or more relevant data than the ECIS technique. Based on the reviewed bibliography others methods can be used to determine others characteristics than the presented technique cannot. The utilization of different electrodes is also suggested. While commercial electrodes where used, they had some fabrication errors, which caused errors and lost information due to the architecture of the proposed system. We

suggest keeping experiments with different electrode configurations to find the most suitable type for the bioimpedance measurements, and to determine the impact of electrode type over the impedance measurement. Also the design of specific electrodes is an idea that cannot be thrown away and should be explored if possible. Additionally, the design of a specific novel impedance reader card with all subsystems integrated arises as an interesting challenge for electronic design; reduction of processing times could be achieved and interconnections that cause noise between subsystems could be eliminated. It is also suggested to use a commercial LCR meter with a specific fixture to measure impedance of liquids, which would corroborate the measurements made by the acquisition card.

The design of an *analytical system* that interprets and fits the data to the desired curves automatically, would reduce the post processing time this research presented. The implementation and creation of model simulations is suggested in order to achieve a better understanding of the experiment. Obtained characteristics of the cells must be verified, and a statistical validation must be driven in order to validate the presented results.

In the *biological area*, more experiments could be performed in order to corroborate the results. Proposed impedance characteristic curves of differentiation pathways must be corroborated in further assays. Different ASCs (human adult stem cells) or different differentiation pathways could be selected to determine if the system is consistent with the reported models in bibliography and to see if its application as an automatic sensor could be of use in laboratory. About differentiation, the performance of late differentiation tests could be of interest to compare the behavior of the late and early differentiated impedance curves. Different types of coatings could be used over the substrate to promote the adhesion of the cells. Analysis changing different parameters in the environment of the cell tissue culture is a strong suggestion.

Microelectrode impedance measurements techniques (ECIS) offer promising possibilities for its use as sensor element in the future automatic culture systems. While more work is required to fully prove the utility of the designed system presented herein, there is clear evidence that cultured cells coupled to biosensors can be a powerful tool for analyzing the behavior and responses of cells to external stimulus. Further advances in cell cultured cell technologies, substrate structures and microelectronic design will improve the power of these techniques and systems, and undoubtedly permit the use of these for its use in the development of reliable automated tissue culture stations.